

**Oxidation of Atmospheric Organic Carbon:  
Interconnecting Volatile Organic Compounds,  
Intermediate-Volatility Organic Compounds, and  
Organic Aerosol**

by

James Freeman Hunter

B.S., University of California, Berkeley (2009)

Submitted to the Department of Civil and Environmental Engineering  
in partial fulfillment of the requirements for the degree of

Doctor of Philosophy in Environmental Chemistry

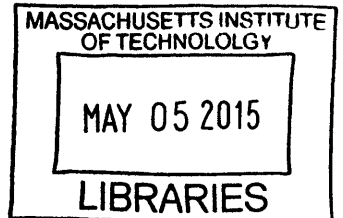
at the

MASSACHUSETTS INSTITUTE OF TECHNOLOGY

February 2015

© Massachusetts Institute of Technology 2015. All rights reserved.

**ARCHIVES**



**Signature redacted**

Author .....  
Department of Civil and Environmental Engineering

January 29, 2015

**Signature redacted**

Certified by .....  
Jesse H. Kroll

Associate Professor of Civil, Environmental, and Chemical Engineering  
Thesis Supervisor

**Signature redacted**

Accepted by .....  
Heidi M. Nepf

Donald and Martha Harleman Professor of Civil and Environmental  
Engineering

Chair, Graduate Program Committee



# Oxidation of Atmospheric Organic Carbon: Interconnecting Volatile Organic Compounds, Intermediate-Volatility Organic Compounds, and Organic Aerosol

by

James Freeman Hunter

Submitted to the Department of Civil and Environmental Engineering  
on January 29, 2015, in partial fulfillment of the  
requirements for the degree of  
Doctor of Philosophy in Environmental Chemistry

## Abstract

Organic molecules have many important roles in the atmosphere, acting as climate and biogeochemical forcers, and in some cases as toxic pollutants. The lifecycle of atmospheric organic carbon is extremely complex, with reaction in multiple phases (gas, particle, aqueous) and at multiple timescales. The details of the lifecycle chemistry (especially the amount and properties of particles) have important implications for air quality, climate, and human and ecosystem health, and need to be understood better. Much of the chemical complexity and uncertainty lies in the reactions and properties of low-volatility oxidized intermediates that result from the oxidation of volatile organic precursors, and which have received comparatively little study thus far. This thesis describes three projects that link together the entire chain of oxidation (volatile to intermediate to condensed) in an effort to improve our understanding of carbon lifecycle and aerosol production. Laboratory studies of atmospherically relevant aerosol precursors show that the slow oxidation of intermediates is critical to explaining the yield and properties of aerosol under highly oxidized (“aged”) conditions, and that the production of organic particles is significantly increased when intermediates are fully oxidized. This aging process is a strong function of molecular structure, and depends on aerosol concentration through the phenomenon of condensational trapping. Further laboratory studies of a series of (poly)cyclic 10 carbon alkanes show that structural effects are largely explained through fragmentation reactions, and that more generally, carbon-carbon bond scission is a ubiquitous and important reaction channel for oxidized intermediates. Finally, direct measurement of oxidized intermediate compounds in field studies shows that these compounds are abundant and important in the ambient atmosphere, with concentrations and properties in between those of volatile and particulate organic compounds. Together with other co-located measurements and complementary techniques, this enables estimates of emission, oxidation, and deposition to be constructed. The results from this thesis can be used to inform more sophisticated models of atmospheric organic carbon

cycling, and to improve prediction of organic particulate matter concentrations.

Thesis Supervisor: Jesse H. Kroll

Title: Associate Professor of Civil, Environmental, and Chemical Engineering



## Acknowledgments

The research described in this thesis was funded in part by the National Science Foundation, under grant number AGS-1056225, as well as by the National Oceanic and Atmospheric Administration under grant NA10OAR4310106.

The author wishes to acknowledge Jesse Kroll for being a fantastic advisor and generally swell guy. The Kroll group (especially the author's cohort, Anthony Carrasquillo and Kelly Daumit) have been extremely helpful throughout the Ph.D. process, and deserve much credit for the author's continued sanity amidst the numerous setbacks typical of graduate school. The author's family (Penny Hunter, Brian Hunter, Emily Carreño and Manuel Carreño) has been extremely supportive, especially through difficult events in the author's life. Finally, life would be much less fun without all of the friends the author has made while in Massachusetts. These friends are too numerous to list individually, but they know who they are and how they've enriched the author's life.

The author also wishes to acknowledge Meena Hussain for miscellaneous contributions to the writing of the thesis.



# Contents

<b>1</b>	<b>Introduction</b>	<b>13</b>
1.1	Organic Compounds in the Atmosphere . . . . .	13
1.2	Thesis Questions . . . . .	16
1.3	Synopsis . . . . .	19
<b>2</b>	<b>Atmospheric Aging &amp; Properties of Organic Aerosol</b>	<b>21</b>
2.1	Introduction . . . . .	21
2.2	Experimental Methods . . . . .	25
2.3	Results & Discussion . . . . .	32
2.3.1	Aging Effects . . . . .	32
2.3.2	OH Exposure Isopleths . . . . .	37
2.3.3	Seed Particle & Humidity Effects . . . . .	40
<b>3</b>	<b>Aerosol Yields &amp; the Role of Fragmentation in Reactive Products</b>	<b>47</b>
3.1	Introduction . . . . .	47
3.2	Experimental Methods . . . . .	49
3.3	Results & Discussion . . . . .	51
3.3.1	Aerosol Formation & Yields . . . . .	51
3.3.2	Comparison With Previous Results . . . . .	51
3.3.3	Influence of Number of Rings on Yields and Mechanisms . . . . .	54
3.3.4	Role of Number of Rings on SOA Elemental Composition . . . . .	59
<b>4</b>	<b>Comprehensive Measurements of Atmospheric Organic Carbon</b>	<b>63</b>

4.1	Introduction . . . . .	63
4.2	Results . . . . .	65
4.3	Discussion . . . . .	76
4.4	Methods . . . . .	80
4.4.1	Data Selection and Averaging . . . . .	80
4.4.2	Estimates of $\overline{\text{OS}}_{\text{C}}$ , $n_{\text{C}}$ , $c^*$ . . . . .	81
4.4.3	Instrument Scope and Overlap . . . . .	82
4.4.4	Flux Calculations . . . . .	83
4.4.5	Key Uncertainties . . . . .	85
4.5	TGO Description, Calibration & Analysis Methods . . . . .	86
4.6	Calibration Methods . . . . .	89
4.6.1	Mass Concentration Calibration . . . . .	89
4.6.2	Volatility Calibration . . . . .	90
4.7	Analysis Methods . . . . .	92
4.7.1	Processing Routines . . . . .	92
4.7.2	Background Subtraction . . . . .	93
<b>5</b>	<b>Conclusion</b>	<b>95</b>
5.1	Summary . . . . .	95
5.2	Implications and Research Prospectus . . . . .	97
<b>A</b>	<b>Glossary of Acronyms</b>	<b>99</b>

# List of Figures

1-1	The lifecycle of atmospheric organic carbon . . . . .	16
2-1	Effect of condensational trapping on OH exposure . . . . .	24
2-2	Validation of aging methodology . . . . .	29
2-3	Effect of aging (increased OH exposure) on selected molecules . . . . .	35
2-4	OH exposure esopleths for cyclodecane . . . . .	41
2-5	Effect of seed particles on cyclodecane aging . . . . .	42
2-6	Effect of relative humidity on $\alpha$ -pinene aging . . . . .	45
3-1	Reaction pathways available to unbranched acyclic, monocyclic, and polycyclic alkanes . . . . .	49
3-2	Time traces for key measurements during a typical experiment (oxidation of cyclodecane) . . . . .	52
3-3	Yields of organic aerosol . . . . .	55
4-1	Campaign average data for the instruments during BEACHON-RoMBAS	68
4-2	Volatility distribution of carbon mass during BEACHON-RoMBAS . . . . .	70
4-3	Total carbon concentration categorized by chemical significance . . . . .	71
4-4	Diurnal trends in chemically significant categories of organic carbon mass . . . . .	73
4-5	Approximate instantaneous carbon fluxes during BEACHON-RoMBAS	77
4-6	Variability in measured quantities during BEACHON-RoMBAS . . . . .	81
4-7	Volatility contours in $\overline{OS_C-n_C}$ space . . . . .	83
4-8	A diagram of the TGO instrument . . . . .	87

4-9	TGO mass calibration . . . . .	90
4-10	Empirical desorption times for alkanes measured by the TGO . . . . .	91
4-11	TGO volatility binning, integration and subtraction . . . . .	92
4-12	Details of TGO data analysis . . . . .	94

# List of Tables

2.1	Magnitude of aging effects . . . . .	38
3.1	Key properties of molecules in this study . . . . .	50
3.2	Yields and elemental composition of SOA from C10 compounds . . . . .	56
4.1	Flux estimates for chemically significant carbon categories . . . . .	75





# Chapter 1

## Introduction

### 1.1 Organic Compounds in the Atmosphere

Organic compounds constitute a diverse group of molecules in the atmosphere, with a wide range of origins, sinks, transformations, chemical properties, and environmental impacts. Volatilities range over many orders of magnitude, with the least volatile organic material in the form of condensed particles ranging from small clusters of molecules up to about 1 micron in diameter. Approximately 1300 Tg carbon/year of non-methane volatile organic compounds (VOCs) are emitted by humans (anthropogenic emissions), plants and other biota (biogenic emissions).<sup>1</sup> Particle-phase organic compounds have a variety of sources, and may be emitted directly as particles from combustion sources like biomass burning and engine emissions (primary organic aerosol, POA) or formed from more volatile precursors through secondary chemistry (secondary organic aerosol, SOA). Organic particulate is much less abundant than VOCs, with an estimated production of approximately 140 (50 to 380) Tg carbon/year,<sup>2</sup> up to 40 Tg of which of results from the oxidation of primary particles.<sup>2</sup>

Transformation of emitted carbon is dominated by oxidation, which can take a variety of pathways. VOCs will mostly undergo gas-phase oxidation by the OH radical or other oxidants. This oxidation leads to the addition of oxygen-containing functional groups that significantly lower the vapor pressure of the oxidation products.<sup>3</sup> This process creates significant quantities of oxidized, low volatility intermediates,

and eventually leads to volatilities low enough for the products to condense through the process of absorptive partitioning.<sup>4,5</sup> Continued oxidation of particles occurs but is much slower,<sup>6-8</sup> partly because partitioning to the condensed phase reduces the amount of material that can react in the gas phase, and partly because particle-phase oxidation (e.g. heterogenous oxidation and direct photolysis) is itself usually slow. Mass spectrometric measurements of ambient organic aerosol indicate however, that most of the total organic aerosol burden is oxidized and resembles SOA.<sup>9</sup> This suggests that emitted POA does continue to oxidize after emission, a conclusion which is supported by laboratory measurements.<sup>10</sup> For molecules with a sufficiently high Henry's law constant (including oxidized intermediates and particles), aqueous oxidation can also occur.<sup>11,12</sup> Collectively these oxidation processes lead to about 100 Tg carbon/year from emitted VOCs,<sup>2</sup> for an overall aerosol yield of about 8%.

VOC carbon that is emitted to the atmosphere can be removed from the atmosphere in one of two ways—either through complete oxidation to CO<sub>2</sub>, or through deposition to environmental surfaces. Oxidation to CO<sub>2</sub> is thought to be relatively slow, with estimates that 20-30% of carbon will be converted to CO<sub>2</sub> over 5 days of oxidation, though this is difficult to constrain with measurements.<sup>1</sup> It is likely that CO<sub>2</sub> production occurs along the entire oxidation pathway (from VOCs to intermediates to particles) via fragmentation that results in small molecules like acetone and formaldehyde. The slow oxidation rate of these molecules, along with the slow oxidation rate of CO<sub>2</sub>'s immediate precursor CO are likely responsible for the slow production rate of CO<sub>2</sub>. Deposition can occur for particles as well as for oxidized intermediates through both dry and wet (associated with precipitation) processes, and depends to a great extent on the chemical properties (e.g. Henry's law constant) of the intermediates.<sup>13</sup> The combination of complete oxidation and deposition of oxidized vapors remove the vast majority of carbon emitted as VOCs (~ 90%), but the lack of detailed knowledge of the reactions and properties of the oxidized intermediates leaves the branching between these processes mostly unconstrained.

Together, emission, transformation and removal form the lifecycle of atmospheric organic carbon, a simplified picture of which is shown in figure 1-1. The branching

between the three sinks—deposition of SOA, deposition of intermediates, and complete oxidation to CO<sub>2</sub>—determines the overall fate of the emitted volatile carbon, but it also determines the overall environmental impact. Though organic compounds can be toxic pollutants themselves (e.g. polycyclic aromatic hydrocarbons), more significant impacts are tied to the lifecycle chemistry. Under most circumstances oxidation leads to production of tropospheric ozone, which is a greenhouse gas and has well documented negative human and environmental health effects.<sup>14–16</sup> Particulate matter also has negative health effects,<sup>17,18</sup> and affects the climate by directly absorbing or reflecting sunlight and by causing changes to cloud formation, longevity, and droplet properties.<sup>15</sup> These effects are large but not well understood, and dominate the overall uncertainty in predictions of future climate (though not the overall radiative forcing).<sup>15</sup> Collectively, oxidation of VOCs leads to smog formation, low air quality, and poor visibility. Because the balance between the sinks affects the total production of particles and ozone from a given emission of volatile carbon, it can exert a significant influence on the total health, climate, and environmental impacts.

Significant research efforts have been directed towards simulation of organic aerosol using regional and global air quality models, but their concentration and properties have been especially difficult to predict. In the past, models have underestimated concentrations by up to an order of magnitude,<sup>19–21</sup> More recently, concentrations have been modeled to within a factor of two, but predictive ability of models is still poor, with modeled versus measured time series R<sup>2</sup> on the order of 0.2.<sup>22</sup> Much less effort has been directed toward predicting the concentrations of oxidized intermediates, even though the reaction and loss of these species determines how much PM is made as well as the overall fate of carbon. This is partly because these molecules have not been the focus of targeted study until very recently, and partly because they are difficult to measure (they are efficiently lost to instrument surfaces). Parameterizing oxidation intermediates in models requires experiments in which the role of these intermediates is characterized, experiments that simply have not yet been performed.

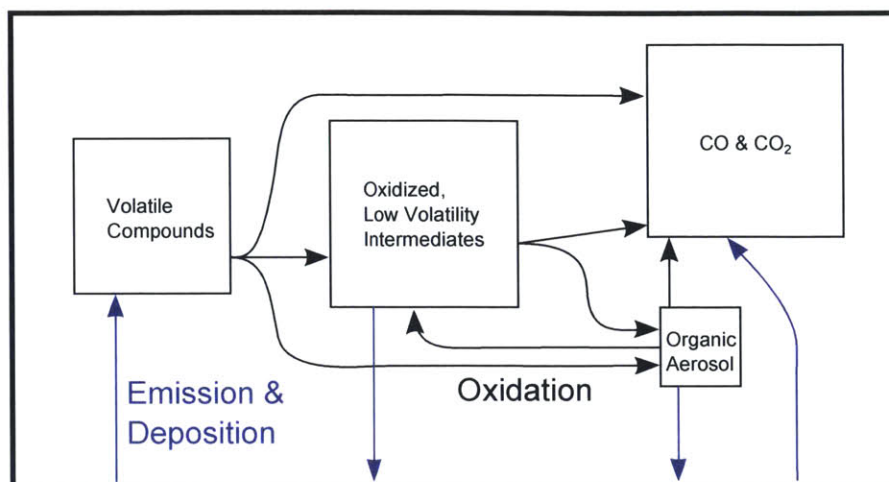


Figure 1-1: The lifecycle of atmospheric organic carbon. Volatile organic compounds (VOCs) undergo oxidation, yielding intermediates with lower vapor pressure. The initial oxidation step may also lead to some organic aerosol (material with vapor pressure low enough to condense into particles) and  $\text{CO}_2$ . The intermediates can undergo further oxidation steps and form additional organic aerosol and  $\text{CO}_2$ , and are also subject to deposition processes. The formation of  $\text{CO}_2$  and deposition constitute the overall sinks for volatile carbon emitted to the atmosphere, the balance of which is largely controlled by the relative strength of the loss processes for oxidized intermediates.

## 1.2 Thesis Questions

Considering the state of our knowledge, several central unanswered questions are apparent concerning the role of oxidized intermediates in atmospheric organic chemistry. In an abstract sense, we want to know what these compounds do in the atmosphere, and how they influence the fate of carbon especially with respect to the formation of particles. We would specifically like to know how the reactions of these intermediate influence the yield and properties of organic aerosol over the full lifetime of the emitted carbon. This is in turn dependent on the the key reactions of these intermediates, and how these reactions determine how much of the carbon is deposited or is oxidized to  $\text{CO}_2$  as opposed to organic aerosol. The full effect will ultimately also be a function of how abundant these intermediates are in the ambient atmosphere, and what fraction of the total carbon is tied up in these hard to measure, low volatility, oxidized compounds. The goal of this thesis is to provide a first step toward answering these

questions through the description of several related research projects. These projects are closely connected to existing lines of inquiry in atmospheric chemistry, but unique in the focus on the role of oxidized intermediates.

The formation of aerosol is thought to be a multigenerational oxidation process, in which several reactions are necessary and several groups of intermediates are produced prior to vapor pressure decreasing enough to cause condensation. This gradual conversion of intermediates to aerosol is closely linked to the concept of atmospheric aging, which refers to the collection of processes that occur in the atmosphere that lead to modification of emitted carbon over time. This includes physical processes such as coagulation and growth of particles, as well as the oxidation chemistry under consideration here.<sup>23</sup> Gas-phase OH aging chemistry has been hypothesized to lead to the significant quantities of highly oxidized aerosol that have been observed to rapidly form in the ambient atmosphere,<sup>10,21,24</sup> but attempts to replicate ambient aerosol in the lab typically result in lower aerosol yields and much less oxidized aerosol. These laboratory experiments have typically focused on the amount of hydrocarbon precursor reacted relative to aerosol formed, but the implication of multigenerational oxidation is that even after this precursor has reacted, significant quantities of unreacted intermediates may remain, and additional oxidation will be necessary to achieve maximum aerosol yields. Experiments were conducted specifically in order to fully oxidize these intermediates, and demonstrate the maximum effect of aging for a series of atmospherically relevant organic molecules. The relationship between yield, degree of oxidation, and aerosol concentration is also investigated, as is the feedback of condensational trapping on aerosol yield and composition.

As organic compounds oxidize, each step has a branch for products that are smaller and eventually lead to CO<sub>2</sub>, as well as a branch that leads to lower volatility products, and eventually to aerosol particles. Although the chemistry is likely more complicated, this can be understood in terms of the likelihood of fragmentation (leading to oxidized but more volatile products) versus functionalization (adding oxygenated functional groups and decreasing vapor pressure). This branching is a function of molecular structure,<sup>25-28</sup> and almost certainly changes with degree of oxidation, such that the

branching may be very different for intermediates than for the initial structure. Most studies however, have only investigated the effect of the initial structure, and have attempted to explain the overall yield of aerosol based on the first oxidation step. However, most compounds (including those in the referenced studies) are expected to require multiple generations of oxidation to yield aerosol, and other examples exist where the result of the initial oxidation is not consistent with the overall outcome. For example, linear alkanes are not expected to fragment upon oxidation,<sup>26,27,29</sup> and yet the linear alkane *n*-decane has a very low aerosol yield of only a few percent. This yield cannot be achieved without significant fragmentation, and has remained largely unaddressed and unexplained in the literature so far. Experiments were conducted for this thesis that investigate the branching for oxidized intermediates, and specifically how the tendency to fragment changes with structure for multigenerational aerosol formation processes. The effect of condensational trapping on the degree of fragmentation is also assessed.

Significant total concentrations of intermediates should be present both in the ambient atmosphere as well as transiently during laboratory experiments as a result of the the oxidation of volatile precursors to CO<sub>2</sub> and organic aerosol. The concentrations of individual compounds are likely very low due to the large number (many thousands) of possible products that can result of oxidation of VOCs.<sup>1</sup> Low volatility, oxidized intermediates are also challenging to measure because they tend to stick to environmental and instrument surfaces. This means that conventional approaches for measuring VOCs are ineffective for these molecules, and that a complete (even by mass) accounting of intermediates on a molecular level is not likely to be possible. Because of the importance of directly measuring these intermediates for completely understanding aerosol formation and the fate of carbon, novel techniques are required that can overcome these issues. This thesis describes measurements taken by a suite of such instruments, several of which were essentially new to field deployment. In conjunction with supporting measurements of VOCs and organic aerosol, these measurements allow first order questions about the relative amount, volatility and degree of oxidation of intermediates to be answered. More complex questions about the

sources and the relative magnitudes of oxidation and deposition are also addressed.

### 1.3 Synopsis

Collectively, the experiments described constitute a significant advancement in knowledge of the role of intermediates in the production of aerosol and the fate of carbon. The experiments and field data are organized into three chapters within the thesis. The role of intermediates in aging processes is discussed primarily in Chapter 2. This chapter describes how aerosol yields and properties are a function of the oxidation chemistry of multiple generations of intermediates. The aging methods are also central to the work on fragmentation of intermediates in multigenerational oxidation which is discussed in Chapter 3. The central theme of this work is that the branching of pathways for oxidation intermediates is highly important for determining the overall fate of emitted carbon, and further that fragmentation (and more generally carbon-carbon bond scission) is the dominant pathway over multiple generations of oxidation. The direct measurements of intermediates are described in Chapter 4. The key point of Chapter 4 is that oxidized intermediates are abundant and highly active in the local ambient photochemistry. The work in Chapter 4 additionally involved the deployment of a new instrument, much of the characterization of which is described for the first time within this work. Details of the instrument operation and data analysis procedures are provided in Appendix 4.5.





## Chapter 2

# Atmospheric Aging & Properties of Organic Aerosol

### 2.1 Introduction

The formation of secondary organic aerosol (SOA) in the atmosphere is characterized by the conversion of volatile compounds into oxidized products that have a low enough volatility to condense into liquid or semisolid particles according to absorptive partitioning theory.<sup>4,5</sup> This process is complex, and though some aerosol may be formed from the first oxidation step, multiple generations of oxidation reactions are expected to be required to fully convert partially oxidized intermediates to organic aerosol. The details of this chemistry are important because of the key role of aerosol in the lifecycle of atmospheric organic carbon, as well as the health and climate impacts of aerosol particles.<sup>15</sup> Organic aerosol is a relatively minor channel in the overall transformation of organic carbon, with a disproportionately large impact. Because only a small fraction of the emitted carbon is ever converted to particles, small changes to the gas-phase chemistry over multiple oxidation steps (a few percent) can lead to large relative changes in the amount of aerosol formed.

Simulating aerosol has been the focus of a significant body of research. In spite of this, photochemical models have had great difficulty in predicting the loading and properties (degree of oxidation) of organic aerosol, and historically have underpre-

dicted loading by up to a factor of ten.<sup>19-21</sup> More recently, the average loading has been modeled within a factor of two, but with little ability to predict time series, indicating that the detailed processes are still not understood.<sup>22</sup> The treatment of SOA in models is based on parameterized laboratory experiments in which artificial SOA is made in large reaction chambers. These experiments themselves have had limited success reproducing observations of ambient aerosol. Most laboratory SOA tends to have moderate yields ( $< 30\%$ ) even at high, non-atmospherically relevant loadings ( $> 100 \mu\text{g}/\text{m}^3$ ), and a low degree of oxidation ( $\text{O}/\text{C} < 0.4$ ). Under ambient conditions however, yields can be as high as 25% at much lower loadings,  $\text{O}/\text{C}$  values can be in excess of 0.7, and organic aerosol can be formed rapidly (less than 6 hours).<sup>9,21,24</sup> A key hypothesis for explaining this discrepancy (in experiments and in models), is the notion of atmospheric aging, in which continued oxidation of intermediates and vapors in equilibrium with condensed particles leads to increasing aerosol yield and degree of oxidation. This leads to aerosol yield and properties being a function of both loading and OH exposure (the product of OH concentration and time). A Simple theoretical treatment of aging was created by Robinson et al.,<sup>10</sup> and later modified by Grieshop et al.,<sup>30</sup> but these and subsequent approaches have been hampered by a lack of observational constraints on aging processes.<sup>23</sup> Laboratory studies typically reach OH exposures equivalent to only a few hours of ambient oxidation,<sup>25-28</sup> leaving open the possibility that aerosol yields and properties may be different under more aged conditions, and motivating experiments specifically designed to explore these conditions.

The details of gas-phase aging chemistry may also be much more complex than the simple Robinson-Grieshop model. SOA properties have previously been observed to be a function of loading, with more oxidized aerosol appearing at lower loadings.<sup>31</sup> This has been explained through absorptive partitioning theory, where lower volatility, more oxygenated products are required for condensation to occur at lower loadings. However, higher effective OH exposures are also expected at lower loadings due to the phenomenon of “trapping,” in which condensed materials undergo a much slower overall OH-mediated oxidation rate because heterogeneous oxidation is so much slower

than gas-phase oxidation.<sup>6-8</sup> This effect is shown quantitatively in figure 2-1, which shows OH exposure as a function of product saturation concentration for a synthetic experiment. The OH exposure is higher both for more volatile products (higher saturation concentration) within a single experiment, and higher for all products for experiments with lower aerosol concentrations. The magnitude of this effect can be quite large—for example, for a hypothetical product with a saturation concentration of  $0.1 \mu\text{g}/\text{m}^3$  at an absorptive organic aerosol loading of  $10 \mu\text{g}/\text{m}^3$ , the fraction partitioned to the gas phase is given by  $0.1/(0.1 + 10) \sim 0.01$ , resulting in gas-phase oxidation slowed by a factor of 100. Since a greater number oxidation steps are required to condense at lower loadings, organic material will spend more time in the gas-phase prior to condensation, and thereby have a greater average OH exposure. Other condensed phase chemistry (e.g. due to light absorption) can still occur, and has been observed for aerosol produced by  $\alpha$ -pinene ozonolysis,<sup>32,33</sup> but does not appear to be dominant in the present experiments (discussed further in Section 2.3 below). Other experiments have suggested that oxidized intermediates may be lost to the teflon walls of reaction chambers, leading to lowered yields<sup>34,35</sup> and possibly affecting aerosol properties. The lowest volatility, most oxidized vapors are thought to be most affected by wall losses, which may lead to systematically lower observations of aerosol O/C in chambers. Finally, low relative humidities (<30%, and often <5%) typically used in chambers may lead to extremely slow diffusion within particles, and greatly slowed gas-particle equilibrium timescales.<sup>35-42</sup> This can lead to “burial” of more volatile material within particles, and effectively prevent oxidation that would be expected by gas-particle partitioning theory. None of these effects, however, have been investigated in the context of aging processes, and their relative importance is therefore not clear.

The present work describes several sets of experiments designed to address these gaps in our knowledge of aging chemistry and the role of low volatility oxidation intermediates. The first set was conducted to assess how much additional aerosol mass may be formed and what effects on aerosol properties result from increased OH exposures. These experiments represent a baseline for how large the aging effect can

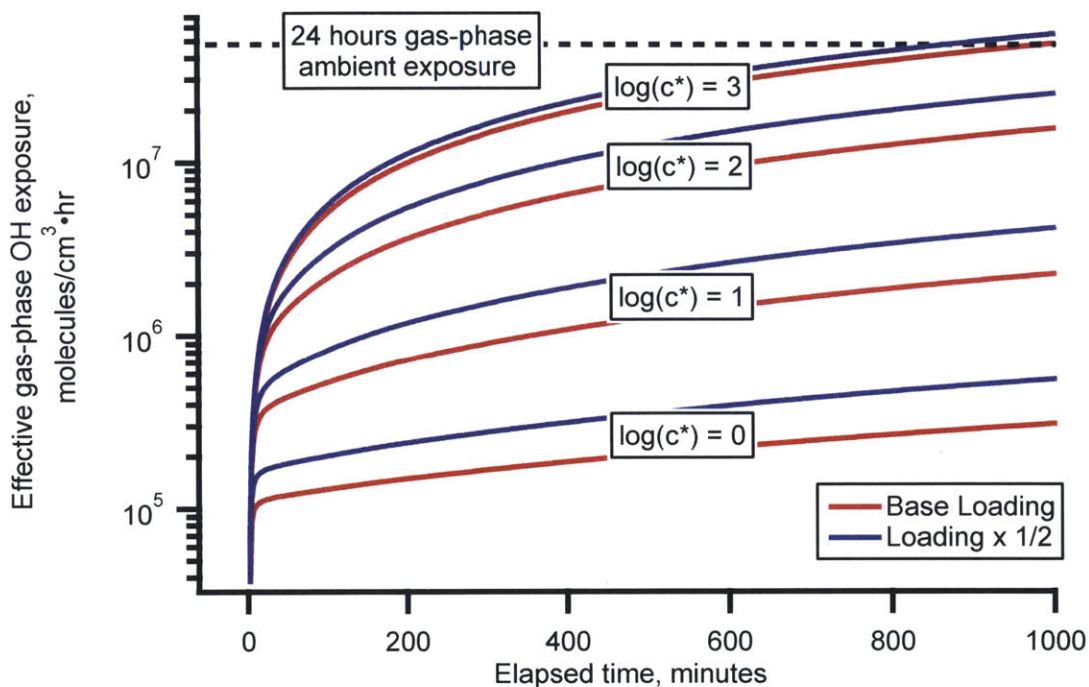


Figure 2-1: Effect of condensational trapping on OH exposure. The traces show OH exposure versus time for two synthetic experiments that rapidly forms  $300 \mu\text{g}/\text{m}^3$  of organic aerosol (red traces, base case), or half that amount (blue traces). Each trace shows OH exposure for products with a set saturation concentration assuming a constant OH concentration of  $3.8 \times 10^6$ . This OH concentration as well as the organic aerosol loading are similar to the experiment for  $\beta$ -caryophyllene shown in figure 2-3. Products with lower saturation concentrations (less volatile material) have systematically lower OH exposures because they have lower equilibrium gas-phase concentrations. Similarly, all compounds have higher OH exposures at lower organic aerosol loading because less absorbing material is present and gas-phase concentrations are therefore higher. The saturation concentration of the condensed products must be at least as low as the aerosol concentration for condensation to occur, suggesting that limited OH exposures due to trapping is significant for the experiments in this study.

be, and were conducted using a set of atmospherically relevant aerosol precursors to determine how variable the aging effect is as a function of structure. In order to conduct these experiments, an entirely new chamber-based aging technique had to be developed, since previous methodologies have only been able to achieve modest OH exposures.<sup>25–28</sup> This technique (described in more detail in the Experimental Methods below) is able to produce elevated, relatively constant OH concentrations through the constant addition of HONO, which photolyzes to produce OH and NO. A second set of experiments was conducted in order to disambiguate the effects of OH exposure and loading. This used the aging methods developed for the previous set of experiment, and varied the initial hydrocarbon concentration in order to achieve the same loading at different OH exposures. A final set of experiments was run in order to gauge the effects of slow particle-phase diffusion and loss of oxidized vapors against the magnitude of aging effects. The effect of vapor loss was assessed by varying the concentration of seed particles as described in Zhang et al. (2014)<sup>35</sup> while using the same aging methods as the previous experiments. The effect of diffusion was investigated by running aging experiments at high relative humidities that are known to result in higher particle-phase diffusivities.<sup>42</sup> These experiments were conducted primarily as a check that the qualitative aspects of aging chemistry were not dominated by diffusion and vapor-loss effects.

## 2.2 Experimental Methods

The compounds used for the experiments in this work include *n*-decane (C<sub>10</sub>H<sub>22</sub>, Sigma-Aldrich, ≥ 99%), cyclodecane (C<sub>10</sub>H<sub>20</sub>, Sigma-Aldrich, 95%), isoprene (C<sub>5</sub>H<sub>8</sub>, Sigma-Aldrich, 99%), (–)- $\alpha$ -pinene (C<sub>10</sub>H<sub>16</sub>, Sigma-Aldrich, 98%), (–)-*trans*-caryophyllene (C<sub>15</sub>H<sub>24</sub>, Sigma-Aldrich, ≥98.5%), and *m*-xylene (C<sub>8</sub>H<sub>10</sub>, Sigma-Aldrich, >99%). These molecules are all noted for their direct atmospheric relevance and use in numerous previous studies.<sup>24</sup> Decane and cyclodecane may not have large emissions to the ambient atmosphere but are representative of linear and cyclic alkanes that are emitted in large quantities.<sup>43,44</sup>

All experiments were conducted in a 7.5 m<sup>3</sup> environmental (“smog”) chamber constructed of 0.005 inch thick perfluoroalkoxy (PFA) Teflon film (Ingeniven). The chamber is housed in an environmental room that maintains a constant temperature of 15-40 °C. All experiments in this study were conducted at 20 °C and, and most had RH <10% (measured by a Vaisala HMP50 probe). Several experiments (with corresponding blank experiments) were conducted with an RH of ~80% in order to assess the effects of aging on deliquesced particles with much higher internal diffusion rates. High relative humidities were maintained by flowing make-up air through a bubbler containing milliQ water. The bubbler was heated to compensate for evaporative cooling, with temperature controlled by a PID. The chamber is flanked by two sets of 24 40-watt blacklights (Sylvania BL350 eco). The lamps have a standard 300-400 nm spectrum, centered at 350 nm. Full lamp intensity was used for all experiments, resulting in a J<sub>NO<sub>2</sub></sub> of ~0.12 min<sup>-1</sup>. The chamber is operated in a constant-volume (“semi-batch”) mode in which clean air (Aadco 737A/C) is continuously added to make up for instrument sample flow. The lack of chamber deflation allows for relatively long (~6-12 hours) experiments at a constant surface-to-volume ratio (and therefore an approximately constant wall loss rate). Pressure in the chamber, measured with a pressure transducer (Omega Engineering), is maintained at 20-30 mTorr above the ambient atmospheric pressure. When the excess pressure exceeds 30 mTorr, a valve is automatically opened to a vacuum pump until it drops to 20 mTorr, ensuring a constant volume. The continuous addition of 5 liters per minute (LPM) of clean air produces a constant dilution lifetime of 25 hours, in agreement with measured dilution lifetimes of 22.4 to 24.0 hours (determined from GC measurements, as described below). For high humidity experiments, 3 LPM of the inflow was humidified to maintain a constant RH. PFA film is noted for very low gas permeability, which limits the risk of contaminants diffusing into the chamber through the walls. Water vapor diffuses relatively rapidly through fluoropolymer film, and was therefore used to calculate an upper limit contamination from diffusion. Water vapor has a permeability coefficient of approximately 0.8 g•mm/m<sup>2</sup>/atm/day in PFA film. For a day with 50% relative humidity at a temperature of 20 °C, approximately 2-3 g/day of water are expected

to diffuse into the chamber, given the film thickness of 0.127 mm. This increases the internal RH of the chamber by approximately 2%. Molecules of greater concern (e.g. hydrocarbons) are expected to have vastly lower concentrations and diffusion rates than water vapor, and therefore diffusion is not expected to be a significant source of contamination.

Prior to each experiment, ammonium sulfate particles (serving as condensation nuclei), hexafluorobenzene (HFB, the dilution tracer), HONO (the oxidant precursor), and the precursor hydrocarbon were added to the chamber. Seed particles were atomized from a 2 g/L solution of reagent-grade ammonium sulfate (Aldrich), generating particles with a number-weighted average diameter of 200 nm. Most experiments had a mass concentration of 40 to 50  $\mu\text{g}/\text{m}^3$  (corresponding to a number concentration of 20,000 to 25,000  $\text{cm}^{-3}$ ). Some experiments used higher concentrations of 140 to 150  $\mu\text{g}/\text{m}^3$  to assess the effects of higher seed concentration on wall losses of oxidized vapors.<sup>34,35</sup> For most experiments the particles passed through a diffusion dryer and radioactive charge neutralizer to minimize electrostatic wall losses of particles. For high humidity experiments, particles bypassed the drier and neutralizer. This ensured that the particle population was uniformly deliquesced, as the chamber RH of  $\sim 80\%$  is well above the ammonium sulfate efflorescence RH.<sup>14</sup> Hydrocarbons (15 to 150 ppb, depending on the molecule) and HFB (60 ppb) were added through a silicone septum into a 4 LPM flow through a coated stainless steel line (Silcotek Sulfinert) heated to 50 °C in order to aid evaporation.

Two aging methods are used in the present experiments, both of which rely on photolysis of nitrous acid (HONO) as a source of OH radicals. HONO was generated in a bubbler containing 25 mL of 1 M sodium nitrite by adding 1 M sulfuric acid via a syringe pump (Chemyx Fusion 100). The HONO produced escapes to the 1 LPM air stream of the bubbler and is sent into the chamber. For both aging methods, an initial HONO concentration of  $\sim 50$  ppb was achieved in the chamber by adding 7.6  $\mu\text{L}$  of sulfuric acid 30 minutes prior to initiating photochemistry. For the first aging method (“continuous mode”), this is followed by adding  $\sim 2$  ppb per minute (0.33  $\mu\text{L}$  acid per minute) concurrently with the UV illumination in order

to to maintain a constant OH concentration. Estimates of OH concentrations and exposures were made from hydrocarbon concentrations and OH rate coefficients using methods similar to Barmet<sup>45</sup> (described below). These methods indicate that the average OH concentration remains high ( $7 \times 10^6$  to  $3 \times 10^7$  molecules/cm<sup>3</sup>, dependent on the total OH reactivity) for at least as long as the hydrocarbon remains measurable. This is typically the case for the first half of the experiment; the OH concentration is likely to remain approximately constant thereafter.<sup>31,45</sup> The second aging method (“discontinuous mode”) is identical to the first, except that the onset of steady HONO addition is delayed until the SOA production ceases. This typically takes a few hours, and results in reaction of most (75 to 100%) of the precursor hydrocarbon. OH exposures are limited by OH concentrations that rapidly decline as the initial pulse of HONO photolyzes. This portion of the experiment is identical to the methodology for typical experiments that use HONO as an OH source<sup>25-27</sup> that simulate near-source conditions on account of the relatively low OH exposures. Oxidant concentrations rapidly rise again after HONO addition starts, reacting any remaining hydrocarbon and explicitly demonstrating changes to aerosol yields and properties that may occur under more aged conditions.

This aging approach was further validated by performing an experiment in which two successive aliquots of cyclodecane were added, with the second aliquot added when the first had completely oxidized away, shown in figure 2-2. The concentration of OH can be estimated from the slope of the log of cyclodecane concentration, which is constant valued in both parts of the experiment, indicating that the OH concentration is also constant. The OH concentration does decrease to a lower constant value after the second aliquot is added as a result of the increased OH reactivity (the sink of OH is larger). This implies that the OH reactivity is a function of the initial amount of hydrocarbon added rather than the instantaneous concentration of hydrocarbon, and likely reflects the fact that OH continues to react with gas-phase intermediates in addition to the initial precursor.

Mass concentration and elemental composition of particles were measured using an Aerodyne high-resolution time-of-flight aerosol mass spectrometer (HR-ToF-



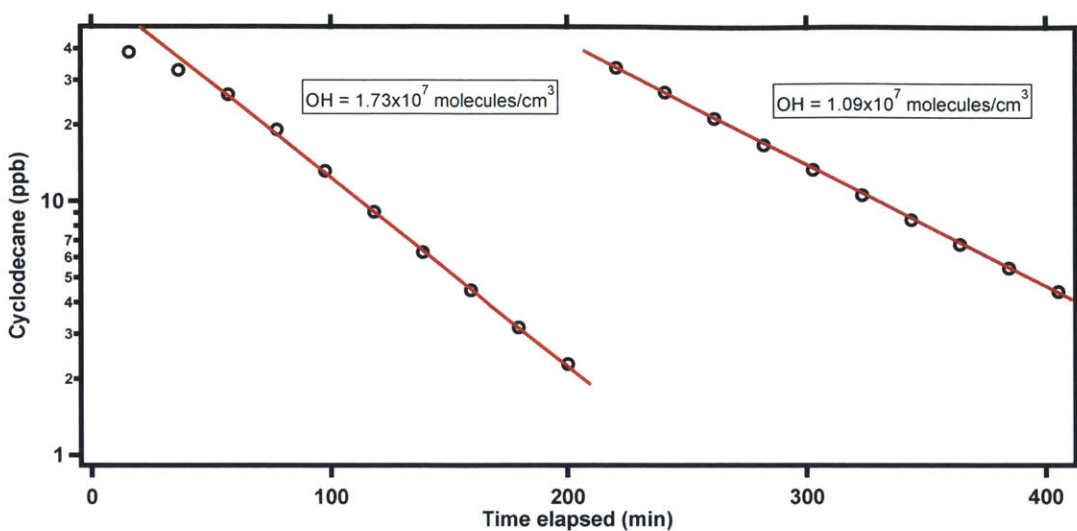


Figure 2-2: Validation of aging methodology. The experiment investigates OH concentration over long experimental timescales by adding a second aliquot of cyclodecane when the first has completely reacted away. The constant slope in both parts of the experiment implies a constant OH concentration. The OH concentration decreases to a new constant value when the second aliquot is added because OH reactivity increases, but is expected to remain constant otherwise.

AMS).<sup>46,47</sup>  $\text{NO}^+$  and  $\text{NO}_2^+$  (from organic nitrates) were not added to the AMS organic mass or O/C measurements in order to maintain comparability of yield data to previous work. Particle number and volume were measured using a scanning mobility particle sizer (SMPS, TSI, Inc.). Concentrations of hydrocarbon precursors and dilution tracers were measured with gas chromatography-flame ionization detection (SRI). Other measurements include ozone by UV absorption (2B Tech) and  $\text{NO}/\text{NO}_x$  by chemiluminescence (Horiba Inc.).

The correction of particle mass concentration for wall loss and dilution follows the methods of Hildebrandt et al (2009).<sup>48</sup> Loadings are corrected primarily using the organic-to-sulfate method (“AMS case 2”) and in some cases (and in extensively in Chapter 3) using the decay-rate method (“SMPS case 1”). The organic-to-sulfate method involves multiplying the time-dependent organic-to-sulfate ratio measured by the AMS by the initial sulfate mass concentration (measured by the SMPS) to produce a corrected organic mass concentration. This accounts for loss of particles to the walls, loss of vapors via equilibration with such particles (with no mass-transfer

limitation), and dilution of the chamber, but not for loss of vapors to the walls themselves. As discussed in section below (2.3.3), loss of vapors to the walls does not appear to be a dominant process for the present experiments, and thus this approach provides an upper limit for calculating organic mass.<sup>48</sup> The decay-rate method involves correcting aerosol mass using the particle mass loss rate (which includes wall losses and dilution), determined from 30-60 minutes of SMPS data once dilution flow is stable (after the addition of all reagents). This rate is used to separate the sulfate and organic contributions to the SMPS volume using the density of ammonium sulfate (1.77 g/cm<sup>3</sup>) and an assumed SOA density of 1.4 g/cm<sup>3</sup>. The corrected organic mass concentration is found by integrating the product of the particle loss rate with the suspended concentration and adding this loss term to the suspended concentration. This method assumes no partitioning of suspended vapors to the walls, and is a lower limit for estimating organic mass.<sup>48</sup> For high RH experiments (in which particles also contain significant water mass), the initial sulfate concentrations are calculated using the known volume fraction of ammonium sulfate as a function of relative humidity.<sup>14</sup> SMPS case 1 yields are not calculated for any high RH experiments due to uncertain effects on the overall particle density.

SOA yields (Y) were calculated via Equation 2.1,

$$Y = \frac{\Delta c_{\text{OA}}}{\Delta \text{HC}} \quad (2.1)$$

in which  $\Delta c_{\text{OA}}$  is the wall-loss and dilution-corrected change in total organic aerosol concentration and  $\Delta \text{HC}$  is the mass concentration of hydrocarbon lost to reaction with OH. Hydrocarbon concentrations were obtained by fitting GC-FID measurements (25 minute resolution) with an exponential decay and interpolating onto the timebase of the AMS (2 minutes). The amount of hydrocarbon lost to OH reaction is determined from Equation 2.2,

$$\Delta \text{HC} = \Delta \text{HC}_T \times \frac{k_r}{k_r + k_d} = \Delta \text{HC}_T \times \frac{k_t - k_d}{k_t} \quad (2.2)$$

where  $\Delta \text{HC}_T$  is the decrease in hydrocarbon,  $k_d$  is the dilution rate,  $k_r$  is the OH

reaction loss rate, and  $k_t$  is the total loss rate.

The chamber was cleaned between experiments by flushing with 35 LPM clean air at 40 °C overnight. Blank experiments were run at regular intervals to check for background aerosol. The blank experiments used an identical methodology except that the hydrocarbon precursor was omitted. These experiments generally produced less than 1  $\mu\text{g}/\text{m}^3$  of SOA, suggesting a negligible background effect on aerosol yields and properties. High RH experiments had a higher background of about 7  $\mu\text{g}/\text{m}^3$  of highly oxidized aerosol, necessitating subtraction. The subtraction was performed by interpolating the time series of wall loss corrected background aerosol onto that of a given experiment. Mass was subtracted element wise (carbon, hydrogen and oxygen) so that corrected O/C and H/C ratios could be calculated. For experiments other than high RH experiments, this had only a small effect. To investigate the possible effect of chamber history on SOA composition and yield, a back-to-back repeat experiment was conducted using cyclodecane. The yield increased by a factor of 1.075 and O/C decreased by a factor of 1.074 for the second experiment relative to the first. These magnitudes are on the order of typical experimental variability ( $\sim 10\%$ ), suggesting that carryover does not play a major role in the results.

The continual addition of HONO leads to  $\text{NO}_x$  concentrations that start low but increase roughly linearly in the chamber over time, producing NO and  $\text{NO}_x$  levels of up to 240 ppb and 475 ppb respectively. The effect of such high levels of  $\text{NO}_x$  on the SOA chemistry was assessed by performing experiments with 500 ppb of added NO. This had no measurable effect on the aerosol O/C and increased the maximum yield by a factor of 1.087 for cyclodecane; these effects are again within typical experimental variability, suggesting the  $\text{NO}_x$  addition did not have a major effect on results, and that the  $\text{RO}_2$  chemistry is dominated by reaction with NO when using these oxidation methods.

Several differences exist between the conditions in this smog chamber method and the ambient atmosphere. The first is that the OH concentrations are often elevated above ambient OH concentration by approximately an order of magnitude. This accelerates gas-phase and heterogeneous oxidation, but does not affect other important

timescales, most notably the gas-particle partitioning timescale. This can potentially lead to enhanced gas-phase oxidation relative to ambient conditions. Photolysis may also be affected by differences in light sources between the chamber and the atmosphere. The ambient atmosphere has a small but important photon flux below 300 nm that leads to the production of OH from ozone photolysis, and may enhance condensed-phase photolysis relative to the 350 nm centered UV lamps used for chamber experiments. The ambient atmosphere also has a variety of chemical regimes with respect to the production and consumption of ozone and OH radicals, as well as the concentration and influence of NO radicals. The experiments described here are most consistent with polluted conditions characteristic of urban outflow.

## 2.3 Results & Discussion

### 2.3.1 Aging Effects

The effects of aging chemistry are shown in Figure 2-3, which shows upper limit (organic-to-sulfate corrected)  $c_{OA}$ ,  $\Delta HC$ , O/C and aerosol yield for the study molecules. Each of the traces shown is from a discontinuous aging experiment, as described in the methods (Section 2.2) above. This technique involves oxidizing hydrocarbons with a 50 ppb initial pulse of HONO, which oxidizes most or all of the hydrocarbon precursor (Figure 2-3, Panel B), and producing a rapid increase in aerosol concentrations that levels off as HONO and oxidant concentrations fall to negligible levels. Particle diameter increases by as much as 50 nm due to the condensation of organic aerosol onto seed particles, indicating absorption into a thick organic layer rather than adsorption onto the seed surface. Cessation of new aerosol formation is indicated by the first point in Panel A of Figure 2-3 where organic-sulfate corrected concentrations level off. This is the point at which most typical experiments stop the oxidation, leading to maximum OH exposures that are determined by the relative quantities of HONO and the hydrocarbon precursor.<sup>25-27</sup> After the initial oxidation stage is complete, continual addition of HONO is initiated, leading to increased oxidation and enabling an

estimate of the magnitude of the aging effect. From panel A, it is apparent that this increased oxidation leads to some additional aerosol for all of the study molecules (the “bump” in  $c_{\text{OA}}$  in each trace) and that this quantity depends to a large extent on molecular identity. From panel B, it is evident that the second oxidation period is associated with a small or zero increase in  $\Delta\text{HC}$ , such that the change in  $c_{\text{OA}}$  must be ascribed to aging chemistry rather than direct formation from the reaction of the precursor. It is also evident that all of the molecules reach a point where organic aerosol formation ceases (the second leveling off point). Comparison with this second point allows the overall effect of aging to be quantitatively determined. Upper limit carbon yields (shown in Table 2.1) are below 100% for all the molecules except  $\beta$ -caryophyllene, indicating that OH aging chemistry does not result in yields that always increase to the strict upper limit of a 100% carbon yield. Lower limit yields are approximately a factor of 2 smaller, dominating the overall measurement uncertainty,<sup>48</sup> and explaining carbon yields above 100%. The lower limit carbon yield for aged  $\beta$ -caryophyllene for example is only 37%. The effects of aging on  $c_{\text{OA}}$  and yield are summarized in Table 2.1, which shows that the magnitude of the yield enhancement (the ratio of the aged maximum upper limit yield to the initial “freshly oxidized” upper limit yield) ranges from 1.06 for  $\beta$ -caryophyllene to 2.3 for isoprene.

Compositional changes to the organic particle phase during aging chemistry can be elucidated from the O/C data shown in Panel C of Figure 2-3 and Table 2.1. In general, O/C does increase with increased OH exposure, but the changes are very small. Only decane has a aging-induced change to O/C greater than 0.06. It appears, therefore, that OH aging under these conditions is apparently not capable of generating the highly oxidized aerosol found in the ambient atmosphere, even at exposures equivalent to greater than a full day of ambient oxidation. The significant changes to yield that occur are instead likely the result of gas-phase aging chemistry, which generates products that condense and mostly stop oxidizing once they have a low enough vapor pressure (at the trapping point). This occurs at roughly the same level of molecular oxidation (and volatility) for the whole experiment. In other words, aging appears to simply generate more aerosol that is very similar in composition to

the aerosol from the initial oxidation. Loading dependent effects on composition (more volatile, less oxidized material condenses at higher  $c_{OA}$ ) are still expected to occur, and are discussed separately in section 2.3.2. Further evidence for uniform composition before and after aging chemistry comes from the yield curves in Panel D of Figure 2-3. These yield curves appear to be smooth and change uniformly, without jumps or discontinuities that might be expected with significant changes to composition. The aging effect thus described is consistent with a multi-generation oxidation process creating a delay between complete oxidation of the hydrocarbon precursor and complete formation of aerosol. Oxidation of the hydrocarbon precursor leads to oxidized intermediates, and oxidation of these intermediates leads to yields of condensable products, and ultimately, aerosol formation. In typical experiments at lower OH exposures, only a fraction of these intermediates oxidize ( $\leq \Delta H C$ ), leading to aerosol yields that are smaller than their full potential. The relative kinetics of precursor and intermediate oxidation determine the overall aging effect of a given molecule with respect to yield—the faster the intermediate oxidizes relative to the precursor, the less additional aerosol formation will take place after the precursor has been completely oxidized. This suggests the differences in the aging effect reflect a difference in the oxidation rates of oxidized intermediates, and suggests that aerosol formation kinetics may be useful in informing estimates for these reaction rates as they relate to complex mixtures present in these experiments.<sup>49,50</sup>

The small changes to O/C suggest that a small amount of particle oxidation does occur, the slow speed of which is consistent with slowed oxidation due to trapping.<sup>49</sup> This continued oxidation could also come from a small amount of heterogenous oxidation and possibly also from direct photooxidation of the condensed phase. From Figure 2-3 Panel A, it is also apparent that different molecules undergo slightly different particle phase aging chemistry, and that there can also be differences in the evolution of the particle phase before and after the OH aging phase of the oxidation. Cyclodecane and *m*-xylene are both characterized by very flat particle concentrations in both phases, suggesting that no further particle formation is occurring (or alternatively that formation and loss are balanced). In contrast, decane,  $\alpha$ -pinene,

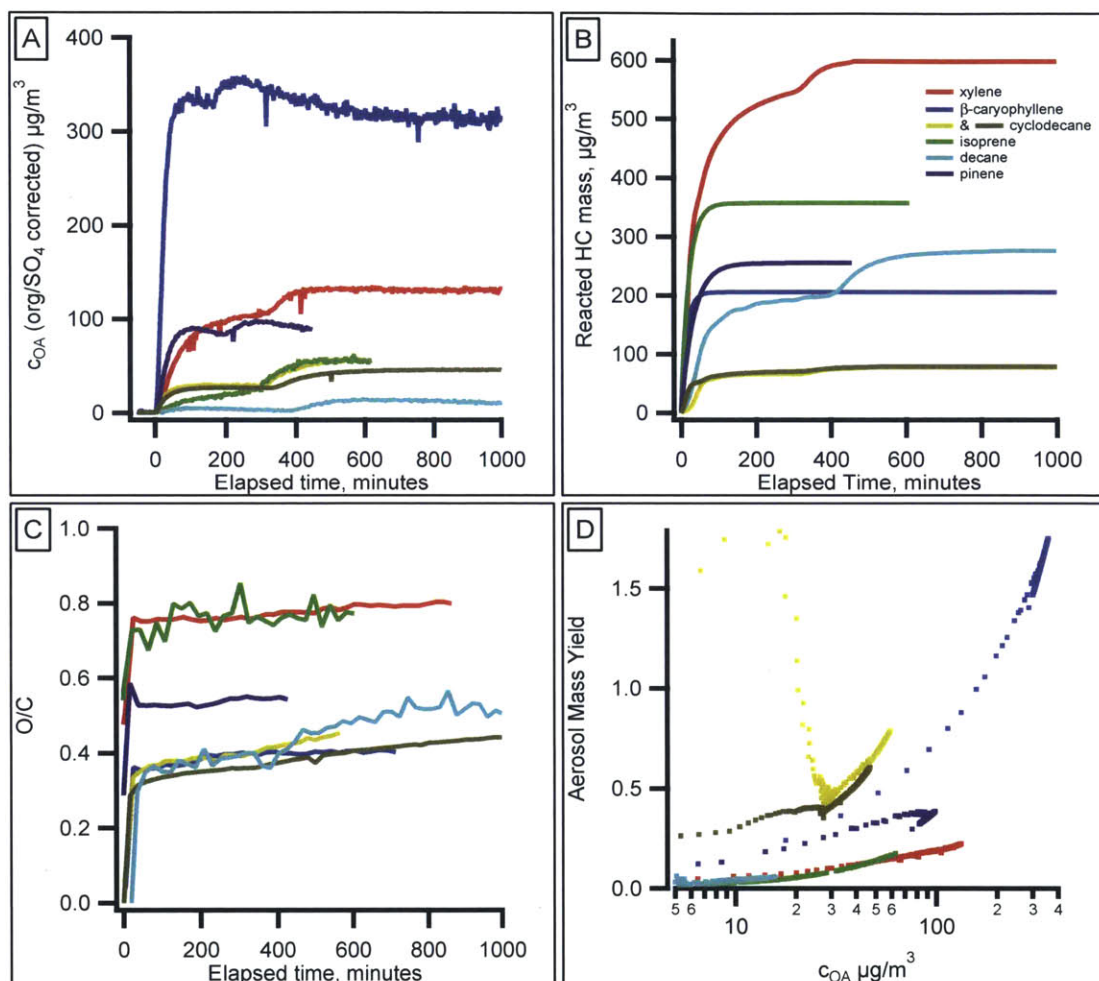


Figure 2-3: Effect of increased OH exposure on selected molecules during discontinuous aging experiments. Time series of  $c_{\text{OA}}$  (Panel A) show two distinct periods of aerosol formation: the first increase in response to the initial pulse of OH at early time, and the second increase in response to the initiation of OH aging later in the experiment. Panel B shows the associated total  $\Delta\text{HC}$  for these experiments, and demonstrates that the increase in  $c_{\text{OA}}$  upon OH aging is not simply due to oxidation of additional precursor. Panel C shows 20 minute averaged O/C for the experiments, which indicate that OH aging is generally not associated with large increases in O/C or changes in composition. Instead, aging appears to affect the total yield of products with a composition determined mainly by the trapping point.<sup>49</sup> Panel D shows yield versus  $c_{\text{OA}}$  for the experiments, which generally do not change significantly with aging, thereby supporting the lack of significant changes to composition.

and  $\beta$ -caryophyllene have a total particle concentration that actually decreases after reaching a peak in both phases of the oxidation. This decrease eventually levels off for  $\beta$ -caryophyllene, suggesting that an equilibrium has been achieved. Interestingly, the rate of decrease for  $\alpha$ -pinene appears to be similar before and after the initiation of OH aging (beginning of the second oxidation phase). Because OH concentrations are very different before and after this point, it is likely that this change in particle concentration is related to a non-OH aging mechanism, such as photolysis.<sup>32,33,51</sup> By contrast, isoprene has a particle concentration that rises slowly and uniformly even at the end of the initial oxidation phase when OH concentrations should be relatively low. This may be explained by particle-phase oligomer formation, another non-OH aging process that has been invoked previously in the literature.<sup>26</sup>

Direct comparisons to literature values for aerosol yield and properties are possible in principle for the initial oxidation stage, which has a methodology that is qualitatively identical to many experiments described in the literature. However, differences in relative quantity of HONO and hydrocarbon can lead to initial-stage OH exposures that are different for the present experiments and those in the literature even with an otherwise identical methodology. Comparison is also complicated by the fact that OH exposures are generally estimated crudely (e.g. by assuming values for unmeasured OH concentrations) or not at all in most experiments described in the literature. Despite this, the initial yields and properties from this work are not extremely dissimilar to those in the literature. For example, decane from Presto et al.<sup>52</sup> has a measured upper limit yield of 1.5% at an aerosol concentration of 7  $\mu\text{g}/\text{m}^3$  and OH exposure of approximately  $1.2 \times 10^7$  molecules/ $\text{cm}^3$ , as compared to an upper limit yield of 3.1% at an aerosol concentration of 5.4  $\mu\text{g}/\text{m}^3$  and an OH exposure of  $2.4 \times 10^7$  molecules/ $\text{cm}^3$  in the present work. A detailed comparison of yields would need to account explicitly for differences due to both organic aerosol concentration and the effects of OH exposure. This is possible for cyclodecane for which experiments were specifically performed to disambiguate these effects, and is discussed in the next section. For this reason however, an exhaustive comparison to literature yields for the other compounds in this study is not provided.



The key effect of aging chemistry discussed thus far is that significant additional aerosol mass may be generated with increased OH exposures, but that little additional change to O/C occurs. This effect appears to be caused by intermediates continuing to oxidize after the initial hydrocarbon has been consumed, leading to a delay in the peak aerosol yields. Aerosol properties are not highly affected, because the degree of oxidation is mainly set by the total aerosol concentration through the phenomenon of trapping, such that the intermediates condense as they achieve composition similar to that of the particle phase. These results also confirm the expectation that particle-phase aging mechanisms such as heterogenous oxidation, direct photooxidation and photolysis are slow under the experimental conditions, and lead only to modest increases in aerosol O/C and changes to aerosol yield. If photolysis were important, for example, significant decreases in wall loss corrected particle mass should be observed. These results are consistent with recent theoretical treatments, which suggest that gas-phase chemistry should be unable to create highly aged aerosol without exotic chemical pathways or extremely low aerosol concentration.<sup>53</sup> Explicitly accounting for the changes to O/C resulting from the condensational trapping effect requires additional experiments in which the concentration and OH concentration are varied independently. These experiments have been performed for cyclodecane and are discussed in the next section.

### 2.3.2 OH Exposure Isoleths

It is expected that changes in  $c_{\text{OA}}$  lead to changes to yield and composition due to the combined effects of absorptive partitioning (more volatile, less oxidized material will condense at higher  $c_{\text{OA}}$ ) and trapping (material that condenses undergoes much slower oxidation). Disambiguating these effects from OH aging effects is challenging, because OH exposure and  $c_{\text{OA}}$  covary within any single experiment, such that multiple experiments are required for this analysis. Figure 2-4 shows a series of continuous aging experiments for cyclodecane that start from a variety of concentrations so that they reach the same OH exposures at different organic aerosol concentrations. Panel A of Figure 2-4 shows clearly that increased yields versus  $c_{\text{OA}}$  are associated with

Table 2.1: Magnitude of aging effects for atmospherically relevant compounds

Compound	$c_{\text{OA}}$ $\mu\text{g}/\text{m}^3$	$\Delta\text{HC}$ $\mu\text{g}/\text{m}^3$	O/C	OH exp. $\text{molec.}/\text{cm}^3\cdot\text{hr}$	Aging Eff. (Yield) Upper / Lower <sup>a</sup>	Aging Eff. (O/C) <sup>b</sup>	Carbon Yield Upper / Lower <sup>c</sup>
Decane (i)	4.6	197	0.35	$1.4\times 10^7$			0.01 / 0.015
Decane (f)	13	275	0.48	$6.8\times 10^7$	2.02 / 1.04	0.13	0.03 / 0.016
Cyclodec. (i)	27	70	0.35	$2.2\times 10^7$			0.28 / 0.13
Cyclodec. (f)	46	79	0.40	$1.2\times 10^8$	1.51 / 1.3	0.05	0.41 / 0.17
Cyclodec. (i)	32	66	0.39	$2.9\times 10^7$			0.35 / 0.13
Cyclodec. (f)	57	77	0.45	$1.0\times 10^8$	1.53 / 1.3	0.06	0.51 / 0.17
Isoprene (i)	23	356	0.76	$3.3\times 10^7$			0.03 / 0.027
Isoprene (f)	54	356	0.77	$5.7\times 10^7$	2.3 / 1.9	0.01	0.08 / 0.052
$\alpha$ -Pinene (i)	90	253	0.53	$2.2\times 10^7$			0.22 / 0.082
$\alpha$ -Pinene (f)	98	255	0.55	$4.4\times 10^7$	1.07 / 0.76	0.02	0.24 / 0.062
$\beta$ -Cary. (i)	336	205	0.37	$6.0\times 10^6$			1.14 / 0.36
$\beta$ -Cary. (f)	355	205	0.40	$1.5\times 10^7$	1.06 / 1.07	0.03	1.18 / 0.37
<i>m</i> -Xylene (i)	106	547	0.76	$2.5\times 10^7$			0.10 / 0.047
<i>m</i> -Xylene (f)	132	599	0.79	$7.1\times 10^7$	1.14 / 1.12	0.03	0.12 / 0.051

Data shown are from discontinuous aging experiments designed to measure the effect of additional aging for a set of atmospherically relevant compounds. Initial values (i) are from the time points corresponding to the maximum upper limit (organic-to-sulfate) corrected particle mass concentration from the first HONO pulse. Final values (f) are from the time points corresponding to the maximum upper limit corrected particle mass concentration after continuous HONO addition has been initiated. <sup>a</sup>Calculated as the ratio of the initial and final upper and lower limit yields. The enhancement is expected to be a function of  $c_{\text{OA}}$  and of the initial degree of oxidation. <sup>b</sup>Calculated as the difference in initial and final O/C. <sup>c</sup>Calculated using elemental composition data. Carbon yields above 100% indicate the upper limit organic-to-sulfate correction is an overestimate.

increased OH exposures. Contour lines are drawn to guide the eye, but are not strictly quantitative. In general, at any given OH exposure, yields are relatively flat at lower  $c_{\text{OA}}$ , and rise steadily starting around a  $c_{\text{OA}}$  of  $50 \mu\text{g}/\text{m}^3$ . Panel B of figure 2-4 shows the O/C versus  $c_{\text{OA}}$  for the same set of experiments. OH isopleths are not included in this Panel because the measurements essentially fall onto a single curve (although there is some scatter at low  $c_{\text{OA}}$ ), with an O/C of approximately 0.55 at low  $c_{\text{OA}}$ , and an O/C of 0.3 at higher  $c_{\text{OA}}$ . The transition point for O/C appears to be the same as for yield, occurring at a  $c_{\text{OA}}$  of about  $50 \mu\text{g}/\text{m}^3$ . Evidence for aging-induced changes to O/C can be found in Panel B (e.g. the increase in the red points around a  $c_{\text{OA}}$  of  $100 \mu\text{g}/\text{m}^3$ ), but these increases are small compared to changes with larger changes due to changing  $c_{\text{OA}}$ .

The relationship of O/C and  $c_{\text{OA}}$  suggests that two product populations are generated—one with an average O/C of about 0.55 and a very low vapor pressure (such that yield is a weak function of  $c_{\text{OA}}$  at low  $c_{\text{OA}}$ ), and one with an O/C of about 0.3 and a  $c^*$  (saturation concentration) of approximately  $50 \mu\text{g}/\text{m}^3$ . The yield of the first product can be evidently quite high at low enough  $c_{\text{OA}}$ . This yield is likely a function of the relative amount of fragmentation and functionalization that occurs, which is expected to be a strong function of structure, discussed in detail in chapter 3. At higher  $c_{\text{OA}}$ , the less oxidized products are apparently trapped before the more oxidized products form, resulting in lower O/C. A key effect of trapping, therefore, is to reduce the yield of less volatile, more oxidized, later generations of oxidation. At even higher  $c_{\text{OA}}$  it is expected that the yield contours will level off due to reaching a 100% carbon yield. They may even decrease, since at high enough  $c_{\text{OA}}$  an even lower O/C may be required for condensation, resulting in a lower oxygen mass for the same amount of carbon mass. This will occur far above atmospherically relevant loadings for cyclodecane, but may be relevant to the oxidation of compounds that start with a much lower volatility.

As discussed in the previous section, disambiguating the effects of loading and OH exposure enable a much more careful comparison of aerosol yield to literature values to be made. Tkacik et al. reports an upper limit yield of 0.25 for cyclodecane at a

concentration of  $15 \mu\text{g}/\text{m}^3$  and an OH exposure of  $6.0 \times 10^6$  molecules/ $\text{cm}^3$ , calculated in a similar manner to the OH exposures in this work. From Figure 2-4, this OH exposure and concentration corresponds to an upper limit yield of approximately 0.35 in the present experiments. This is well within the experimental variability evident in Figure 2-4, which is approximately one contour line of OH exposure. This comparison is especially good considering that the low concentration, low OH exposure portion of the isopleth plot is the least well constrained, and generally gives confidence that this method works well for reconciling differences in yield across multiple experiments.

The findings for the relationship between OH aging and  $c_{\text{OA}}$  are consistent with the general aging narrative from Section 2.3.1 above, and underline the importance of considering the trapping effect in the evolution of organic carbon and production of aerosol. In order to properly represent the time series and properties of atmospheric organic aerosol, it is not sufficient to consider oxidation of the hydrocarbon precursor with fixed yields at fixed volatilities. Instead, air quality models must include oxidation as a multigenerational process, in which evolving  $c_{\text{OA}}$  is a key feedback controlling the evolution of aerosol properties and partitioning. The results also suggest that even higher O/C values may be associated with lower concentrations, such that even moderate concentrations in experiments may be a significant barrier to reproducing the high O/C values found for ambient aerosol. Significant dilution (present in ambient conditions but not in chambers) also has the capacity to decrease the condensational trapping volatility as a pollution plume ages, thereby leading to higher O/C values as vapors evaporate and undergo gas-phase oxidation.

### 2.3.3 Seed Particle & Humidity Effects

The previous two sections provide an explanation for the apparent effects of OH aging on yields and properties. One key result is that the oxidation of the initial precursor yields oxidized intermediates which may react more slowly. This creates the risk that chamber wall losses of these low volatility vapors can reduce yields.<sup>34</sup> This effect has been used to explain yields that increase with increasing seed particle concentration by other researchers.<sup>35</sup> Based on the results from the discontinuous aging experiments in

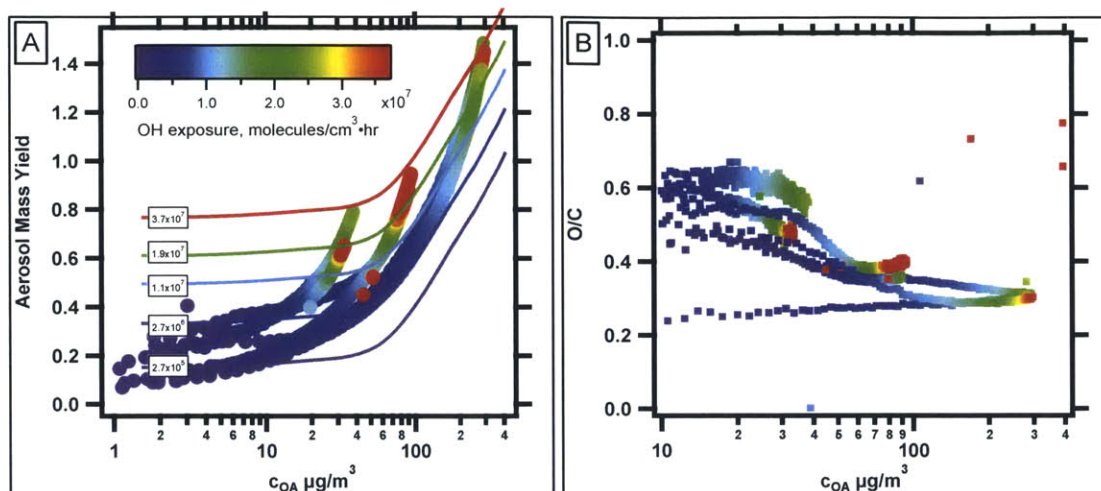


Figure 2-4: OH exposure isopleths for cyclodecane yield and O/C versus  $c_{\text{OA}}$ . Panel A shows yield versus  $c_{\text{OA}}$  for series of continuous aging experiments for cyclodecane. The yields are colored by OH exposure, showing a clear trend for increased yields under more aged conditions. Approximate contours of constant OH exposure are drawn to guide the eye. Panel B shows O/C versus  $c_{\text{OA}}$  for the same experiments. O/C depends mainly on  $c_{\text{OA}}$  rather than OH exposure, with a changing composition resulting from trapping at a lower volatility and higher O/C occurring at lower  $c_{\text{OA}}$ .

Figure 2-3 and Table 2.1, this is not expected to be a dominant effect simply because all the compounds generate significant additional aerosol upon aging even after the oxidized vapors have spent several hours in the environmental chamber. Figure 2-5 shows a series of discontinuous cyclodecane oxidation experiments conducted at two different seed particle concentrations in order to specifically look for this effect in the present experiments. Cyclodecane has a relatively large aging effect (Table 2.1), suggesting that the oxidized intermediates may react relatively slowly, and may be subject to enhanced wall losses if they are important. Panel A of Figure 2-5 shows  $c_{\text{OA}}$  versus time for these experiments, while Panel B shows yield versus  $c_{\text{OA}}$ . Taken as a pair, the experiments with higher ( $\sim 140 \mu\text{g}/\text{m}^3$ ) seed particle concentrations do have higher yields than do the experiments with lower ( $\sim 40 \mu\text{g}/\text{m}^3$ ) seed particle concentration. However, the variability between identical experiments appears to be larger than this effect (the magnitude of the variability in Figure 2-5 is typical). For example, the experiments with seed concentrations of 44 and 139  $\mu\text{g}/\text{m}^3$  (yellow and green traces) have virtually identical maximum yields and yields vs  $c_{\text{OA}}$ . O/C (not

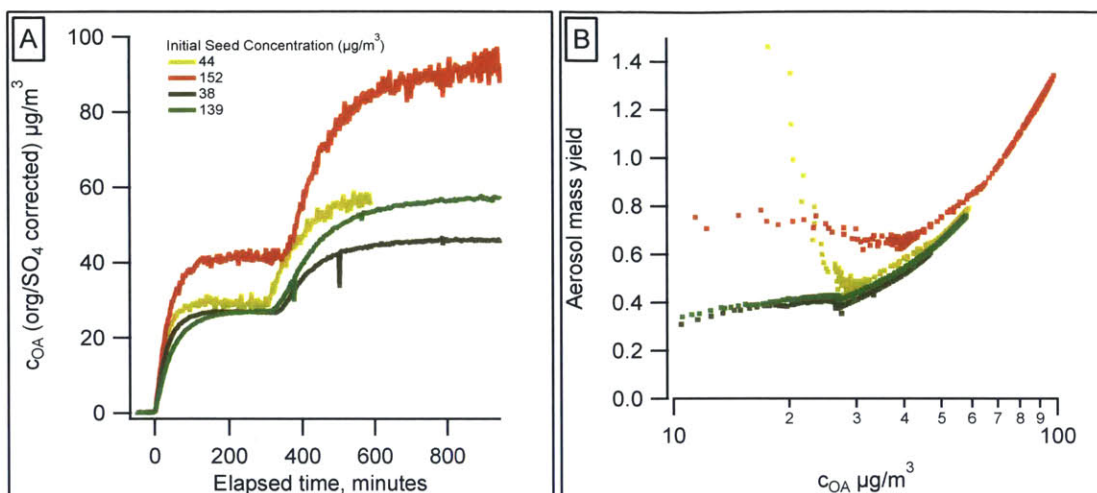


Figure 2-5: Effect of seed particles on cyclodecane aging. Two pairs of identical discontinuous aging experiments (with initial seed concentrations of  $\sim 140 \mu\text{g}/\text{m}^3$  and  $\sim 40 \mu\text{g}/\text{m}^3$ ) were conducted in order to check for effects on yields that have been observed in other SOA forming systems.<sup>35</sup>  $c_{\text{OA}}$  versus time is shown in Panel A and yield versus  $c_{\text{OA}}$  is shown in Panel B. The two pairs of experiments do not have significantly different results, suggesting that the effect of seed concentration is not large compared to the ordinary variability in experiments, and that wall loss of oxidized vapors does not play a dominant role in the present experiments.

pictured) is also similar for the experiments, suggesting a similar composition that is independent of seed concentration. So, it appears that a kinetic effect due to wall loss of vapors is not significant in the present experiments. It is also worth noting that the trapping effect should reduce the flux of vapors to the walls for the same reason that it reduces gas-phase oxidation rates, namely reduced gas-phase concentrations, so that the magnitude of a wall loss effect should be most pronounced at the earliest phases of the oxidation.

Another key feature of aging is the importance of the trapping effect in determining the extent of aging, yield and properties by slowing gas-phase oxidation of material that partitions to the condensed phase. This effect can be enhanced if particles have slow enough diffusion rates that gas-particle equilibrium times are significantly lengthened. Evidence for slow diffusion rates at the low relative humidities typical of chamber experiments is abundant, as is evidence that these particle diffusivities are much higher at high RH.<sup>35-42</sup> Because the trapping effect is key in preventing

significant oxidation of the particle phase, understanding the contribution of slowed particle-phase diffusion to this effect in the present experiments is important. A series of continuous oxidation experiments of  $\alpha$ -pinene was conducted at high ( $\sim 80\%$ ) and low ( $<10\%$ ) RH in order to assess these effects. For  $\alpha$ -pinene ozonolysis, the work of Renbaum-Wolff et al.,<sup>42</sup> suggests that these relative humidities should result in particles with diffusivities that are fairly high at high RH and extremely low at low RH. If particle-phase diffusion has a significant effect therefore, high and low RH experiments should reveal differences due to this effect. The results of these experiments are shown in Figure 2-6. Both experiments use ammonium sulfate seed particles, with these particles being deliquesced in the high RH case.<sup>14</sup> Panel C shows wall loss corrected  $c_{\text{OA}}$  versus time, which exhibits unusual and very interesting behavior—a very rapid rise in aerosol concentration is observed for the high humidity experiments relative to the dry experiment, followed by a precipitous drop in aerosol concentration back down to approximately the same level as the dry experiment. This indicates that a significant amount of additional aerosol is being formed and then lost through oxidation chemistry. This unusual time series has an equally unusual yield curve, shown in Panel A of Figure 2-6, in which the initial points begin at high yield and then decrease, curving back underneath the earlier part of the trace (red and blue traces). The end points lie within the yield curve for the dry trace, suggesting the end products are fairly similar to those in the dry trace.

Additional compositional information can be deduced from the O/C, which is slightly elevated for the high RH cases. O/C does not change significantly over the large changes in yield, suggesting that the composition of the reactive part of the SOA (spike) and more stable part of the SOA (tail) have a similar degree of oxidation. Taken together, the yield and O/C data suggest that the effects may not be due to coincidental changes in particle-diffusion rates, but rather due to changes in partitioning and chemistry that result from the presence of an aerosol aqueous phase. When aerosol water is present, small, oxygenated compounds with large Henry's law constants and relatively large vapor pressures can partition to the condensed phase. An example of this type of molecule is glyceraldehyde, which has a Henry's law con-



stant of  $2 \times 10^{10}$ , and a log saturation concentration of  $1.4 \times 10^5 \mu\text{g}/\text{m}^3$ . In the absence of aerosol water, this compound will not undergo significant absorptive partitioning to the organic condensed phase below a loading of  $1000 \mu\text{g}/\text{m}^3$ . With an aerosol water content of  $10 \mu\text{g}/\text{m}^3$  however, this compound will be found entirely in the condensed phase.<sup>12</sup> Glyceraldehyde is not necessarily generated in these experiments, but other molecules with similar properties are likely to be generated. Aging chemistry using HONO photolysis at high RH has never previously been investigated, but chamber based aging using other sources of OH at high RH have shown significant differences from the features of gas-phase aging previously described, including rapid oxidation and significant photolysis fragmentation and volatilization of the resulting aerosol.<sup>12,32</sup> This may occur as a result of the formation of singlet oxygen and other reactive oxygen species, which has been observed for cloud droplets and may also be relevant to aqueous aerosol where water content is much smaller.<sup>54</sup> Regardless of the source and fate of the organic material in the initial pulse, the high RH aging eventually generates aerosol that appears to be similar to that of the dry experiment. Even under the high RH, high diffusivity conditions present in these experiments, the particle phase still does not undergo significant enhancement of the O/C. Diffusivity, therefore, does not appear to be the factor preventing OH aging from reproducing the high O/C found in ambient aerosol. Under ambient conditions and in the presence of metal ions, aqueous chemistry may have significantly different outcomes,<sup>12</sup> but these do not appear to result simply from diffusion effects.

The picture of OH aging that emerges from these studies is of a multigenerational oxidation process in which the reaction of oxidized intermediates plays a key role in determining the yield and properties of aerosol, and in which the trapping effect provides a key feedback. These effects appear to be at work for all of the systems studied, and are likely ubiquitous in the atmosphere. The aging effect with respect to yield is a function of the number of oxidation steps required to convert from the initial precursor as well as how much slower or faster these oxidized intermediates react with OH, and depends highly on the properties of the initial structure. The results do not appear to be significantly impacted by losses of organic vapors to the Teflon



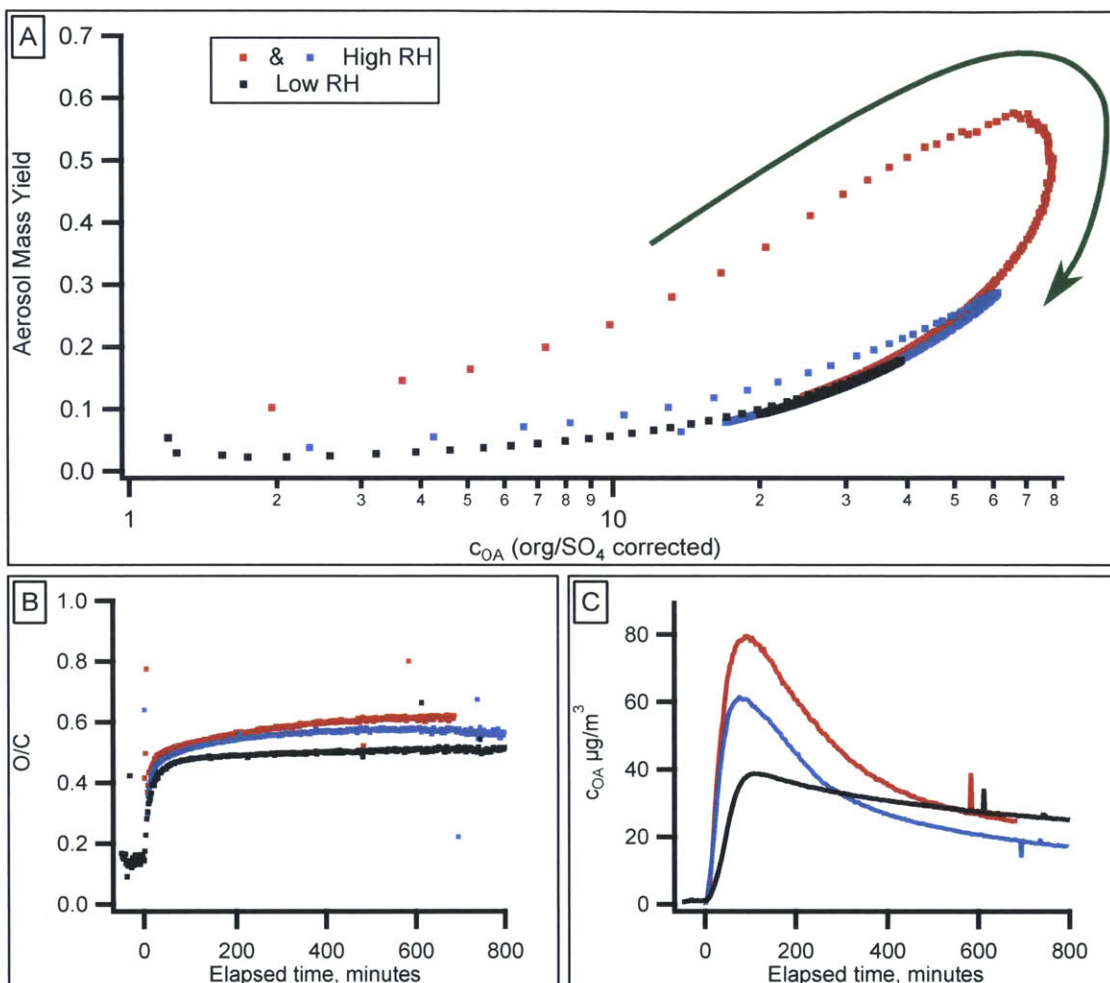


Figure 2-6: Effect of relative humidity on  $\alpha$ -pinene aging. Panel A shows yield versus  $c_{OA}$  for a set of three continuous aging experiments, two at high ( $\sim 80\%$ , red and blue traces) RH, and one at low ( $< 10\%$ , black trace) RH. The green arrow indicates the time progression. The high RH experiments show greatly enhanced yield initially, followed by rapid loss of mass that causes they yield curves to converge onto the dry yield curve. Panel B shows the O/C for these experiments, which is only mildly elevated for the humid experiments and does not change significantly in response to the large changes in yield. Similar to the dry experiment, the O/C does not increase significantly even though the aqueous particles presumably undergo rapid internal diffusion and minimal gas-particle equilibration timescales. Panel C shows wall loss corrected  $c_{OA}$  versus time, highlighting the dramatic rise and fall of the organic aerosol for the humid experiments, followed by eventual convergence onto the dry trace.

reaction chamber walls, and although interesting differences in the chemistry occur during humid chamber experiments, low particle-phase diffusivity present in the dry aging experiments do not appear to be responsible for lack of large increases in aerosol O/C with OH aging. Although important for yield, the continued oxidation of intermediates through OH aging is simply not capable of generating the highly oxidized material found in the ambient atmosphere under the conditions of the experiments in this study. Neither particle diffusivity nor loss of vapors appears to explain this, though significant dilution present in the ambient atmosphere is expected to lead to higher O/C values than are observed in chambers. Instead, condensational trapping dominates the aerosol composition through feedback on the oxidation and multigenerational chemistry: vapors reach an O/C prior to condensation that depends on  $c_{\text{OA}}$ , and undergo much slower oxidation after this point. Disambiguating the competing effects of  $c_{\text{OA}}$ /trapping and OH aging/kinetics on yields requires conducting aging experiments over a wide range of concentration in order to create yield contours at constant OH exposures. These experiments are necessary in order to improve the model treatment of aerosol, which is currently based on yields parameterized from historical experiments in which total OH exposures and degree of oxidation are not well constrained. Because additional aerosol will generally be produced at high OH exposures, these current methods are expected to lead to underestimates of organic aerosol mass, especially at locations farther downwind from emissions sources. The results from the present experiments are most relevant to historical experiments that have used a HONO pulse to oxidize precursors. However, for these and for experiments that use different oxidation methods, the exact enhancement in yield will be a function of the details of these historical experiments, which are highly variable.

## Chapter 3

# Aerosol Yields & the Role of Fragmentation in Reactive Products

This work is adapted from material previously published as "Secondary Organic Aerosol Formation from Acyclic, Monocyclic, and Polycyclic Alkanes," *Environmental Science and Technology* 2014, 48, 10227-10234, authored by James F. Hunter, Anthony J. Carrasquillo, Kelly E. Daumit, and Jesse H. Kroll.<sup>55</sup>

### 3.1 Introduction

A significant fraction of all hydrocarbons emitted into the atmosphere have molecular structures with cyclic moieties; these include cycloalkanes, aromatic species, and most mono and sesquiterpenes. Many such species are known to be efficient precursors of secondary organic aerosol,<sup>25-28,56,57</sup>

Figure 3-1 shows the classes of reaction available to unbranched acyclic, monocyclic and polycyclic alkanes in the gas phase, including functionalization (addition of oxygen-containing functional groups) and carbon-carbon bond (C-C) scission. For acyclic structures, C-C scission causes fragmentation, forming two smaller compounds (path 1b). For cyclic alkanes, the free ends of C-C scission products remain tethered together (path 2b).<sup>6,25,26</sup> This prevents fragmentation and leads to more functional groups on the single product, thereby promoting the formation of low-volatility species

which can condense into the particle phase (and subsequently undergo oligomerization reactions).<sup>26</sup> Polycyclic compounds with  $n$  fused rings can resist up to  $n$  fragmentation reactions in this way (paths 3b and 3e). However, polycyclic alkanes differ from monocyclic alkanes in that their scission products are substituted rings (with functionalized alkyl substituents on the ring) rather than unbranched structures (path 3b versus 2b). These substituted rings may undergo enhanced fragmentation (path 3f), similar to the enhanced fragmentation of branched alkanes relative to linear alkanes.<sup>26-29</sup> Some work has examined the importance of the initial ring opening for monocyclic alkanes (path 2a versus 2b),<sup>26</sup> but not to our knowledge for polycyclic alkanes. The branching for later-generation oxidation pathways (2c-2d and 3c-3h) also remains highly uncertain. For simplicity, all of the reactions are shown leading to carbonyl groups, representative of the simplest radical termination chemistry. These products are possible, but in many cases alkoxy radical isomerization will also take place, leading to products with a hydroxyl group as well as a carbonyl group.<sup>58,59</sup> For cyclic structures isomerization can follow scission, leading to terminal hydroxy-aldehydes rather than dialdehydes as pictured.<sup>58,59</sup> The goal of this study is to investigate the oxidation chemistry of cycloalkyl structures and to determine the effect of additional rings on SOA formation, and specifically the relative importance of ring opening, fragmentation, and addition of functional groups. We report the aerosol yields and chemical properties for the reaction of the hydroxyl radical (OH) with a set of C10 alkanes that have zero to three rings. The role of branched cycloalkanes has been studied previously,<sup>26,28</sup> and is not examined here in great detail (only one such structure is included in the study) because of the present focus on the effect of additional rings. Experiments are conducted at high organic aerosol concentrations ( $c_{\text{OA}}$ ) in order to increase sensitivity to more volatile products, and at high OH exposures to include the effects of oxidative aging. The aim of this study is not to provide detailed yields for individual molecules, but rather to use SOA yields and composition to constrain the various reaction channels shown in Figure 1, and to better understand how such channels relate to SOA formation.

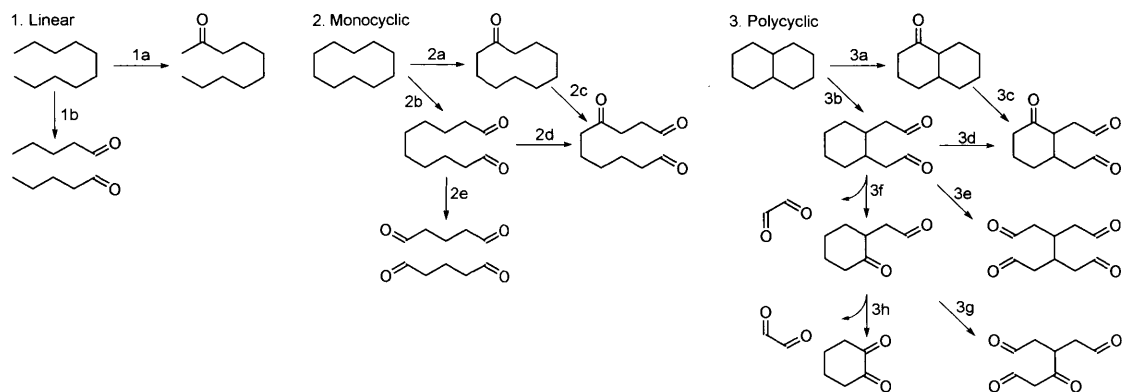


Figure 3-1: An illustration of different reaction pathways available to unbranched acyclic, monocyclic, and polycyclic alkanes. All arrows represent OH oxidation steps, with horizontal arrows corresponding to functionalization, diagonal arrows to C-C scission with tethering, and vertical arrows to C-C scission with fragmentation of the carbon skeleton. For simplicity, all OH oxidation reactions are shown adding carbonyl groups (the simplest termination products) to the carbon skeleton (one for functionalization, two for C-C scission). Isomerization is also possible, leading to hydroxy-carbonyls.<sup>58,59</sup> Additional fragmentation and functionalization reactions of the product species (omitted for clarity) can also occur, as can oligomerization reactions following condensation.

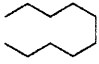
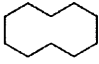
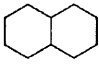
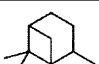
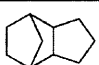

## 3.2 Experimental Methods

The C<sub>10</sub> compounds used in this study are shown in Table 3.1 along with their key properties. They include *n*-decane (no rings, C<sub>10</sub>H<sub>22</sub>, Sigma-Aldrich, ≥ 99%), cyclodecane (1 ring, C<sub>10</sub>H<sub>20</sub>, Sigma-Aldrich, 95%), decalin (bicyclo[4.4.0]decane, 2 rings, C<sub>10</sub>H<sub>18</sub>, Sigma-Aldrich, cis + trans, 99%), pinane (2,6,6-Trimethylbicyclo[3.1.1]heptane, 2 rings, C<sub>10</sub>H<sub>18</sub>, Santa Cruz Biotech, endo + exo, ≥ 99%), JP-10 (tricyclo[5.2.1.0<sup>2,6</sup>]decane, 3 rings, C<sub>10</sub>H<sub>16</sub>, TCI America, ≥ 94%), and adamantane (tricyclo[3.3.1.1<sup>3,7</sup>]decane, 3 rings, C<sub>10</sub>H<sub>16</sub>, Sigma-Aldrich, ≥ 99%).

The instruments and methods used for the present experiments are generally identical to those described in Section 2.2, with differences noted below.

Dry ammonium sulfate particles seed particles were used for all experiments. These were atomized from a 2 g/L solution of reagent-grade ammonium sulfate (Aldrich) for 15-25 minutes. This produced a number-weighted average diameter of 200 nm, number concentration of 25,000 to 50,000 cm<sup>-3</sup> and mass concentration

Table 3.1: Key properties of molecules in this study

Name	Alkane Type	Structure	Formula	Vapor Pressure at 298 K (Pa) <sup>a</sup>	$k_{OH}^b$ (cm <sup>3</sup> molecule <sup>-1</sup> sec <sup>-1</sup> )	Ring Strain <sup>c</sup> (kJ mol <sup>-1</sup> )
Decane	Acyclic		C <sub>10</sub> H <sub>22</sub>	191	1.10x10 <sup>-11</sup>	N/A
Cyclodecane	Monocyclic		C <sub>10</sub> H <sub>20</sub>	74	1.59x10 <sup>-11</sup>	53
Decalin	Bicyclic		C <sub>10</sub> H <sub>18</sub>	163	1.88x10 <sup>-11</sup>	1.3 (trans); 12 (cis)
Pinane	Bicyclic, Substituted		C <sub>10</sub> H <sub>18</sub>	292	1.24x10 <sup>-11</sup>	>110 <sup>d</sup>
JP-10	Tricyclic		C <sub>10</sub> H <sub>16</sub>	263	1.06x10 <sup>-11</sup>	95
Adamantane	Tricyclic		C <sub>10</sub> H <sub>16</sub>	230	2.15x10 <sup>-11</sup>	18-28

<sup>a</sup>Estimated from MPBPWIN, a component of EPI Suite.<sup>60</sup> <sup>b</sup>Atkinson et al 2003.<sup>29</sup>

<sup>c</sup>Atkinson et al 1983.<sup>61</sup> <sup>d</sup>Lower-limit ring strain from four membered ring.<sup>62</sup>

of 50 to 100 µg/m<sup>3</sup>. Approximately 40 ppb of hydrocarbon precursor was used for each experiment.

All experiments used the “continuous aging” methodology described previously. The average OH concentration ranged from 8.3x10<sup>6</sup> to 2.6x10<sup>7</sup> molecules/cm<sup>3</sup>, and stayed approximately constant over each experiment.<sup>31,45</sup>

As in the previous chapter, NO<sup>+</sup> and NO<sub>2</sub><sup>+</sup> from organic nitrates were not included in organic mass or O/C calculations for the HR-ToF-AMS.<sup>46,47</sup> These ions were however included in the calculation of the nitrogen-to-carbon ratio in order to provide an estimate of organic nitrate abundance. For this calculation the relative ionization efficiency of the nitrate ions was set to 1.1 rather than the value of 1.4 used for organic mass.

Wall loss and dilution corrections for particle mass follow the methods described previously, but for these experiments the lower-limit “SMPS case 1” correction is calculated for all experiments in addition to the upper-limit organic-to-sulfate method

(“AMS case 2”).<sup>48</sup>

## 3.3 Results & Discussion

### 3.3.1 Aerosol Formation & Yields

Figure 3-2 shows key time traces for a typical experiment (43 ppb cyclodecane): cycloalkane concentration, organic and sulfate mass loadings, and the organic mass loadings corrected by the organic-to-sulfate (upper limit) and decay-rate (lower limit) approaches described above. AMS O/C and H/C are also shown, and are discussed in a later section. Initially sulfate signal decays due to wall losses, then sharply increases as organics condense onto the sulfate seeds and increase the AMS collection efficiency.<sup>63</sup> The corrected organic loading increases rapidly and eventually levels off, marking the point where the maximum SOA yield has been achieved (at an OH exposure of  $1.1 \times 10^8$  molecules  $\text{cm}^{-3}$  hr). The two correction methods diverge with time and lead to significantly different final concentrations; these differences are substantially larger in the present experiments than in previous studies<sup>48</sup> because aerosol production is sustained over a longer time (6-10 hours) than in typical chamber experiments (1-4 hours).<sup>25,26,48,52</sup> The disparity between the wall loss correction methods dominates the overall uncertainty in yields (the measurement errors are on the order of 10%), underlining the importance of future research aimed at better quantifying losses of particles and vapors to the chamber walls.

Table 3.2 summarizes yield results for all experiments, with maximum SOA yields versus  $c_{\text{OA}}$  shown in Figure 3-3. The  $c_{\text{OA}}$  ranges from 80 to 300  $\mu\text{g}/\text{m}^3$ ; this is higher than typical atmospheric levels but enables precise measurements of the aerosol composition without requiring background subtraction procedures.

### 3.3.2 Comparison With Previous Results

Results from previous SOA studies of C10 species are also given in Table 3.2. Chamber studies of SOA have previously been made for *n*-decane<sup>26,52</sup> and cyclodecane,<sup>25,26</sup> but

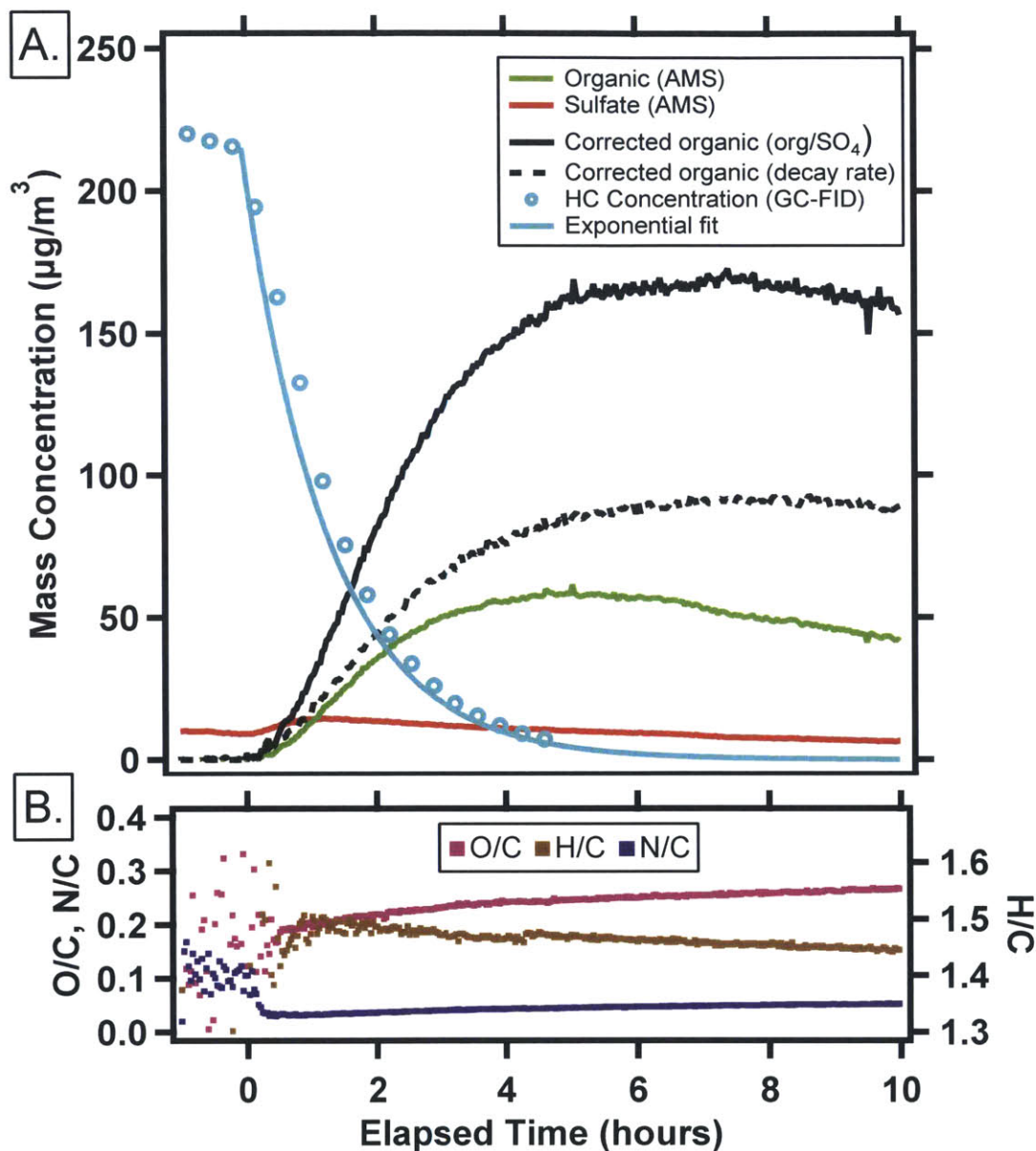


Figure 3-2: Time traces for key measurements during a typical experiment (oxidation of cyclodecane). Photochemistry is initiated at  $t=0$ . Panel A: Cycloalkane concentrations, AMS measurements of organic and sulfate aerosol, and corrected aerosol loading measurements. AMS mass loadings are not corrected for collection efficiency (CE), but corrected loadings take into account wall loss, dilution and changes to CE. Panel B: Elemental ratios.



not for any of the other compounds in this study. For the chamber studies,<sup>25,52</sup> volatility basis set (VBS) fits (for  $c^* = 0.1$  to  $100 \mu\text{g}/\text{m}^3$ ) are given in Figure 3-3.<sup>5</sup> Extrapolations to higher  $c_{\text{OA}}$  are also shown (dashed lines), but these are highly uncertain.<sup>64</sup> More volatile material ( $c^* \geq 1000 \mu\text{g}/\text{m}^3$ ) may contribute SOA at high  $c_{\text{OA}}$ , so these extrapolations represent lower limits. Results by Lim and Ziemann<sup>26</sup> are not included in Figure 3-3 since those experiments were run at much higher organic loading. In fact, yields for *n*-decane and cyclodecane are substantially higher here than those reported by Tkacik et al.,<sup>25</sup> Presto et al.<sup>52</sup> and Lim and Ziemann.<sup>26</sup> Although higher yields are expected at higher  $c_{\text{OA}}$  due to absorptive partitioning,<sup>4</sup> differences in  $c_{\text{OA}}$  cannot fully explain the differences between the previous chamber studies and the present work. Yields reported by Lim and Ziemann<sup>26</sup> are actually lower than those achieved here despite the much higher organic loading in those experiments. The differences in yields can instead be explained by differences in OH exposures (given in Table 3.2). The OH exposures in this work, required in order to reach maximum SOA yields, are up to a factor of 25 higher than comparable chamber experiments. This suggests that the yields and properties reported here are more representative of SOA formed after substantial aging (multiple days in the atmosphere) than those reported in previous chamber studies.

By contrast, the measured yields for *n*-decane are lower than those measured in the flow-reactor experiments of Lambe et al.<sup>65</sup> (also included in Figure 3-3 and Table 3.2), and yields from JP-10 are in reasonable agreement with the results from that study. Those experiments were carried out under  $\text{NO}_x$ -free conditions, with higher OH concentrations ( $8 \times 10^8$  to  $2 \times 10^{10}$  molecules/ $\text{cm}^3$ ) and much shorter residence times (100 s) than the chamber experiments. Yields were corrected for wall loss using the measured size-dependent particle transmission efficiency of the flow reactor.<sup>65</sup> This method does not include losses of vapors to wall-bound particles and is most similar to the decay-rate correction method. The OH exposures were higher than in the present chamber study, but only by a factor of  $\sim 3$ . That the yields in the present study agree more closely with the flow-reactor study than previous chamber studies again suggests the importance of multigenerational oxidation in SOA formation. However,

differences in reaction conditions (e.g., NO<sub>x</sub> level, irradiation) make it difficult to directly compare results from the two experiments.

### 3.3.3 Influence of Number of Rings on Yields and Mechanisms

Figure 3-3 shows yields computed using both the organic-to-sulfate (upper limit) and decay-rate (lower limit) correction methods. These limits diverge over a given experiment, as shown in Figure 3-2, so that uncertainty in organic aerosol concentration and yield increases with time (and hence degree of aging). The mass yields may be constrained further by carbon yields, computed from the mass yields and the mass fraction carbon determined from AMS elemental analysis data. The upper-limit and lower-limit carbon yields for this study are given in Table 3.2. In many cases the upper-limit carbon yields are above the strict maximum of 100%, indicating that the organic-to-sulfate method is an overestimate (by up to 30%). Such high carbon yields imply that losses to the chamber walls (either to wall-bound particles or to the Teflon itself) are not a dramatic sink of organic vapors in the present experiments, in contrast to chamber studies of other SOA-forming systems.<sup>34,35</sup>

All cyclic species (except pinane) have a substantially higher SOA yield than *n*-decane; this is consistent with previous results<sup>25,26,52,65</sup> and can be explained by the “tethering” effect discussed above. However, no clear additional increase in yield is observed as the number of rings increases beyond one. This lack of dependence on ring number may arise from differences in multigenerational oxidation pathways for monocyclic and polycyclic alkanes, as illustrated in Figure 3-1. C-C scission of monocyclic species (pathway 2b) results in an acyclic product with terminal oxygen-containing functional groups. The high yield indicates that fragmentation (2e) does not occur to a major extent, and/or that it is associated with minimal carbon loss. For polycyclic alkanes, C-C scission results in substituted cyclic structures (e.g., the product of pathway 3b). These structures likely fragment more than in the monocyclic case (3f is enhanced relative to 2e), much like branched alkanes fragment more readily than linear alkanes.<sup>26,27</sup> This likely also explains the low yield of pinane, which has a branched starting structure analogous to the product of 3b; this effect may also be

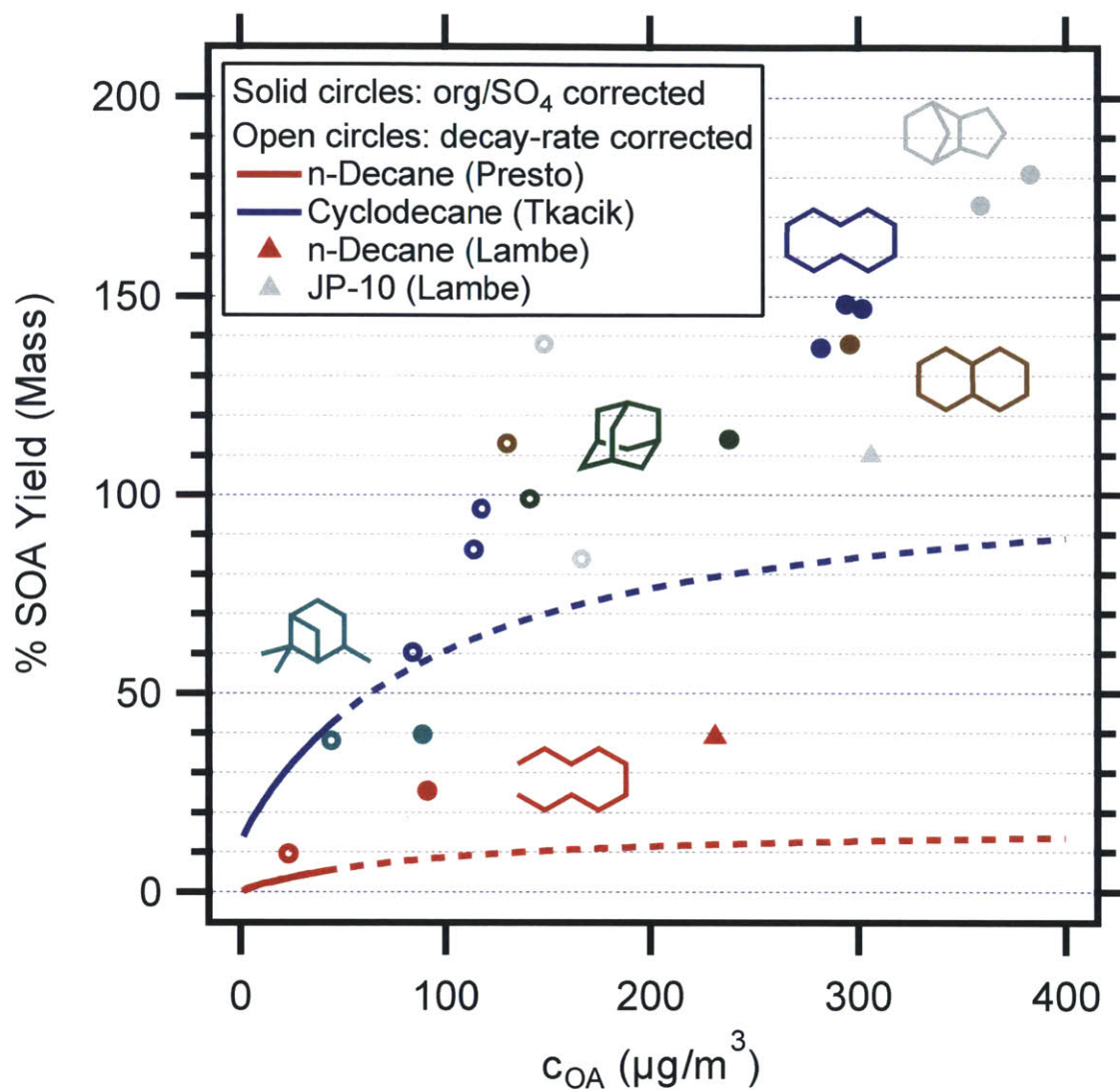


Figure 3-3: Yields of organic aerosol computed using both the organic-to-sulfate (closed circles) and decay-rate (open circles) correction methods, and comparison with previous yield measurements (lines and triangles). Color denotes SOA precursor (red: *n*-decane; dark blue: cyclodecane; brown: decalin; light blue: pinane; green: adamantane; grey: JP-10). VBS fits of *n*-decane and cyclodecane mass yields from Presto et al.<sup>52</sup> and Tkacik et al.<sup>25</sup> are shown, with extrapolated fits indicated by dashed lines. The maximum reported yields of *n*-decane and JP-10 from the flow-tube study of Lambe et al.<sup>65</sup> are also shown. Overall uncertainties in yields are dominated by differences between lower limit and upper limit wall loss corrections rather than uncertainty in the measurement techniques (10%).

Table 3.2: Yields and elemental composition of SOA from C10 compounds<sup>a</sup>

compound	% SOA yield (mass)		% SOA yield (carbon)		$c_{\text{OA}}$ ( $\mu\text{g}/\text{m}^3$ )		O/C <sup>e</sup>	H/C <sup>e</sup>	N/C <sup>e</sup>	DBE <sup>f</sup>	excess DBE <sup>f</sup>	OH exposure (molec/cm <sup>3</sup> ·hr)
	upper <sup>b</sup>	lower <sup>c</sup>	upper <sup>b</sup>	lower <sup>c</sup>	upper <sup>b</sup>	lower <sup>c</sup>						
<b><i>n</i>-Decane</b>												
this study	25.4	9.6	19.6	7.4	91.4	23.4	0.33	1.58	0.031	3.1	0	$4.5 \times 10^7$
Presto	1.5	–	–	–	6	–	–	–	–	–	–	$1.2 \times 10^7$
Lim	–	14.6	–	–	–	828	–	–	–	–	–	$2.9 \times 10^7$
Lambe	–	39 <sup>d</sup>	–	29 <sup>d</sup>	–	231 <sup>d</sup>	0.35	1.53	–	3.3	0.2	$1.4 \times 10^8$
<b>Cyclodecane</b>												
this study	147	60.3	115	47.2	302	84.3	0.28	1.47	0.054	3.6	0.5	$1.6 \times 10^8$
this study	137	86.2	104	65.4	282	114	0.28	1.48	0.049	3.6	0.5	$9.6 \times 10^7$
this study	148	96.4	111	72.3	294	118	0.33	1.42	0.043	3.9	0.8	$8.5 \times 10^7$
Tkacik	25	–	17	–	15	–	0.30	1.34	–	4.3	1.2	$6.0 \times 10^6$
Lim	–	64.1	–	–	–	3325	–	–	–	–	–	$7.7 \times 10^6$
<b>Decalin</b>												
this study	138	113	98.3	88.5	296	131	0.35	1.38	0.045	4.1	1.0	$2.4 \times 10^7$
<b>Pinane</b>												
this study	39.6	38.0	24.6	23.6	89.0	44.2	0.53	1.31	0.050	4.4	1.3	$5.4 \times 10^7$
<b>JP-10</b>												
this study	181	138	125	95.3	383	149	0.39	1.33	0.046	4.3	1.2	$9.1 \times 10^7$
this study	173	83.8	130	62.9	359	167	0.34	1.30	0.047	4.5	1.4	$1.6 \times 10^8$
Lambe	–	110 <sup>d</sup>	–	72 <sup>d</sup>	–	306 <sup>d</sup>	0.74	1.22	–	4.9	1.8	$2.6 \times 10^8$
<b>Adamantane</b>												
this study	114	99.0	77.1	67.0	238	142	0.42	1.26	0.064	4.7	1.6	$5.2 \times 10^7$

<sup>a</sup>Quantities that were not measured/reported in previous studies are denoted with a “–” <sup>b</sup>Yields computed using organic-to-sulfate wall loss correction method. <sup>c</sup>Yields computed using decay-rate wall loss correction method assuming an SOA density of  $1.4 \text{ g}/\text{cm}^3$ . <sup>d</sup>Maximum yields measured from oxidation within a flow reactor, corrected for wall loss using methods detailed in Lambe et al.<sup>65</sup> <sup>e</sup>Determined from W-mode AMS data from the final hour of each experiment, associated with the maximum SOA yield achieved. N/C includes  $\text{NO}^+$  and  $\text{NO}_2^+$  and therefore provides a measure of organic nitrate abundance. <sup>f</sup>Double Bond Equivalents, computed from Equation 2.2 assuming condensed-phase products retain all 10 carbon atoms. “Excess DBE” computed by subtracting 3.1 from the DBE to account for carbonyl functionalities.

relevant to other branched cyclic species as well. However, enhanced fragmentation for polycyclic species may be offset by additional ring opening pathways (3g), ultimately leading to comparable yields for monocyclic and polycyclic compounds. As discussed below, the elemental ratios of the SOA provide additional evidence for the enhanced ring opening of polycyclic compounds and increased fragmentation of ring-opened products.

Once product vapor pressure is sufficiently low to condense, the oxidation rate slows significantly due to the “trapping” effect, in which species are protected from further gas-phase OH oxidation due to partitioning into the condensed phase. Heterogeneous oxidation may still occur, but is much slower than gas-phase oxidation.<sup>6-8</sup> Oxidation processes caused by direct absorption of UV light are also possible, but given the relatively unchanging aerosol properties do not dominate the chemistry of the present experiments. The “trapping point” depends on the volatility of the products, the aerosol loading, and the extent to which the condensed-phase products rapidly form oligomers. The uniformly high SOA yields for all unbranched polycyclic compounds suggest that under the conditions of this study (high aerosol loading), trapping follows the second generation of oxidation, since if further oxidation were to occur, there would likely be differences in the yields of the monocyclic and polycyclic compounds. For example, a third oxidation step for cyclodecane would likely result in fragmentation, because second-generation products are likely to be ring-opened and functionalized. For polycyclic species, although the remaining rings are less effective at preventing fragmentation once the first ring has opened, some “tethering” may still occur, increasing the yield of lower volatility products relative to a structure with no remaining rings. Thus, gas-to-particle conversion after two generations of oxidation leads to similar yields for all cyclic structures examined in this study; however differences might emerge if further oxidation is possible. This could result either from lower aerosol loadings or reduced carbon number of the precursors. At lower loadings, products must have a lower volatility to partition into the condensed phase, potentially requiring additional oxygenated functional groups and therefore additional oxidation steps. Similarly, compounds with lower carbon numbers start with a higher volatility,

and require a larger number of oxidation steps to achieve the same low volatility as a larger compound. In either case, the more oxidation steps that take place, the less effective rings are expected to be in producing high SOA yields, since fragmentation should increase on increasingly ring-opened and oxygenated structures.

The carbon yields in Table 3.2 help to further constrain the relative importance of the multigenerational fragmentation pathways. The upper limit carbon yields for the cyclic, unbranched structures are 77 to 130%, while lower limit carbon yields are 47 to 95%. The carbon yields, like the mass yields, do not vary with number of rings. The fraction of remaining gas-phase carbon (0-53%) suggests that fragmentation occurs somewhat for the cyclic alkanes, and is not necessarily prevented by the presence of multiple rings. However this fraction is small, suggesting that fragmentation (e.g. pathways 2e, 3f and 3h) is a relatively minor channel for the cyclic structures under the conditions of this study (high aerosol loading, 10 carbon atoms per precursor). Conversely, the larger fraction of carbon present in the gas phase for linear or branched compounds (75-93%) suggests that fragmentation dominates overall gas-phase reactivity for such species. Fragmentation is unlikely in the first oxidation step for linear alkanes,<sup>26,27,29</sup> and instead likely dominates in later generations, as expected for oxygenated species.<sup>66</sup>

Lim and Ziemann<sup>26</sup> previously explained the high yields of monocyclic alkanes in terms of the relative probability of C-C scission and isomerization/functionalization (e.g., path 2a versus 2b in Figure 3-1). In that analysis, greater ring strain energy increases C-C scission for cyclic alkanes. This scission results in ring-opened products that are multifunctional and possibly subject to enhanced oligomer formation,<sup>26</sup> and thereby increases aerosol yield. No trend in yield with ring strain (given in Table 3.1) is apparent in the present study, suggesting that the probability of ring opening in the first oxidation step does not govern SOA formation. Instead, it appears that multiple generations of oxidation are required, reducing the relative importance of any individual ring opening step. Furthermore, ring strain is expected to change over a multigenerational oxidation process. Functionalized rings have increased ring strain<sup>62</sup> which may increase the likelihood of ring opening in subsequent oxidation

steps.

### 3.3.4 Role of Number of Rings on SOA Elemental Composition

Aerosol elemental ratios (averaged over the final hour of each experiment) are given in Table 3.2. Typical time traces for O/C, H/C and N/C are also shown in panel B of Figure 3-2; changes in these ratios are relatively minor despite significant changes in loading and OH exposure. The O/C for SOA from all precursors (except pinane) ranges from  $\sim 0.3$  to  $\sim 0.4$ , indicating that a 10 carbon skeleton acquires 3 to 4 oxygen atoms before reaching a low enough volatility to condense at the loadings in the present study. Since each oxidation step is likely to add 1-2 functional groups, this is consistent with the second oxidation step leading to SOA formation. O/C increases slightly with increasing ring number. This suggests enhanced ring opening, since this reaction channel adds more functional groups per oxidation step. The relatively unchanging O/C implies little oxidation of condensed-phase organic species, consistent with slowed oxidation due to “trapping” after these two steps. The high O/C of pinane is an exception, likely due to increased fragmentation; fragmentation products have a reduced carbon number and are more volatile, leading to both reduced yields and increased O/C.

Aerosol organic nitrogen is entirely due to  $\text{NO}^+$  and  $\text{NO}_2^+$  such that the abundance of organic nitrates can be inferred from the N/C values given in Table 3.2. Assuming that the oxidation products in SOA retain all 10 carbon atoms, the organic nitrate yield ranges from 31% to 64%. Because the maximum nitrate yield for a single reaction step is expected to be approximately 30%,<sup>59</sup> this suggests multiple oxidation steps are required. Nitrate yields appear to be systematically higher for all the cyclic compounds, but do not exhibit a trend with increasing ring number. Inclusion of nitrate in the organic mass increases aerosol mass by an additional 10 to 20%, but would not affect any of the overall trends or conclusions of this work.

The relative importance of functionalization and ring-opening reactions in the

oxidation of the cyclic alkanes can be constrained by the average number of double bond equivalents (DBE) of the molecules within the SOA, calculated via

$$DBE = n_C + 1 - \frac{n_H}{2} = 1 + n_C \left( 1 - \frac{1}{2} \frac{H}{C} \right) \quad (3.1)$$

in which  $n_C$  and  $n_H$  are the number of carbon atoms and hydrogen atoms in an average molecule. Calculated DBE values are given in Table 3.2; we assume that  $n_C > 10$  (i.e., SOA contains no fragmentation products), though small decreases in  $n_C$  do not strongly affect DBE values. Carbon-carbon double bonds are unlikely to be stable under the highly oxidizing conditions of the present experiments, suggesting the DBE is roughly equal to the total number of intact rings and carbonyl functionalities. The DBE of *n*-decane SOA indicates that, on average, 3.1 carbonyl groups are added to each carbon skeleton; the remaining functional groups involve C-O single bonds. Assuming that the SOA functional group distribution is similar for all precursors studies, the number of retained rings can be approximated from the “excess DBE” (equal to  $DBE - 3.1$ ). By comparing this to the number of rings that each molecule started with, the average number of ring opening reactions that the SOA components have undergone can be estimated: 0.2-0.5 for cyclodecane, 0.7 to 1.0 for the bicyclic compounds, and 1.4 to 1.8 for the tricyclic compounds. Although these values are only approximate, due to differences in functional group distribution (and possibly the importance of oligomerization<sup>26</sup>), there is a clear increasing trend in the degree of ring opening with number of rings. Were additional oxidation steps to occur (e.g., at lower loadings or carbon number), additional ring opening might be expected to occur.

Consistent with the yield measurements, the elemental ratio measurements point to the ubiquity of ring opening for all the cyclic structures, and the importance of both additional ring opening and fragmentation in polycyclic moieties over the multiple generations of oxidation required to form SOA in these experiments. Although “tethering” implies that a polycyclic compound with  $n$  rings can resist up to  $n$  C-C bond scissions without fragmenting, in practice fragmentation of early-generation



products may be important, since the first ring-opening product has a branched structure. For pinane, a precursor that has both rings and branches, this competition exists in the first oxidation step, leading to lowered yields. Finally, unbranched monocyclic compounds comprise a special case in which ring opening results in a linear molecule with primary oxygenated functional groups, with little fragmentation of gas-phase products. The yield and chemical composition measurements show that aerosol formation from cyclic compounds is a multigenerational process, and that the degree of fragmentation (which is a strong function of molecular structure and oxidation generation) is critical to the amount and properties of the aerosol that is eventually formed.



## Chapter 4

# Comprehensive Measurements of Atmospheric Organic Carbon

### 4.1 Introduction

Organic compounds play a central role in the chemistry of the atmosphere by forming secondary species such as ozone and secondary organic aerosol (SOA), by controlling the concentrations of oxidants, and by serving as pollutants and nutrients in their own right. They are therefore closely linked to air quality, ecological health, and global climate.<sup>1,67</sup> The contribution of organic compounds to the formation and evolution of SOA is especially complex, because the amount and properties of SOA depend not just on the gas-phase precursors that react initially, but also on the oxidized, low volatility, intermediates and the semivolatile compounds that are in equilibrium with the condensed phase once formed. Accurate representation in models depends on a thorough understanding of the entire lifecycle of atmospheric organic carbon—emission, chemical transformation, and loss (deposition or oxidation to CO<sub>2</sub>). The complexity of the gas-phase is a large part of why the formation and evolution of SOA has been difficult to capture in models, leading to significant disagreement in loadings, properties and variability.<sup>22</sup> This is especially true for the oxidized intermediates and semivolatile compounds, which may have large deposition velocities<sup>13</sup> and reaction rates<sup>49</sup> but have been poorly constrained thus far.

Viewed holistically, the loadings, properties, and effects of atmospheric organic carbon (aerosol and key gas-phase species) depend critically on the balance between the lifecycle processes, and the details of these processes individually (the relative amounts of species, emissions, and details of the oxidative transformations). Characterizing this whole has been extremely challenging for several reasons. Atmospheric organic carbon is made up of a very large number of unique organic compounds that exhibit extraordinary structural diversity, reactivity, and have volatilities that range over many orders of magnitude. The number of compounds may be greater than 10,000 in a given air sample,<sup>1</sup> making a complete inventory on the molecular level impractical both for measurement and simulation based on number alone. This is made even more complex by adding the transformations (e.g. oxidation chemistry) that link all of these compounds together. This diversity in properties also leads to difficulty in measuring many of the species at all. The oxidized intermediates and semivolatile compounds are especially challenging, because low volatility, gas-phase, oxygenated, organic compounds are efficiently lost to environmental and instrument surfaces, and conventional measurement techniques are not well suited to measuring these types of molecules. Attempts to measure total organic carbon loading have been made, starting with the work of Gagosian as part of SEAREX, and more recently by Roberts, Chung, and Lee.<sup>68-71</sup> Although useful, these methods are all based on a limited number of measurement techniques that only allow the organic carbon to be apportioned into aerosol and a small number of speciated VOCs, and so are not able to describe the full breadth of atmospheric organic complexity. Finally, even when concentrations are known, interpretation of those concentrations is greatly complicated by the diversity in timescales of oxidation, transport, mixing, and deposition. Timescales for oxidation can range over 6 orders of magnitude, from a few minutes (sesquiterpenes) to a decade (methane). Practically, this means that short lived compounds may have large oxidative fluxes but have very low concentrations and be poorly mixed and therefore difficult to measure. Long lived compounds may be easier to measure, but because of extensive advection and mixing, their high concentrations are not necessarily related to local emissions or photochemistry. Although this level

of complexity is daunting, all of these compounds and processes must be included in a comprehensive and accurate picture of atmospheric organic chemistry. This is a necessary goal if we would like to significantly improve our predictive capabilities for organic aerosol and other important organic species.

A number of theoretical approaches have been created for describing the chemical transformations of these organic compounds in simpler terms. Generally, these involve 2D and 3D reduced dimensionality spaces involving some metric of oxidation or polarity and some metric of size or volatility.<sup>72-76</sup> These methods are useful as model frameworks and as methods for addressing the complexity, but outside of laboratory SOA studies, have not been populated with actual data. In this work, we describe a synthesis of measurements taken by multiple co-located instruments in an effort to provide a comprehensive characterization of atmospheric organic carbon. This analysis takes advantage of new advanced mass spectrometric techniques that were used during the BEACHON-RoMBAS campaign in the Colorado Rocky Mountains in the summer of 2011. This field campaign has been described previously,<sup>77</sup> and is notable for having several instruments for atmospheric organic compounds that were essentially new to field deployment. Collectively the instrument set provides information over 19 orders of magnitude in volatility space, and also provides information on carbon number ( $n_C$ ) and average oxidation state of carbon ( $\overline{OS}_C$ ) (details in the Methods). These data are used to populate the novel analysis frameworks, and the results of this analysis are used to constrain the rates of key processes including emission, transformation, and deposition fluxes. This work describes the widest range of organic compounds and processes that has so far been reported, and represents a significant advancement in the complete characterization of total atmospheric organic carbon.

## 4.2 Results

The analysis in this work primarily uses data from a set of five instruments, all of which have been described previously in the literature. All the instruments use

high resolution time of flight mass spectrometry, but differ in the methods of analyte collection and ionization, resulting in comparatively little overlap in the types of organic molecules measured (as a function of volatility and degree of oxidation). This overlap is discussed in more detail in the Methods at the end of this chapter, as are instrument-specific methods for estimating volatility and carbon number. A brief description of each instrument/measurement follows. The Aerodyne aerosol mass spectrometer with thermodenuder (TD-AMS) measures bulk (average of the overall mixture) aerosol composition and volatility, binned decadally in  $c^*$  space.<sup>46,78</sup> The proton transfer mass spectrometer (PTR-MS) measures speciated (individual ions/compounds) VOCs, excluding alkanes.<sup>79-81</sup> The chemical ionization mass spectrometer with micro-orifice volatilization impactor (MOVI-CIMS) measures speciated gas and particle-phase acids, excluding acetic acid (the reagent ion).<sup>82,83</sup> The semivolatile thermal-desorption aerosol gas chromatography-mass spectrometer (SV-TAG-AMS) measures both speciated semivolatile tracer compounds as well as bulk hydrocarbons decadally binned by volatility.<sup>84,85</sup> The TGO measures bulk composition of semi and intermediate volatility compounds decadally binned by volatility.<sup>86</sup> Many of the features and analysis procedures for the TGO were developed for this data set; additional details (including calibration) are provided in section 4.5.

The data are visualized using the two dimensional volatility basis set and the  $\overline{OS_C}$  versus  $n_C$  spaces shown in figure 4-1. These data are overall (24 hr) averages for the entire campaign for each instrument. The sampling periods for the instruments did not completely overlap in all cases, but the relative uniformity of the campaign time series (Shown in Methods) suggests that comparing campaign averages (and average diurnal profiles) is reasonable. The open circles in Figure 4-1 all represent gas phase compounds, while the solid circles represent particle phase compounds. The circles are sized such that the area of the circles is proportional to the total mass concentration of organic carbon for each compound or bulk point (hydrogen and oxygen mass are not included). Figure 4-1 shows a few broad trends. Panel A shows  $\overline{OS_C}$  for species or the average  $\overline{OS_C}$  for that volatility bin for the bulk measurements versus the base ten log of the saturation vapor pressure ( $C^*$ ) at room temperature

in units of  $\mu\text{g}/\text{m}^3$ . It is apparent that as the volatility decreases, the  $\overline{\text{OS}}_C$  increases and the mass concentration decreases. This is clearest following the smooth and continuous trajectory from the PTR-MS (purple open circles) through the TGO (red open circles) and into the TD-AMS (blue closed circles). The MOVI-CIMS (yellow open circles) roughly brackets this overall trend, though it is biased somewhat high as is expected due to the requirement that analyte molecules contain an acid functional group. Large contributions from formic and oxalic acid are also evident in the MOVI data. The TAG-AMS bulk data (dark green circles) lies somewhat below the average trend as expected, since this measurement is purely of hydrocarbons. Panel B shows the same  $\overline{\text{OS}}_C$  and concentration data as panel A, instead plotted versus the number of carbon atoms ( $n_C$ ). In this space, important VOCs are more identifiable (e.g. monoterpenes, MBO, acetone, and methanol), and several other overall trends are apparent. Interestingly, the bulk trend is for the  $\overline{\text{OS}}_C$  to increase with increasing carbon number, such that the least volatile points in the TD-AMS and TGO are also associated with both the highest  $\overline{\text{OS}}_C$  values and the highest average carbon numbers. The average carbon number for the least volatile particle phase bin is 15, higher than the 10 carbons of a monoterpene. The TAG-AMS bulk data has average carbon numbers up to about 19. Acid species have even higher carbon numbers, though little mass is associated with these ions.

The overall trend in mass concentration with volatility can be seen most clearly in figure 4-2, which shows the campaign average concentration of carbon in  $\mu\text{g}/\text{m}^3$  versus the volatility in  $c^*$ . The concentrations are summed into decadal spaced  $c^*$  bins, and these bars are stacked, representing the assumption that there is no overlap between the different measurements (discussed further in Methods). The notable exception is the MOVI-CIMS particle phase acids (diagonally striped bars), which are expected to be included in the TD-AMS mass concentrations, since the AMS is expected to measure all classes of organics equally well.<sup>46</sup> The CIMS particle phase does not perfectly align with the TD-AMS in volatility space when using the recommended volatility estimation methods from Yatavelli et al.<sup>83</sup> Since the TD-AMS is expected to provide a more robust estimate of volatility, this can be taken

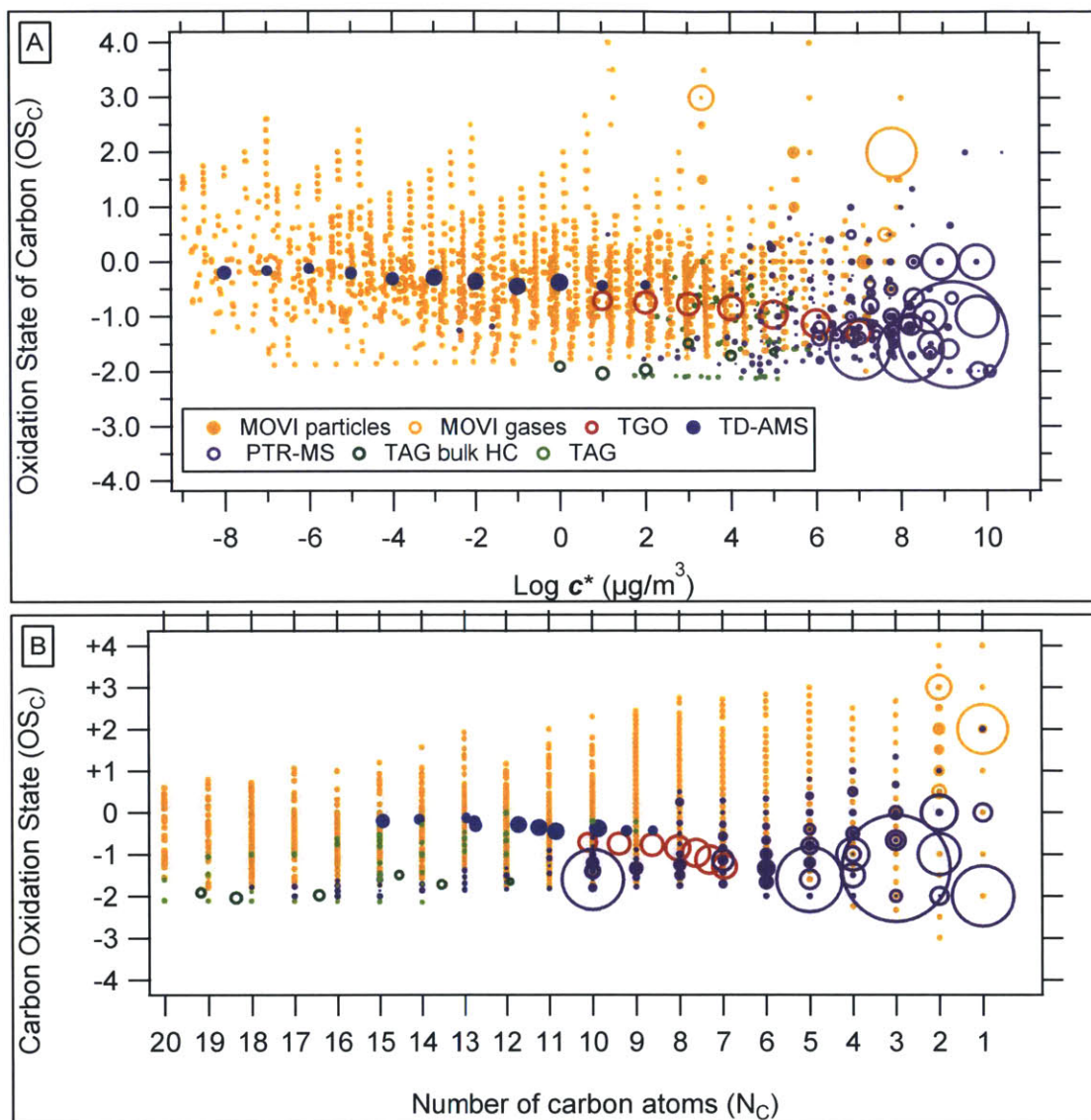


Figure 4-1: Campaign average data for the instruments during BEACHON-RoMBAS. All circles are sized such that area corresponds to concentration. Panel A shows a 2D-VBS<sup>74</sup> plot, in which a general trend towards more oxidized composition at lower volatility can be seen. Panel B shows  $\overline{OS}_C$  vs  $n_C$  for the same data. Individual key compounds (e.g. monoterpenes, MBO, acetone, and methanol) can be picked out in this space, as can a trend towards more oxidized products at higher  $n_C$ . The  $n_C$  of 15 for the least volatile aerosol components suggests that oligomerization or sesquiterpene oxidation is important.



as an indication of the level of uncertainty in the MOVI-CIMS volatility estimation methods. It is also likely that the TAG-AMS bulk data is measured as part of the TGO bulk data, but neither this nor the uncertainty in the CIMS has a large effect on the total measured carbon in a given  $c^*$  bin. From figure 4-2, it is apparent that VOCs dominate the total mass concentrations, followed by IVOCs, and then organic particulate. Total concentrations for the bins with  $c^* = 7, 8$ , and 9 are shown on the bars themselves so that the figure may be scaled appropriately. It is also evident though that the total concentrations smoothly decrease with decreasing volatility, and that there are no obvious gaps or missing carbon from the distribution. The new instruments and methods (TAG, TGO, MOVI) provide most of the mass in the middle of the distribution, and fill an otherwise conspicuous measurement gap.

The high concentrations of VOCs can give a misleading impression of their overall contribution to the local photochemistry, and specifically to the production of aerosol. Figure 4-3 shows a redistribution of total carbon concentrations that incorporates information about the  $\overline{OS}_C$ , the volatility and the atmospheric lifetime in order to give a better sense of what portion of the carbon is active in what role. Lifetimes were calculated using the known rate coefficients when available, and using a structure activity relationship based on  $n_C$  and O/C otherwise.<sup>49</sup> Long lived VOCs have a lifetime longer than 24 hours, and make up very little of the total oxidative activity. VOCs are reactive, reduced, biogenic emissions with aerosol production potential. Oxidized VOCs are reactive but oxidized and volatile and therefore likely to contribute little to SOA production. IVOCs have low volatility and are for the most part oxidized, with significant SOA forming potential. The condensed category is simply the measured particulate. Again, the figure is an upper-limit (stacked) plot, where the MOVI particulate data can be considered to overlap with the TD-AMS. From figure 4-3, it is apparent that although the total concentration is dominated by VOCs, a significant portion of these have very low reactivity or SOA forming potential. Furthermore, the two categories that are relevant to SOA production (VOCs and IVOCs) have approximately equal total mass concentrations.

Diurnal profiles follow patterns attributable to temperature and light profiles

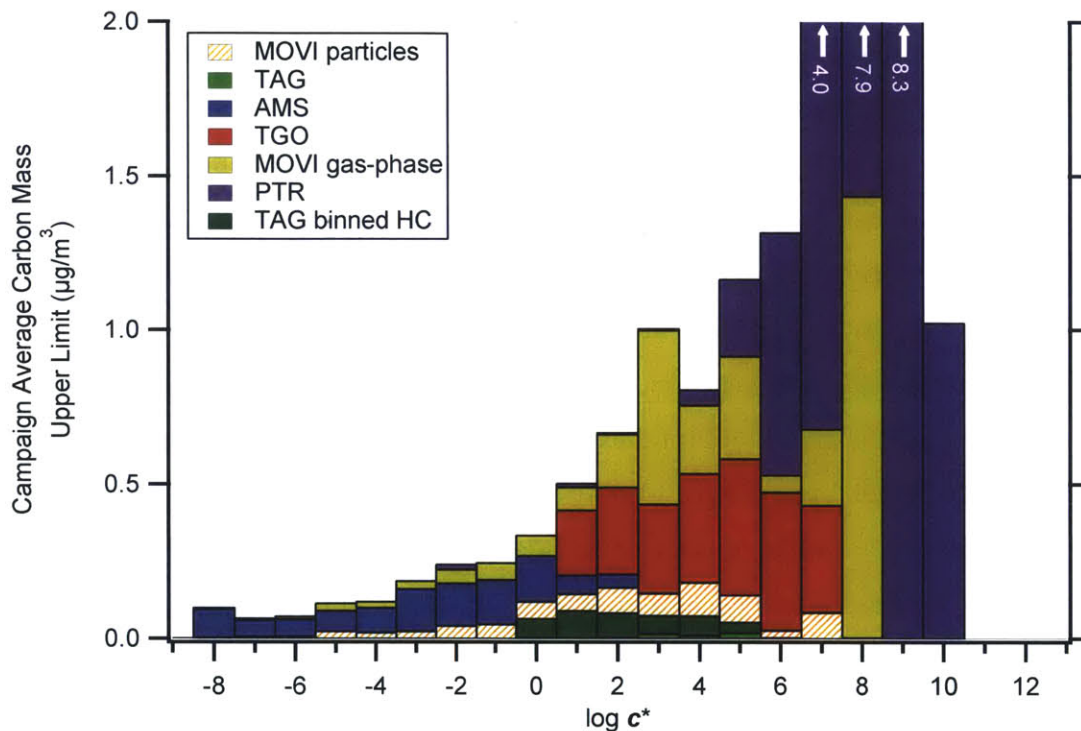


Figure 4-2: Volatility distribution of carbon mass during BEACHON-RoMBAS. The compounds shown in Figure 4-1 are binned decadally by volatility and stacked, representing an upper limit. The stacking does not strongly affect the overall trend, where the most volatile compounds have the highest concentrations, and concentrations smoothly decrease with decreasing volatility. The distribution highlights the importance of the intermediate volatility compounds, fill a conspicuous gap in the middle of the distribution. The MOVIE-CIMS particulate (diagonally striped bars) is a subset of the total PM, but is shown stacked here for simplicity.

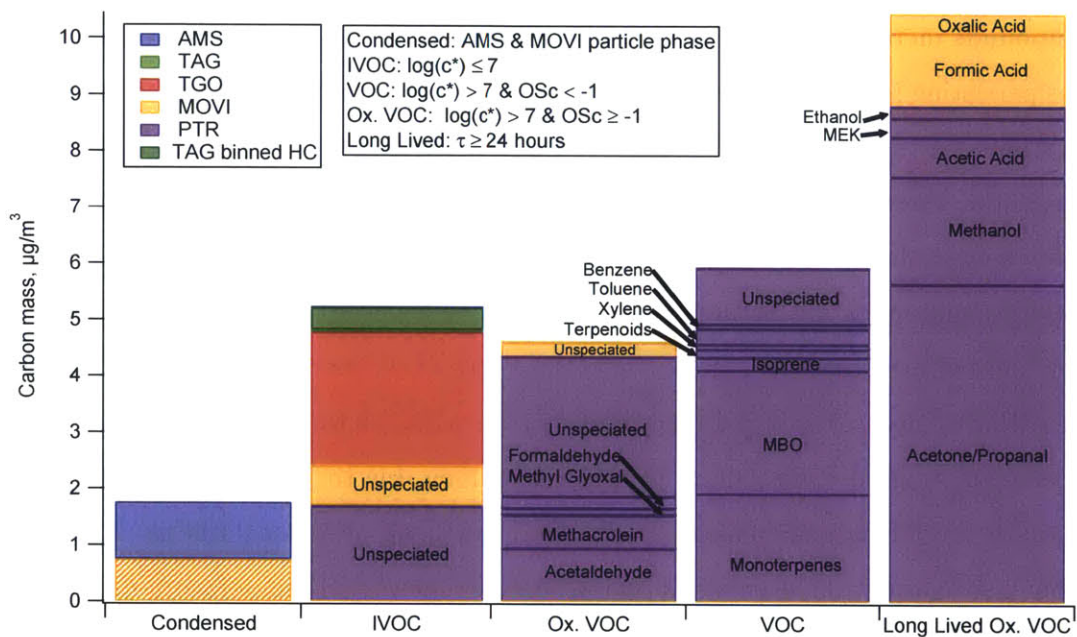


Figure 4-3: Total carbon concentration categorized by chemical significance. Information about the level of oxidation, the volatility and the oxidation lifetime is used to roughly apportion the carbon by its role in the local atmospheric organic chemistry. The categories correspond to reactive emissions (VOCs), oxidative intermediates unlikely to contribute to aerosol production (OVOCs), oxidative intermediates likely to contribute (IVOCs), particulate matter, and locally non-reactive carbon (LLVOCs).

(Temperature in °C and photosynthetically active radiation (PAR) are shown in panel F), oxidant concentration, and changing boundary layer height (shown in panel E).<sup>77,87</sup> These profiles are shown in figure 4-4 for the same organic carbon categories used in figure 4-3. Temperature and light increase at the same time starting around 6 am, with temperature reaching a maximum of 26 °C (from a low of 9 °C) around 1 pm. Light intensity reaches a maximum slightly earlier, and decreases much more rapidly than does temperature. This leads to emissions of temperature and light dependent compounds increasing sharply together in the morning, and temperature driven emissions persisting longer than light driven emissions in the afternoon. The resulting concentrations are also a function of the boundary layer height and the intensity of photochemistry, both of which peak in midday and lead to lower concentrations of most species even though emission rate of primary compounds and formation rates of secondary compounds are highest at this time. The general trends are well illustrated by the behavior of VOCs. Concentrations (panel A) increase sharply in the morning with the onset of light-driven emissions (e.g. MBO) into a shallow boundary layer. Concentrations decrease sharply in the afternoon due to photooxidation and the boundary layer height increasing to an afternoon peak of about 1100 m. Concentrations rise again in the evening as photochemistry slows and temperature-driven emissions (e.g. monoterpenes) continue into a shrinking boundary layer that reaches a midnight minimum of about 110 m. This temporal pattern of MBO and monoterpene emissions is reflected in the average carbon number for VOCs (panel B). Other carbon categories are variations on this sequence. For example, long lived VOCs are similar to VOCs except that they undergo far less oxidation during the afternoon. As a result, the background concentrations are much higher, and concentrations remain high throughout the afternoon, with no characteristic dip. Other broad trends can be extracted from the diurnal data. Most categories are more oxidized in the afternoon, at the peak of photochemical activity (panel C). Carbon number (panel B) however is flat for most categories, suggesting that within any given category the molecular distribution is not on average shifting towards oxidized fragments.

The oxidation flux can be estimated using the oxidation lifetime estimates. In con-

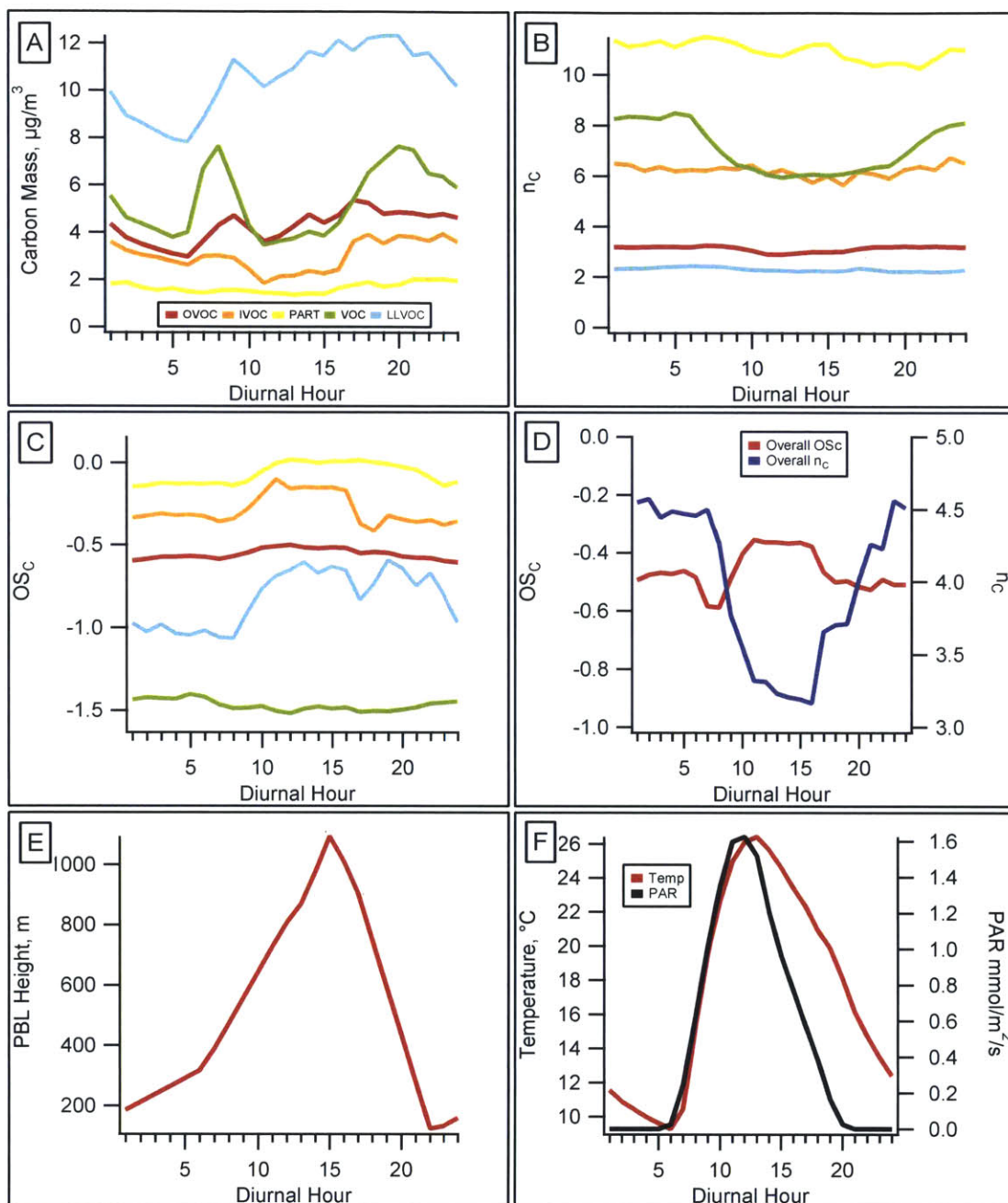


Figure 4-4: Diurnal trends in chemically significant categories of organic carbon mass. The observed profiles result from emissions and oxidation that are a function of boundary layer height (panel E), temperature, and light (panel F). Panel A shows concentrations, which tend to increase in the morning and evening due to the shallow boundary layer, and decrease in the afternoon due to the higher boundary layer and intensified photochemistry. Panel B shows average carbon numbers, which are mainly flat except for VOCs due to the changing relative amounts of monoterpenes and MBO. Panel C shows average oxidation state, revealing slightly more oxidized products during the afternoon peak of photochemistry.

junction with estimates of emission and deposition fluxes, this allows an approximate picture of the overall flow of carbon to be constructed for this site. These fluxes are provided in table 4.1 and shown in figure 4-5. These quantities are campaign averages  $\pm$  one standard deviation calculated from diurnally detrended averaged concentrations. The uncertainty ranges therefore reflect day to day variability and instrument noise for the whole campaign rather than the average variability over a single day. These categories are identical to those in Figure 4-3 except that 1) IVOCs and OVOCs have been combined for simplicity, and 2) known biogenic emissions in the IVOC and OVOC categories have been reassigned to the VOC category. The second change primarily involves sesquiterpenes and acetaldehyde. Dividing the concentrations by lifetimes gives units of  $\mu\text{g}/\text{m}^3/\text{hr}$ . If the concentrations are representative of the average column concentration (the species are vertically well mixed), the reaction rates can be scaled by the average boundary layer height to give an instantaneous reactive flux. This will be the case as long as the oxidation lifetimes are sufficiently long relative to the vertical mixing timescales. Estimates of this mixing time can be estimated using the meteorological parameters of roughness velocity ( $u^*$ ) and Monin-Obukhov length ( $L$ , a measure of atmospheric stability) available for the field site. The diurnal average timescale ranges from 8 minutes during midday up to a maximum of 6.3 hours at night, with an overall daily average of 1.5 hours. This suggests that all the categories of carbon should be well mixed except VOCs (average lifetime 1.2 hr), though this will change over the course of the day. This reinforces the general point that the concentrations measured at ground level may not be very representative of the average concentration of the PBL for reactive species. Because VOCs are short lived however, the reactive flux can be estimated to be approximately equal to the total emission flux. Measured fluxes of the most important VOCs (and LLVOCs) are available for the BEACHON-ROCS field campaign that took place at the same field site the previous summer in Kaser et al.<sup>87</sup> These measured fluxes are out of the canopy, meaning that the amount of VOCs that react below the canopy must also be accounted for. This component is estimated by simply scaling the measured VOC reaction rate by the average canopy height (16 m), below which even VOCs should

Table 4.1: Flux estimates for chemically significant carbon categories

Category	Emission Flux <sup>a</sup> μg/m <sup>2</sup> /hr	Deposition Flux <sup>c</sup> μg/m <sup>2</sup> /hr	Reaction Rate <sup>d</sup> μg/m <sup>3</sup> /hr	Reactive Flux <sup>e</sup> μg/m <sup>2</sup> /hr
VOCs	1100±600 <sup>b</sup>	—	5.5±4.4	1200±700
OVOCs	—	300±200	1.2±1.2	600±600
PM	—	20±10	—	—
LLVOCs	600±400	—	0.07±0.04	30±20

All quantities are campaign averages  $\pm 1$  sigma calculated from day to day variability of the measured quantities (campaign average variance is calculated after removing the diurnal trend). <sup>a</sup>From Kaser et al.,<sup>87</sup> all fluxes are out of canopy. Includes MBO/isoprene, monoterpenes and acetaldehyde. <sup>b</sup>VOCs react within the canopy, contributing an additional  $90 \pm 70$  μg/m<sup>2</sup>/hr to the total flux. <sup>c</sup>Calculated and scaled using 520 m PBL. <sup>d</sup>From measured concentrations divided by estimated lifetimes. <sup>e</sup>Scaled using 520 m PBL except VOCs, which are sum of VOC emissions and reaction rate scaled by canopy height (16 m).

be well mixed. Gas-phase deposition fluxes are estimated using the average boundary layer height and average deposition velocities as a function of  $c^*$  for  $\alpha$ -pinene oxidation products from Hodzic et al.<sup>13</sup> A deposition velocity for aerosol particles representative of a forested environment was obtained from Zhang et al.,<sup>88</sup> and results in a deposition flux similar to the measured flux of organic particles in a similar forest environment.<sup>89</sup> These calculations are described in more detail in the Methods.

An examination of the fluxes shows that emission, oxidation (by OH and O<sub>3</sub>), and deposition of gas-phase carbon are all locally very important. Figure 4-5 shows the magnitudes of these fluxes as well as the pathways that connect the different categories for a vertical column of air. Carbon enters the system through in roughly equal amount through the emission of reactive VOCs and long lived VOCs. Carbon may also enter through transport, as well as entrainment of free tropospheric air as the planetary boundary layer rises each day, but these sources are difficult to constrain using the available measurements. The LLVOC carbon is largely a dead end with respect to the local oxidation chemistry, since this pool contributes little to the overall reactivity and has little potential to form aerosol through gas-phase oxidation. Reactive VOCs are much more complex, with oxidation leading to reactive OVOC products as well as organic aerosol, LLVOCs, and CO<sub>2</sub>. OVOCs and OA are

characterized by recycling arrows as well as significant deposition fluxes. The recycling arrow indicates that the overall oxidative flux includes a component that leads back to the originating category, and represents that fact that the oxidation products for some portion of the molecules in these categories may be themselves classified in the same categories. Heterogeneous oxidation of OA, for example, may generate oxidation products that remain in the condensed phase. For this reason, the total flux out of a given category may exceed the total flux in. It is also not necessarily the case that the measured concentrations and estimated fluxes represent a steady-state condition. Concentrations of LLVOCs especially would need to be much higher for the oxidation flux to be balanced by the total emissions. The opposite scenario (concentrations that greatly exceed steady state) are expected to occur as the LLVOCs are advected to more remote regions that lack such strong source terms.

### 4.3 Discussion

The trends in  $\overline{OS_C}$ ,  $c^*$ , and  $n_C$  observed are broadly consistent with the reaction of reduced emissions leading to oxidized, lower volatility products, and supports the assignment of IVOCs and OVOCs generally as oxidative intermediates to aerosol and  $CO_2$ . As the species become increasing oxidized through multiple generations of oxidation, more carbon is lost to fragmentation and deposition. This results in a decreasing mass concentration with decreasing volatility. Although some oxidized species are directly emitted, (e.g. acetaldehyde), the smoothly increasing average  $\overline{OS_C}$  indicates that emission is not the primary source of IVOCs and OVOCs. The trend in carbon number indicates that oligomerization and sesquiterpene oxidation play an important role in the reactions. Most of the reactive carbon is emitted with 5 or 10 carbons (MBO and monoterpenes), with a smaller amount at 15 carbons (sesquiterpene emissions are about 10% of monoterpene emissions<sup>87</sup>). Organic material with other carbon numbers presumably arises by a combination of oligomerization and fragmentation reactions. Sesquiterpene oxidation likely contributes both condensed and gas-phase carbon, but oligomerization is necessary to explain the carbon num-



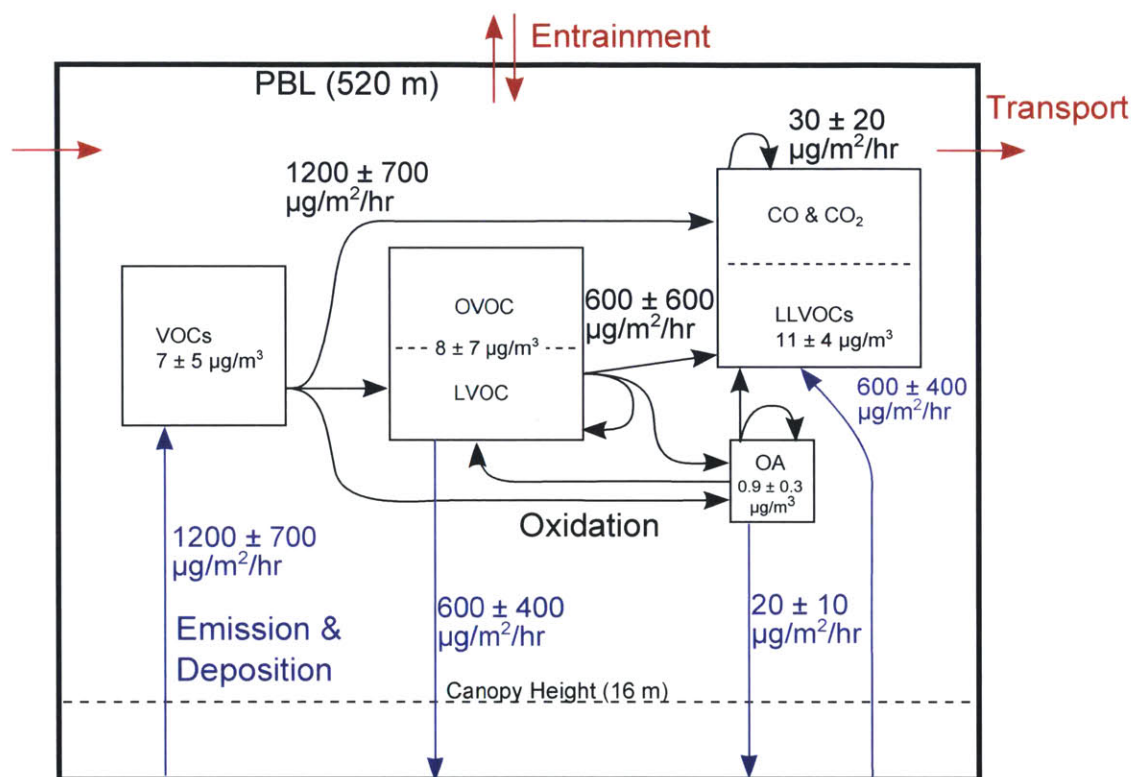


Figure 4-5: Approximate instantaneous carbon fluxes during BEACHON-RoMBAS are shown along with the arrows showing the connections between these carbon pools. The boxes representing each category are sized so that the area of the box corresponds to the measured average campaign concentration. Quantities are campaign averages  $\pm$  one standard deviation of the day to day variability in concentrations and fluxes (diurnal trend removed prior to calculation of variance). The fluxes in and out of each category may not be equal as a result of a lack of steady state conditions, and because some portion of the flux may recycle back into a given category. The overall emissions fluxes of VOCs and LLVOCs are approximately equal, but have a very different fate and contribution to the overall photochemistry.

bers above 15 that are seen for gas-phase acids. It is also important to note that the because the AMS and TGO have average carbon numbers calculated from a single volatility, each point is an average along an isopleth in  $n_C$  space (see Figure 4-7 in Methods). This suggests that the least volatile aerosol bin contains both material with carbon numbers higher than 15 and a lower  $\overline{OS_C}$ , and carbon numbers lower than 15 with a higher  $\overline{OS_C}$ .

Taken together, the new instruments and methods described here (TGO, TAG, MOVI-CIMS and inclusion of small PTR-MS ions) increase the total measured loading of carbon by  $11 \mu\text{g}/\text{m}^3$ . This accounts for 40% of the total, and therefore roughly doubles the observed carbon concentration. Furthermore, the VOCs that are typically measured are not very reactive and unlikely to contribute to aerosol formation. When compared to just the reactive carbon, the new methods account for 75% of the total, or a factor of 4 increase. The measured IVOCs also account for 60% of the total carbon with high aerosol formation potential. Although substantial and compelling, these relative enhancements are likely highly dependent on location and the specific measurement suite. Total observed organic carbon (TOOC) has been reported previously in Heald et al (2008). and de Gouw et al (2009).<sup>90,91</sup> The measurements here are probably most similar to those at the forested Thomson Farm site in Heald et al, although differences in the type of vegetation are significant. This site has a total organic loading of  $17 \mu\text{g}/\text{m}^3$  after subtracting species not measured during BEACHON-RoMBAS (light alkanes like ethane), suggesting that another  $13 \mu\text{g}/\text{m}^3$  of IVOCs and OVOCs might be present, for a total loading of  $32 \mu\text{g}/\text{m}^3$  including light alkanes. Comparisons to other locations can be made by considering how far downfield of emissions sources these locations are. Generally, the farther from emissions sources, the greater the enhancement in longer lived species relative to shorter lived species. In the remotest environments (perhaps representative of the global average), the bulk of the total carbon will be in the form of particulate matter and long lived VOCs simply because these groups have the longest atmospheric lifetime. This again highlights the importance of considering atmospheric lifetime. This also likely tends to increase uniformity by reducing the number of species only to the

most persistent. Locations closer to emission sources are expected to have a larger relative enhancement because the IVOCs and OVOCs are also relatively short lived. Locations closer to strong anthropogenic emission sources are also likely to be very different, and possess qualities of the IVOCs and OVOCs that reflect the difference in source type. Similar studies in a variety of locations would be beneficial in order to understand how the concentrations as well as the fluxes differ. Differences in topography and meteorology between otherwise similar locations especially could have significant effects on deposition, with significant feedbacks into aerosol formation.

The reactive flux measurements underscore the great difference between the reactive VOCs and the long lived VOCs. Total reactivity is dominated by a handful of individual VOCs, representing only 57% of the emissions but 52% of the reactive flux. The long lived VOCs, also a fairly small number of compounds, represent 43% of the total emissions, but only 2% of the reactive flux. The relative importance of LLVOCs is of course expected to increase in more remote locations where the reactive VOCs have all reacted away, but under the conditions present during BEACHON-RoMBAS, these compounds can be considered nearly non-reactive.

Although the approximations and assumptions made in order to construct the fluxes and burdens presented in this manuscript are expected to be reasonable, some drawbacks to using field data remain when considering carbon in a holistic sense. Primary among these is that even if a compelling argument is made that there should be little remaining missing carbon, there is no measurement of total organic carbon (TOC) available to compare to in order to gauge the performance of the instrument suite and the methods. This suggests that a clear next step is to conduct a study with a similarly complete instrument suite under the much more controlled conditions of environmental reaction (“smog”) chamber, where the total carbon may be precisely controlled. With suitable instrumentation, this would allow some of the formation rates (e.g. for CO<sub>2</sub> and LLVOCs) to be estimated, generating a much more complete picture of the fluxes in figure 4-5. This would also enable a careful cross calibration to be performed, greatly improving constraints on measurement overlap. With improved control over the chemistry, it may also be possible to not only estimate the magnitude

of the total reaction rate (the sum of all the reaction arrows exiting each box), but also to estimate the rates of the individual pathways. For the reactive intermediates (IVOCs + OVOCs), this would require precisely constraining the formation rate of LLVOCs and aerosol, thereby determining the feedback term. Developing methods for constraining these formation rates using field data should likewise be an important goal for future research.

## 4.4 Methods

Methodological details are briefly described below.

### 4.4.1 Data Selection and Averaging

The values reported in this work reflect campaign averages for instruments with somewhat different measurement periods. This is expected to be reasonable given the relatively uniform time series, in which the approximately the same concentrations and diurnal patterns were measured day to day for all instruments. Figure 4-6 shows the full time series for monoterpenes (panel A) and OA (panel B) plotted diurnally such that the overall variability is apparent. Monoterpenes are highly reactive and drive much of the oxidation chemistry, and therefore should give an upper limit to the amount of variability within the dataset. OA is much longer lived, and should give a lower limit to the variability due to day to day differences in chemistry. Both quantities have approximately a factor of two spread in their concentrations, with the exception of a few much higher points for monoterpenes which do not significantly impact the overall average. This indicates that there were no significant departures from “typical” chemistry during the campaign, and supports the use of an overall diurnal average. The concentrations and calculated fluxes also vary over the course of the day, but these differences do not significantly change the overall conclusions, and a 24 hour average is therefore used for the non-diurnally-resolved data.

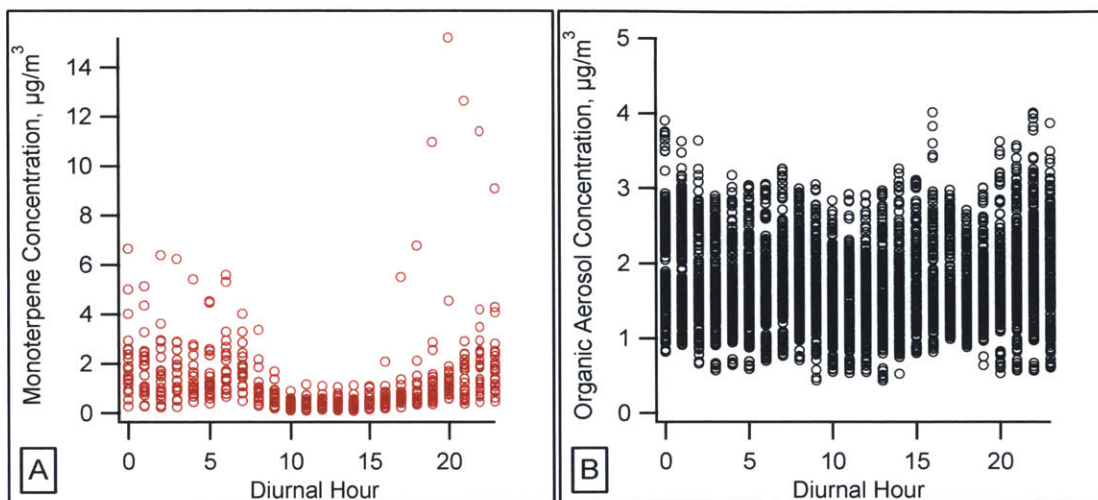


Figure 4-6: Variability in measured quantities during BEACHON-RoMBAS is shown through the campaign time series of monoterpenes (panel A) and organic aerosol (panel B). The variability is approximately a factor of two for both monoterpenes (short lived) and organic aerosol (long lived) with no significant departures from the average diurnal profile excepting a handful of points. This suggests that the chemistry was similar day to day, and supports the comparison of average data from instruments in this study that had different sampling periods.

#### 4.4.2 Estimates of $\overline{OS}_C$ , $n_C$ , $c^*$

The instruments used for this study all have the same ToFwerk time of flight mass spectrometer, which has a sufficient mass resolution to tell apart ions at the same nominal mass (e.g.  $C_3H_7^+$  and  $C_2H_3O^+$  at  $m/z$  43). The estimates of  $\overline{OS}_C$  are generated in two different ways. For the instruments that measure individual species (MOVI-CIMS, PTR-MS as ions, TAG as chromatographic peaks), the  $\overline{OS}_C$  is calculated by applying the formula for  $\overline{OS}_C$  ( $\overline{OS}_C \approx 2 \times O/CH/C$ ) for each ion or identified molecule. Averages (for all instruments and quantities) are calculated by weighting by carbon mass. For bulk measurements using electron impact ionization (TGO, AMS, TAG), the mass spectrum is mostly composed of small fragments.  $\overline{OS}_C$  is calculated from the average O/C and H/C of the ion distribution in this case, as described in Aiken et al.<sup>47,92</sup> Correction factors to account for systematic undercounting of oxygen are available only for the AMS, for which the most up to date factors are used.<sup>93</sup> The O/C may be biased slightly low for the TGO and TAG as a result.

Each instrument provides the  $\overline{\text{OS}}_C$  and either the  $n_C$  or  $c^*$ . The remaining quantity can be estimated (for unidentified constituents) using structure activity relationships that interrelate the three variables. The instruments that measure individual species provide  $n_C$  directly from the ion or molecular formula. The  $c^*$  is estimated for these instruments by starting with the base vapor pressure of an alkane of the same  $n_C$  and adding functional groups according to the  $n_O$  and the best estimate for the predominant type of functional groups present. Although approximate, this method has been used previously for the MOVI-CIMS and is described in Yatavelli et al. 2014.<sup>83</sup> For the MOVI-CIMS, the best estimate for volatility is obtained by assigning the first two oxygen atoms to an acid group and the remaining ions to hydroxyl groups. For the PTR-MS, oxygen atoms are assigned to carbonyl groups, because molecules with these groups are the most likely to pass through the long, unheated Teflon inlet of the PTR. For the TGO, TD-AMS, and the bulk TAG approach the volatility is directly measured (based on interpolating between reference compounds with known volatility, a method discussed further in section 4.5) and the  $n_C$  must instead be estimated. In all cases, this is done using a formula from Daumit et al.,<sup>53</sup> which is based on the approach of Pankow and Asher.<sup>94</sup> Although each volatility bin is assigned a single  $n_C$ , it is likely that a distribution of  $n_C$  is present, corresponding to the distribution of  $\overline{\text{OS}}_C$  in each bin, as shown in Figure 4-7. Uncertainties due to these methods are significant, likely up to several orders of magnitude in  $c^*$  and 3 or more carbon atoms in  $n_C$ . Wherever possible, literature values for  $c^*$  (and all other quantities) have been used (e.g. for the identified/calibrated PTR-MS compounds listed in figure 4-3) in order to reduce these uncertainties.

### 4.4.3 Instrument Scope and Overlap

The instrument suite has only one instance of explicit measurement overlap—formic acid is measured by both the PTR-MS and the MOVI-CIMS. For this analysis only the MOVI-CIMS measurement of formic acid was kept, because it is likely that this is a more robust measurement (formic acid is “sticky” and may sorb to the long unheated Teflon inlet of the PTR-MS). The AMS is also likely a complete measurement of



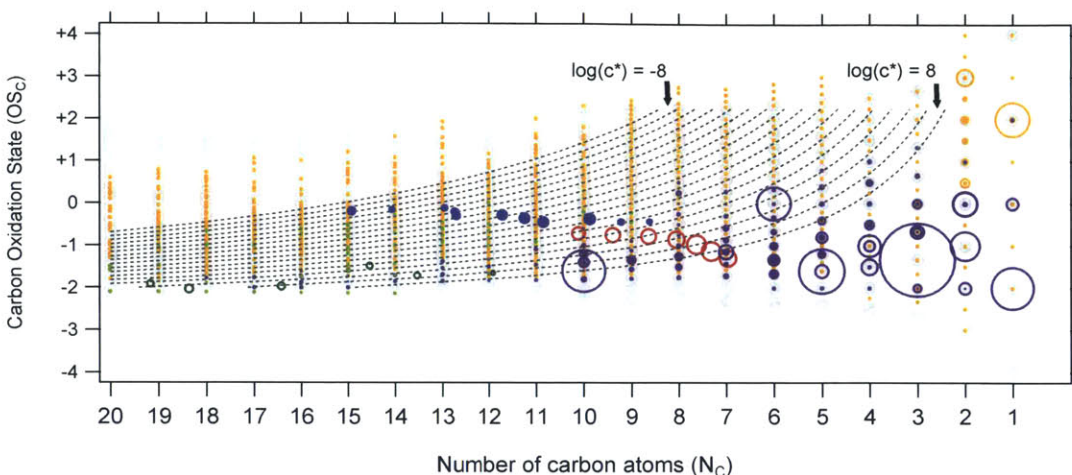


Figure 4-7: Volatility contours in  $\overline{OS}_C$ - $n_C$  space. The contours are calculated using the formula for  $n_C$  from Daumit et al.<sup>53</sup> using the Van Krevelen slope from Heald et al.<sup>73</sup> to convert  $\overline{OS}_C$  to O/C and H/C. The result is that for a point with a given  $c^*$  (e.g. the TD-AMS and TGO bulk average points), the composition will be an average of compounds that lie between a given pair of contour lines.

the particle-phase in itself, and so in most calculations the total concentration and  $\overline{OS}_C$  contribution of the MOVI-CIMS particle phase was not included. It has been included in figures however because it provides important additional information on the composition of the particle phase. Although the instrument suite is relatively complete, and provides new information on the importance of IVOCs and OVOCs, there was one major category of carbon that was not included: light alkanes with  $n_C < 10$ . These species are relatively long lived, with low aerosol formation potential, but would be expected to contribute a few  $\mu\text{g}/\text{m}^3$  to the total carbon measurement, and care should be taken when comparing to other data sets. Other overlaps may exist but are expected to be less significant and more complex.

#### 4.4.4 Flux Calculations

The oxidative fluxes are estimated by dividing the concentrations by the overall (OH + O<sub>3</sub>) oxidation lifetime, and then multiplying the resulting reaction rate by a mixing height (either the canopy or PBL height) to give units of mass per area per time. The OH rate coefficients are taken from the literature when available, and are oth-

erwise estimated using the relationship in Donahue et al.<sup>49</sup> This method accounts for differences in the OH coefficient due to the number of carbon atoms, the number of oxygen atoms as well as the number of remaining abstractable hydrogens. This method also includes the “trapping effect,” wherein oxidation slows for low volatility compounds primarily in the condensed phase. The estimate is fairly approximate, and the predicted rates have not been rigorously compared to literature values in order to estimate uncertainty. The rates could be up to a factor of 3-5 in error. Ozone rate coefficients are more difficult to estimate because they depend almost entirely on the presence or absence of double bonds. Although the number of double bonds can be estimated using the elemental formula, the presence of abundant cyclic structures in biogenic emissions makes this impractical. As a result, literature values for ozone coefficients are used exclusively, and are assumed to be zero for all other ions. This may lead to significant underestimation of the total oxidation rate if reactive double bonds are important for other compounds. The emission fluxes are 24 hour averages of data from the same site from a field campaign the previous year. Although the campaign was during approximately the same time period, year to year variability may lead to differences in the fluxes and to additional uncertainty in the overall estimates of mass balance. The meteorology for 2011 and 2010 was generally very similar (the diurnal temperature profile for 2011 is about 2 °C higher), suggesting that the differences due to meteorology should be small. Deposition fluxes are estimated using the relationships in Hodzic et al for deposition velocity as a function of Henry’s law constant coupled with predictions of Henry’s law constant and  $c^*$  for  $\alpha$ -pinene products produced by the GECKO atmospheric chemistry mechanism generator.<sup>13</sup> The deposition velocities estimated in this way start at 0 cm/s for volatile products and plateau at 4 cm/s for low volatility products. Although this method results in considerable uncertainty, it is an improvement over simply assuming a deposition velocity from a single representative compound as has been done in other cases.<sup>95,96</sup> Deposition velocities for particles are a representative range for forested land from Zhang et al.<sup>88</sup>



#### 4.4.5 Key Uncertainties

The ranges for concentrations and fluxes given in Figure 4-5 are representative of the day to day variation in these quantities, and therefore includes both real differences in the quantities over the campaign as well as instrument noise. Each of these values also has associated measurement and calculation uncertainty that may be significant and is not always well quantified. As discussed in the methods, many of the concentrations measured with speciated instruments are uncalibrated, instead relying on a generic response factor. This might be in error by up to a factor of two for any one ion, though the average for the very large number of ions in the data set should be associated with a correspondingly smaller error. A similar issue exists for the TGO, which has been calibrated for alkanes but not for oxygenated species. TD-AMS concentrations are the most robust, with errors on the order of 10%. The methods for estimating the saturation concentration for speciated compounds are significantly more uncertain. In the best case (for the TGO and TD-AMS) this uncertainty is approximately one order of magnitude, and may be as high as three for the speciated instruments such as the MOVI-CIMS and PTR-MS. The fluxes use the concentrations as inputs and so are at least as uncertain. The uncertainty in the calculation methods for oxidation and deposition is not well quantified, but likely represents another significant source of error. For the oxidation methods this is mainly due to error in calculating OH rate coefficients with a reduced set of information (carbon number and oxygen number). Because the role of molecular structure is important, this error may not be highly reducible, but can at least be estimated by comparing estimated rates to measured rates in a more rigorous manner. A similar approach should be undertaken for deposition rates. Together, the methods for volatility, reaction and deposition represent the greatest source of uncertainty and therefore can give the greatest potential improvement to Figure 4-5 once better methods are available.

## 4.5 TGO Description, Calibration & Analysis Methods

The TGO is a simple, robust and fast technique that can characterize the vapor pressure resolved amount and composition of atmospheric LVOCs. The instrument uses cryogenic trapping of analytes followed by temperature programmed desorption to determine mass concentrations and bulk chemical composition as a function of volatility. The volatility resolved data (thermograms) are not unlike chromatograms, that have been optimized for maximum transmission (e.g. of sticky, oxidized LVOCs) and time resolution over peak resolution. The instrument has been described previously by Cross et al.<sup>86</sup>

A diagram of the TGO is shown in figure 4-8. The basic configuration and operation of the instrument is as follows. Analytes enter the instrument through a heated, passivated stainless steel inlet tube to a six port valve which permits two distinct flow modes. In sample collection mode, air is drawn through a cryogenically cooled sample loop, where gas phase LVOCs condense onto the loop walls. In sample injection mode the sample loop is heated, and condensed materials undergo a temperature programmed desorption. Helium carries the sample through the loop and through a short capillary into the source region of an electron impact (EI) ionizer. Ions are directed into a high resolution time of flight mass spectrometer and data are saved at rates up to 10 Hz. Sample loop temperature data allow the mass spectrometric data to be displayed as thermograms for each collection-desorption cycle. Data are analyzed using standard modules for the Aerodyne HR-ToF-AMS in combination with custom modules for analyzing the MS-thermogram data.

The inlet tubing is constructed primarily of 1/4" stainless steel tubing that has been coated with SilcoNert 2000 (Silcotek Sulfinert) to maximize transfer of oxygenated LVOCs.<sup>97</sup> All fittings are Sulfinert coated stainless steel swagelok. The inlet tubing is uniformly heated using heating tapes composed of nichrome wire covered in fiberglass insulation. Temperature is measured with K-type thermocouples, and a stable, uniform temperature of 250 °C is achieved using commercial PID controllers

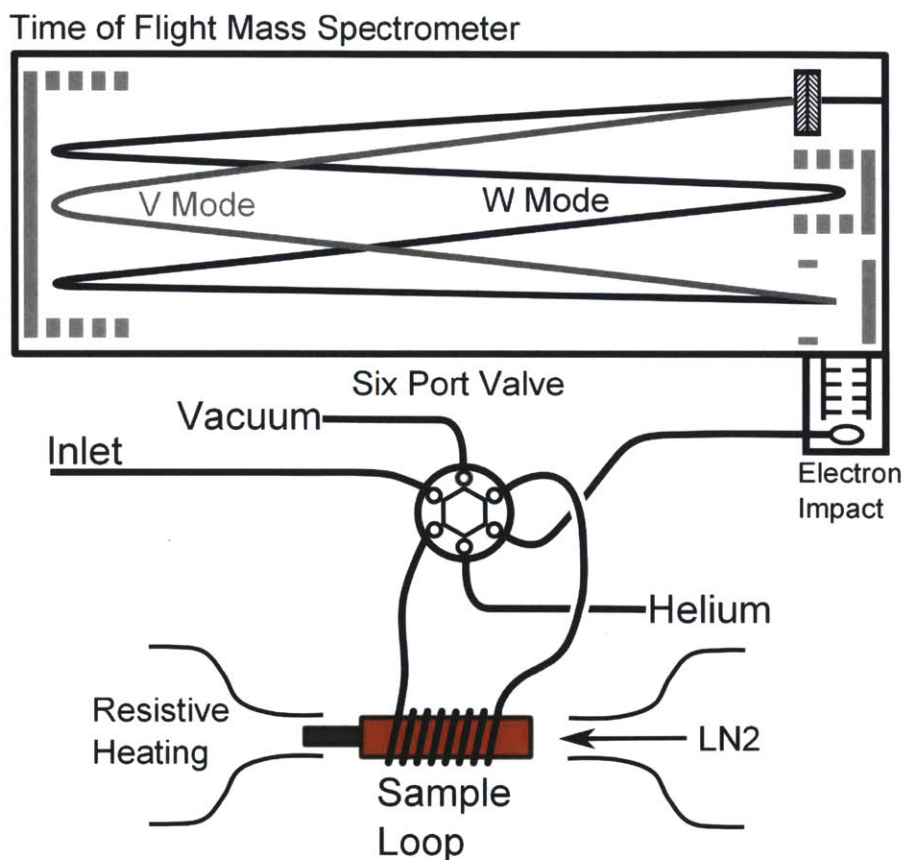


Figure 4-8: A diagram of the TGO instrument. In collection mode, the sample gas is pulled through a 1/4" passivated stainless steel line through a cryogenically cooled sample loop. In desorption mode, UHP helium flows through the sample loop into the electron impact, high resolution, time of flight mass spectrometer. A controlled, linear sample loop temperature ramp separates the analytes by volatility.

(Omega Engineering). The six-port valve is coated with the Inertium coating developed by AMCX, L.L.C.. The sample loop consists of approximately 6" of 1/16" diameter coated stainless steel tubing. The transfer capillary is approximately 30 cm long with a 100  $\mu\text{m}$  I.D. and is also composed of Sulfinert coated stainless steel. The Sulfinert and Inertium coatings are both silica based, and are intended to cover otherwise possibly chemically active metal surfaces. The cryogenic trapping system consists of a sample loop that has been wrapped around a copper cylinder to facilitate thermal energy transfer. Heating of the loop occurs via a cartridge heater that rests in a hole bored down the center of the copper cylinder. Cooling is achieved by directing the gas blow off of a liquid nitrogen dewar at the top of the copper cylinder. Heating utilizes a computer controlled PID for maximum stability, with the heating cycle fully programmable in terms of ramp rate, starting and ending temperature and temperature soak. Typical temperature ramps vary from 3 to 10 minutes depending on the data being collected, and reach a maximum temperature of 280-320  $^{\circ}\text{C}$ . The cooling is computer controlled, and the collection temperature is normally maintained within a few degrees of the desired set point. Collection temperatures range from -15 to 20  $^{\circ}\text{C}$ , with the lower limit for a given air sample being set by the absolute humidity.

The mass spectrometer assembly used is nearly identical to that used for the Aerodyne HR-ToF-AMS, which has been extensively described in the literature.<sup>46,98</sup> The electron impact filament used is a standard Balzer ion cube operating at an energy of 70 electron volts. Ion optics direct the generated ions through a quadrupole and into a rectangular time of flight region that can be operated in two modes. In 'V' mode, the ions are reflected once across the rectangle, forming a V shaped trajectory. The mass spectrometric resolution, defined as  $R = M/\Delta M$  where  $M$  is the nominal mass and  $\Delta M$  is the minimum difference required to distinguish two closely spaced peaks, is approximately 2000 to 2500 for this mode. In 'W' mode, the ions are reflected three times, forming a W shaped trajectory. The longer ion path length results in approximately doubled resolution of 4000 to 5000 at the expense of reduced signal-more ions are lost due to the increased time spent in flight. The ion detection technology utilizes a micro-channel plate (MCP), an array of a large number of very

small electron multipliers arranged to cover a relatively large surface area. The large surface is required to account for both spread and unpredictable positioning in the ion beam during flight. Signals are amplified and transmitted to a data acquisition computer outfitted with an Agilent AP-240 card. The key feature of this card is its 2 GHz bandwidth, required for coping with the nanosecond scale differences in flight time for closely spaced ions in mass to charge space.

## 4.6 Calibration Methods

### 4.6.1 Mass Concentration Calibration

In order to compute mass concentrations, raw data are first converted into ion counts (Hz). Because the ionization probability of a given molecule is dependent on the number of electrons in a molecule, and this is proportional to the mass of the molecule, ion counts are proportional to mass of compound in the ionization region, and may be converted to mass using an appropriate constant. Because ionization efficiency does not vary appreciably for organic molecules, a single conversion factor from ion counts to mass may be used, provided no other biases exist. To compute the total mass of LVOCs in a given mass spectrum, the sum of organic ion counts for a given data point is computed, and an analogous sum computed for a measurement of background signal (usually ultra zero air). For typical unit mass resolution data, organic signal is separated from inorganic signal by applying a filter to the data to exclude ions at  $m/z$  that are primarily inorganic (e.g. 28, 32, 40, 44). The background signal is subtracted from the sample signal, and the difference in ion counts is multiplied by an empirically measured proportionality constant to convert to total mass. This empirical measurement is performed by vaporizing a compound (typically hexadecane or  $\alpha$ -pinene) at a known rate into the sample gas stream using a syringe pump or diffusion cell. For the syringe pump, the flow rate and infusion rate are both known, permitting an accurate calculation of gas phase concentration. The diffusion cell consists of a capillary that has been coated with a given LVOC (by passing a liquid

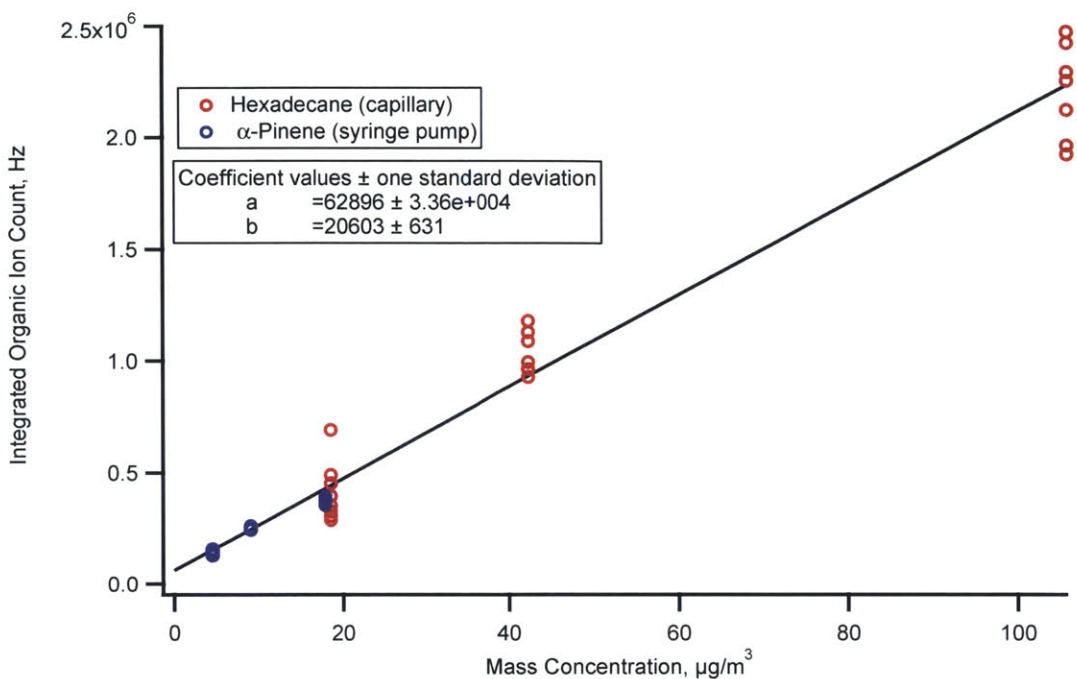


Figure 4-9: TGO mass calibration. A calibration for the conversion of total organic ion counts into organic mass. Known concentrations were produced using a diffusion cell for hexadecane and a syringe pump for  $\alpha$ -pinene. The calibration constant (slope) incorporates the collection and transmission efficiency, which is the same for both molecules for the sampling parameters used during calibration.

drop through). Pressure is then applied to the capillary, resulting in a controlled flow of saturated vapor, the rate of which can be measured using an appropriate flowmeter, or calculated using Poiseuille's equation. Calibrations are performed using at least three gas phase concentrations to check for linearity. A calibration plot from the BEACHON-RoMBAS campaign is shown in figure 4-9. Because oxygenated compounds are important in ambient air and may have different response factors, future calibration work should focus on this category. Preliminary work suggests that molecules with single carbonyl and hydroxyl functionalities should survive the high inlet temperatures, but that acids may be degraded.

#### 4.6.2 Volatility Calibration

To compute LVOC mass as a function of volatility, individual desorptions are split into bins computed using measured desorptions of  $n$ -alkanes with known saturation va-

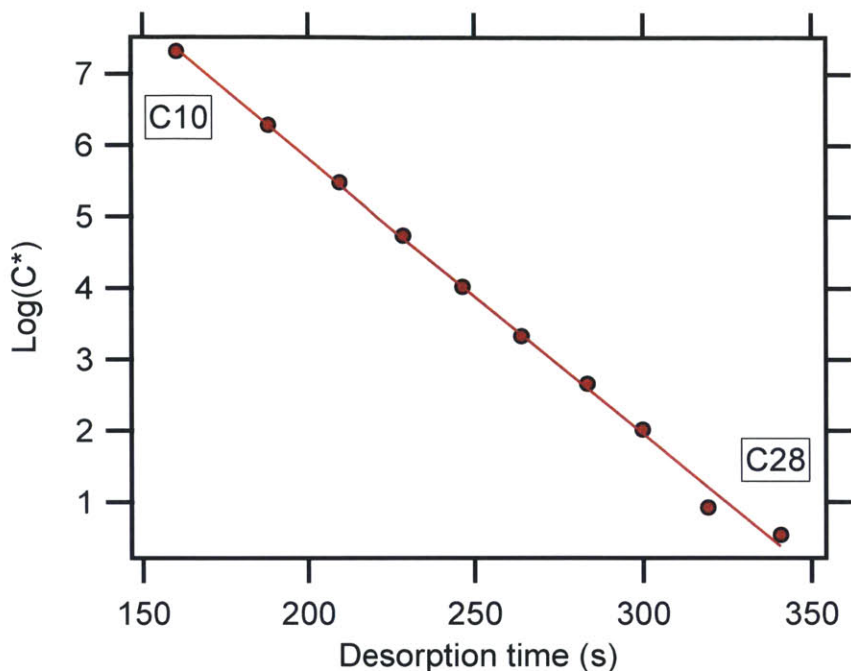


Figure 4-10: Empirical desorption times for alkanes measured by the TGO. The known saturation vapor pressures of these molecules can be interpolated with a linear fit, yielding an estimate of volatility for material desorbing at any time or temperature.

por pressures. The relationship between desorption temperature and vapor pressure is linear, and because the temperature ramp is itself linear, equivalent bin boundaries can be drawn in both temperature and time space. The measured desorption times during the BEACHON-RoMBAS campaign are shown in Figure 4-10. Conversion to  $c^*$  bins involves integrating between the boundaries and subtracting an appropriate background (discussed further in section 4.7 below). The basic binning, integration and subtraction process is illustrated in figure 4-11. The measured desorption times/temperatures are likely to be a function of the sorption characteristics as well as the vapor pressure of a given molecule, and are therefore likely different for oxygenated molecules. The reported volatilities are therefore alkane-equivalent volatilities, and future calibration efforts should be directed at determining the response of other classes.



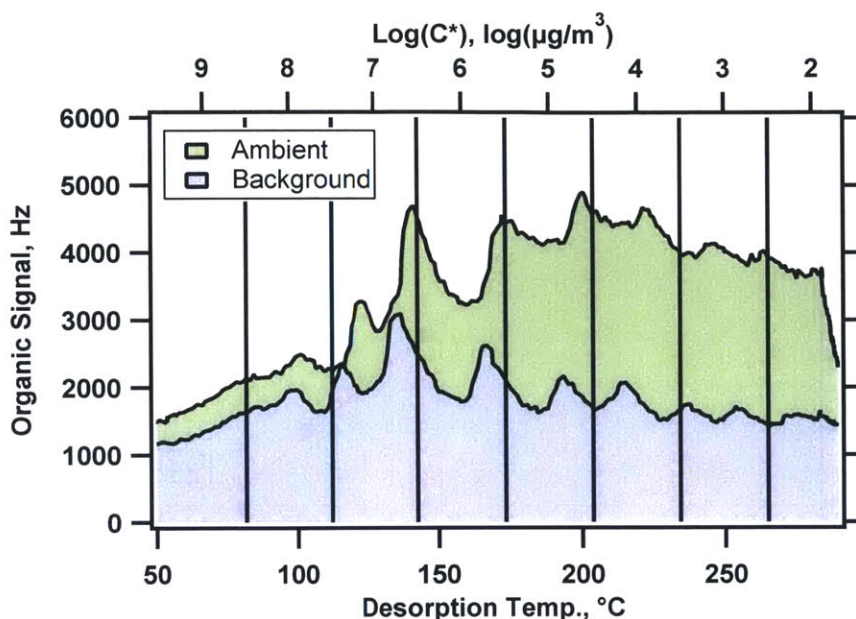


Figure 4-11: TGO volatility binning, integration and subtraction. The concentration for a given volatility bin is found by integrating ambient signal between bin edges and subtracting integrated blank signal.

## 4.7 Analysis Methods

### 4.7.1 Processing Routines

The data analysis procedures for the TGO use the Squirrel and Pika modules available for the computational software Igor Pro (Wavemetrics, Lake Oswego, OR). High resolution data permits a much more sophisticated analysis but requires considerably more processing time (approx. 7.5 hours of computation per 24 hour data collection period). Separation of organic and inorganic ions is greatly simplified, since individual ions can be quantified within a single nominal mass (e.g.  $\text{CO}_2^+$  and  $\text{C}_2\text{H}_4\text{O}^+$  at  $m/z = 44$ ). Since the composition of individual ions is known, elemental analysis is possible by summing the total signal for carbon, hydrogen, oxygen and nitrogen for all ions, a procedure that has been described in the literature.<sup>47,92</sup> The correction factors described in Aiken et al. (accounting for systematic undercounting of oxygen due to electronegativity) have not been measured for the TGO. The TGO is also unable to quantify  $\text{CO}_2^+$  due to significant gas-phase interference. Together, these two effects



likely lead to an estimate of the O/C that is biased low (this may be seen in Figure 4-1. Elemental analysis is performed with same codes for summation and background subtraction as computations of organic mass.

#### 4.7.2 Background Subtraction

Background subtraction procedures involve the subtraction of an appropriate thermogram for an LVOC-free air sample (zero air was used during BEACHON-RoMBAS). Blank thermograms are taken at least twice a day (preferably more often) to check for zero-drift and the possibility of accumulating low-volatility material. At least two blank desorptions are taken in order to assess variability. Once an appropriate blank thermogram is identified, it is subtracted from the sample desorptions. This step can be performed in temperature space or in time space as long as the temperature ramp is sufficiently uniform from desorption to desorption, which was the case during BEACHON-RoMBAS. Several additional steps are necessary to maximize the quality of the resulting data, shown in Figure 4-12. These steps are necessary because of three eccentricities of the TGO instrument. The first is that the tungsten filament is subject to rapid erosion, significantly increasing emission current over the course of the day, and thereby affecting the ionization efficiency (number of ions produced per microgram of sample). To counteract this, a calibration for signal as a function of emission current was performed (Figure 4.7, panel B), and the fit function used to normalize all data points to an emission current of 1.0 mA (matched to the value used for the mass calibration). The second is that the signal intensity fluctuates from desorption to desorption independently of the emission current and independently of the total organic loading. The initial part of each desorption is entirely due to air ions, and should be essentially identical in all desorptions. Sample desorptions are therefore multiplicatively normalized such that the air signal matches that of the blank desorption, shown in 4.7, panel A, region 1. These corrections are on the order of 5%. The last issue is that due to irregularities in the triggering and recording of mass spectra, the desorptions have a small random offset of up to 5 seconds. This is present in temperature as well as time space. The offset is difficult to separate

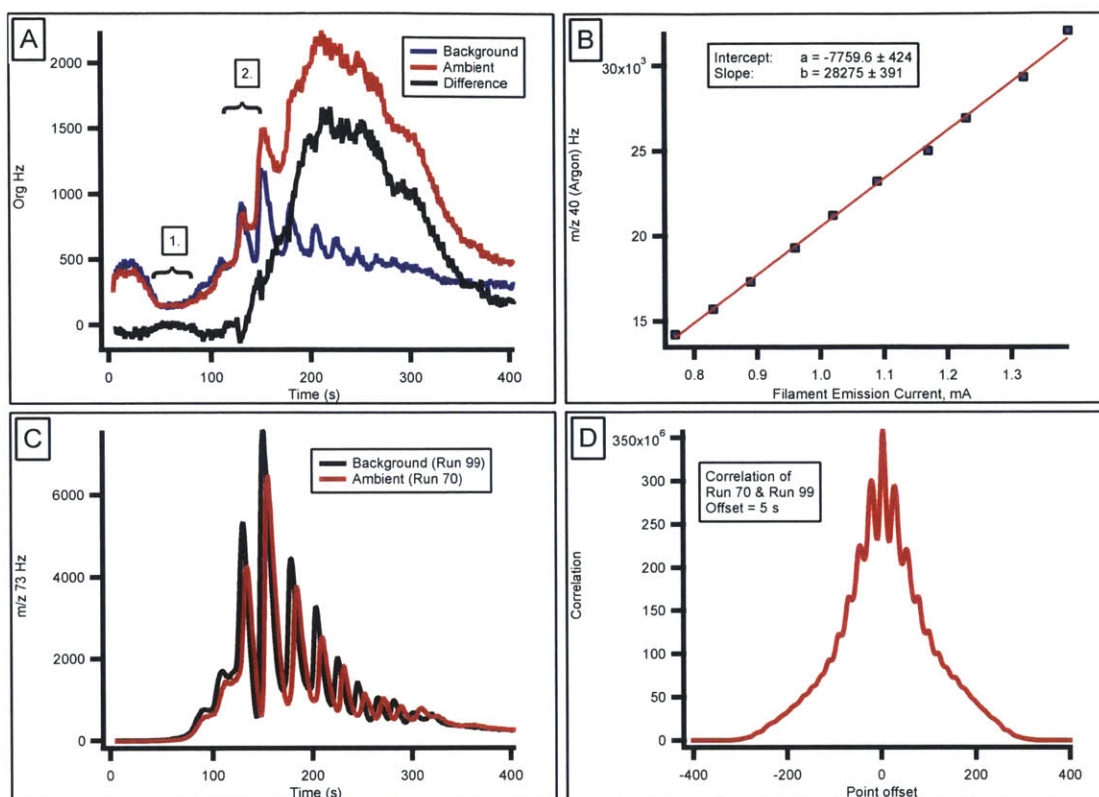


Figure 4-12: Details of TGO data analysis

from real differences in the desorption, and can lead to large changes in the apparent volatility distribution if not accounted for, especially around sharp peaks (see 4.7, Panel A, region 2). Fortunately, the presence of siloxanes functions as an internal standard due to their narrow peak shape and consistent profile run to run with the exception of the time offset, shown in 4.7, panel C. The time offset is determined by correlating m/z 73 (mostly due to siloxane signal) for the sample and blank desorptions, and applying a peak finding routine to the resulting profile (Figure 4.7, Panel D).

# Chapter 5

## Conclusion

### 5.1 Summary

A critical need exists to improve characterization of atmospheric organic carbon and its transformations. Unacceptable uncertainties exist in our ability to predict the effects of organic emissions on human health and climate. Much of this uncertainty is rooted in the transformations of low volatility intermediates of oxidation processes, which has motivated the work described in this thesis. This work constitutes a significant advancement in our understanding of the role of OVOCs in the cycling of atmospheric organic carbon, and especially in the formation and evolution of organic particulate matter.

From studies on aging, we have learned that continued oxidation of intermediates leads to significant additional aerosol formation, but that this oxidation does not lead to the highly oxidized aerosol observed in the atmosphere. These observations were explained through the process of condensational trapping, in which oxidation greatly slows once molecules partition to the condensed phase. Because the condensation point is a function of composition, this leads to aerosol that oxidizes very little with increasing OH exposure. These results are important for explaining the yields of aerosol when OH exposures are elevated (under downfield conditions), and also indicate that means other than simple OH aging must be sought to explain the rapid production of highly oxidized aerosol. In order to properly represent aerosol yields

for use in models it is necessary to account for changes due to aerosol concentration as well as OH exposure, and to design experiments that make this possible.

From studies on the effect of cyclic moieties, we have learned that C-C scission is a key channel for OVOC intermediates, and that the fragmentation pathways increase with increasing generation of oxidation. Because of this, the fate of carbon can be affected by loading, because trapping at earlier generation of oxidation will result in less fragmentation. In order to fully explain the yields and properties of aerosol, it is necessary to understand the effects of carbon-carbon scission over the full multigenerational chemistry that leads to aerosol formation. Although the branching in the first step of oxidation is also important, it is one step in a multi-step process, and even molecules that are extremely unlikely to fragment initially can be dominated by fragmentation in their overall chemistry.

From direct measurements of OVOCs along with VOCs and organic aerosol, we have learned that oxidized intermediates are abundant, and that (at the field site studied) both lower volatility intermediates to aerosol and high volatility fragmentation products account for about as much carbon mass as volatile emissions. New techniques were found to be essential in measuring the full region of volatility space and oxidation state space between volatile emissions and organic aerosol. The results also highlighted the importance of considering reactivity and role when classifying organic carbon, since many compounds that have very high concentrations have very slow reaction rates, such that considering concentration alone can be misleading. Overall, oxidized intermediates were found to play a dominant role in the overall fate of carbon, through their significant concentrations, oxidation and deposition fluxes.

Altogether, intermediates have been shown to be chemically active, ubiquitous, and important in the lifecycle of organic carbon in the atmosphere. When volatile carbon is emitted, it undergoes oxidation and generates large quantities of intermediates. These continue to oxidize, and over multiple generations will form organic aerosol as well as smaller fragments that eventually make CO<sub>2</sub>. The yield and properties of organic aerosol depend not only on the branching between fragmentation and functionalization pathways, but also on the magnitude of deposition. Because depo-

sition of intermediates appears to be significant in the ambient atmosphere, yields may be lower than those in chambers, where vapor losses appear to be less significant (and are certainly different than ambient conditions). By regulating the amount of aerosol, these processes also regulate its degree of oxidation through the phenomenon of trapping. Direct measurements have confirmed the abundance and importance of intermediates and their role in these processes, and despite the challenges associated with making these measurements, it is essential that they be included in the future when organic aerosol and VOCs are also being measured.

## 5.2 Implications and Research Prospectus

The work described in this thesis has significant implications, both for the atmosphere, as well as the conduct of future research on VOC oxidation and aerosol production. In general, in order to properly represent the impact and fate of organic compounds in the atmosphere it is necessary to explicitly include the full range of their oxidation products. To accurately represent aerosol yields and production kinetics for example, it is necessary to include multigenerational chemistry that reflect the fact that initial oxidation of VOCs often does not in itself generate significant concentrations of condensable products. Experiments must be designed to enable the effects of OVOC oxidation to be measured. This means oxidizing VOC and product mixtures to completion, and conducting multiple experiments such that the effects of condensational trapping and OH exposure can be disambiguated. For the atmosphere, including intermediates can lead to significant changes in the overall sinks of carbon, and it is expected that, with better measurements of the production of CO<sub>2</sub> and other long lived oxidized gases, it may be possible to close the budget for emitted organic carbon. Improved measurement technology will allow model output of concentrations of intermediates to be compared to measurements in much the same way as for organic aerosol, opening the door to a wealth of future research opportunities.

This work also motivates specific research objectives that are a direct extension of the work completed so far. Because of the complexity of measuring intermediates

in the ambient environment (e.g. the lack of known total carbon concentration), it is desirable to conduct similar measurements to those described in Chapter 4 (with an equally complete or more complete instrument suite) under more controlled circumstances in an environmental chamber. Similarly, the work on aging and fragmentation in Chapters 2 and 3 would be strengthened through explicit measurements of the intermediates that are implicated in controlling aerosol yield and properties. The scope of the aging work should also be expanded to include oxidation under other conditions (e.g. other oxidants, and other OH sources) in an effort to better constrain oxidative and non-oxidative changes to composition. Oxidized intermediates are expected to play key roles in other aging mechanisms, and so it is essential that they be considered as these systems are investigated. The preliminary work on high RH OH aging is especially interesting due to the differences in the resulting aerosol time series, and future work should focus on exploring the magnitude of these effects for molecules other than  $\alpha$ -pinene, on connections to other modes of aqueous particle aging,<sup>12</sup> and on the role of photolysis in this chemistry.

# Appendix A

## Glossary of Acronyms

**VOC** volatile organic compound

**POA** primary organic aerosol

**SOA** secondary organic aerosol

**PM** particulate matter

**O/C** oxygen to carbon ratio

**H/C** hydrogen to carbon ratio

**N/C** nitrogen to carbon ratio

**RH** relative humidity

**HFB** hexafluorobenzene

**LPM** liters per minute

**HR-ToF-AMS** high resolution, time of flight aerosol mass spectrometer

**SMPS** scanning mobility particle sizer

**c<sub>OA</sub>** concentration of organic aerosol

**HC** hydrocarbon

**DBE** double bond equivalents

$n_C$  carbon number of molecule

$\overline{OS}_C$  average oxidation state of carbon

$c^*$  saturation concentration in  $\mu\text{g}/\text{m}^3$

**TD-AMS** thermodenuder aerosol mass spectrometer

**PTR-MS** proton transfer mass spectrometer

**MOVI-CIMS** micro-orifice volatilization impactor chemical ionization mass spectrometer

**SV-TAG-AMS** semivolatile thermal desorption aerosol gas chromatography mass spectrometer

**TGO** TGO (a non-specific acronym)

**OVOCs** oxidized volatile organic compounds

**LVOCs** low volatility organic compounds

**LLVOCs** long lived volatile organic compounds

**TOC** total organic carbon



# Bibliography

- [1] Goldstein, A. H.; Galbally, I. E. Known and Unexplored Organic Constituents in the Earth's Atmosphere. *Environmental Science & Technology* **2007**, *41*, 1514–1521.
- [2] Spracklen, D. V.; Jimenez, J. L.; Carslaw, K. S.; Worsnop, D. R.; Evans, M. J.; Mann, G. W.; Zhang, Q.; Canagaratna, M. R.; Allan, J.; Coe, H.; McFiggans, G.; Rap, A.; Forster, P. Aerosol mass spectrometer constraint on the global secondary organic aerosol budget. *Atmospheric Chemistry and Physics* **2011**, *11*, 12109–12136.
- [3] Kroll, J. H.; Seinfeld, J. H. Chemistry of secondary organic aerosol: Formation and evolution of low-volatility organics in the atmosphere. *Atmospheric Environment* **2008**, *42*, 3593–3624.
- [4] Odum, J. R.; Hoffmann, T.; Bowman, F. M.; Collins, D.; Flagan, R. C.; Seinfeld, J. H. Gas/particle partitioning and secondary organic aerosol yields. *Environmental Science & Technology* **1996**, *30*, 2580–2585.
- [5] Donahue, N. M.; Robinson, A. L.; Stanier, C. O.; Pandis, S. N. Coupled Partitioning, Dilution, and Chemical Aging of Semivolatile Organics. *Environmental Science & Technology* **2006**, *40*, 2635–2643.
- [6] Kessler, S. H.; Smith, J. D.; Che, D. L.; Worsnop, D. R.; Wilson, K. R.; Kroll, J. H. Chemical Sinks of Organic Aerosol: Kinetics and Products of the Heterogeneous Oxidation of Erythritol and Levoglucosan. *Environmental Science & Technology* **2010**, *44*, 7005–7010.
- [7] Smith, J. D.; Kroll, J. H.; Cappa, C. D.; Che, D. L.; Liu, C. L.; Musahid, A.; Leone, S. R.; Worsnop, D. R.; Wilson, K. R. The heterogeneous reaction of hydroxyl radicals with sub-micron squalane particles: a model system for understanding the oxidative aging of ambient aerosols. *Atmospheric Chemistry and Physics* **2009**, *9*, 3209–3222.
- [8] George, I. J.; Abbatt, J. P. D. Chemical evolution of secondary organic aerosol from OH-initiated heterogeneous oxidation. *Atmospheric Chemistry and Physics* **2010**, *10*, 5551–5563.

- [9] Zhang, Q. et al. Ubiquity and dominance of oxygenated species in organic aerosols in anthropogenically-influenced Northern Hemisphere midlatitudes. *Geophysical Research Letters* **2007**, *34*.
- [10] Robinson, A. L.; Donahue, N. M.; Shrivastava, M. K.; Weitkamp, E. A.; Sage, A. M.; Grieshop, A. P.; Lane, T. E.; Pierce, J. R.; Pandis, S. N. Rethinking Organic Aerosols: Semivolatile Emissions and Photochemical Aging. *Science* **2007**, *315*, 1259–1262.
- [11] Ervens, B.; Turpin, B. J.; Weber, R. J. Secondary organic aerosol formation in cloud droplets and aqueous particles (aqSOA): a review of laboratory, field and model studies. *Atmospheric Chemistry and Physics* **2011**, *11*, 11069–11102.
- [12] Daumit, K. E.; Carrasquillo, A. J.; Hunter, J. F.; Kroll, J. H. Laboratory studies of the aqueous-phase oxidation of polyols: submicron particles vs. bulk aqueous solution. *Atmospheric Chemistry and Physics* **2014**, *14*, 10773–10784.
- [13] Hodzic, A.; Aumont, B.; Knote, C.; Lee-Taylor, J.; Madronich, S.; Tyndall, G. Volatility Dependence of Henry's Law Constants Of Condensable Organics: Application to Estimate Depositional Loss of Secondary Organic Aerosols. *Geophysical Research Letters* **2014**, *41*, 4795–4804.
- [14] Seinfeld, J. H.; Pandis, S. N. *Atmospheric Chemistry and Physics: From Air Pollution to Climate Change*, 2nd ed.; Wiley Interscience, 2006; p 1232.
- [15] Stocker, T. F., Qin, D., Plattner, G.-K., Tignor, M., Allen, S. K., Boschung, J., Nauels, A., Xia, Y., Bex, V., Midgley, P. M., Eds. *Climate Change 2013 - The Physical Science Basis*; Cambridge University Press: Cambridge, 2014.
- [16] Jerrett, M.; Burnett, R. T.; Pope, C. A.; Ito, K.; Thurston, G.; Krewski, D.; Shi, Y.; Calle, E.; Thun, M. Long-term ozone exposure and mortality. *The New England journal of medicine* **2009**, *360*, 1085–95.
- [17] Dockery, D. W.; Pope, C. A.; Xu, X. An association between air pollution and mortality in six US cities. *New England journal* **1993**,
- [18] Pope, C. A.; Dockery, D. W. Health Effects of Fine Particulate Air Pollution: Lines that Connect. *Journal of the Air & Waste Management Association* **2006**, *56*, 709–742.
- [19] Heald, C. L.; Jacob, D. J.; Park, R. J.; Russell, L. M.; Huebert, B. J.; Seinfeld, J. H.; Liao, H.; Weber, R. J. A large organic aerosol source in the free troposphere missing from current models. *Geophysical Research Letters* **2005**, *32*, n/a–n/a.
- [20] de Gouw, J. A.; Middlebrook, A. M.; Warneke, C.; Goldan, P. D.; Kuster, W. C.; Roberts, J. M.; Fehsenfeld, F. C.; Worsnop, D. R.; Canagaratna, M. R.; Pszenny, A. A. P.; Keene, W. C.; Marchewka, M.; Bertman, S. B.; Bates, T. S.

- Budget of organic carbon in a polluted atmosphere: Results from the New England Air Quality Study in 2002. *Journal of Geophysical Research* **2005**, *110*, D16305.
- [21] Volkamer, R.; Jimenez, J. L.; San Martini, F.; Dzepina, K.; Zhang, Q.; Salcedo, D.; Molina, L. T.; Worsnop, D. R.; Molina, M. J. Secondary organic aerosol formation from anthropogenic air pollution: Rapid and higher than expected. *Geophysical Research Letters* **2006**, *33*, L17811.
- [22] Heald, C. L. et al. Exploring the vertical profile of atmospheric organic aerosol: comparing 17 aircraft field campaigns with a global model. *Atmospheric Chemistry and Physics* **2011**, *11*, 12673–12696.
- [23] Tsigaridis, K. et al. The AeroCom evaluation and intercomparison of organic aerosol in global models. *Atmospheric Chemistry and Physics* **2014**, *14*, 10845–10895.
- [24] Jimenez, J. L. et al. Evolution of organic aerosols in the atmosphere. *Science* **2009**, *326*, 1525–1529.
- [25] Tkacik, D. S.; Presto, A. A.; Donahue, N. M.; Robinson, A. L. Secondary Organic Aerosol Formation from Intermediate-Volatility Organic Compounds: Cyclic, Linear, and Branched Alkanes. *Environmental Science & Technology* **2012**, *46*, 8773–8781.
- [26] Lim, Y. B.; Ziemann, P. J. Effects of Molecular Structure - Supplemental. *Environmental Science & Technology* **2009**, *43*, 1–11.
- [27] Ziemann, P. J. Effects of molecular structure on the chemistry of aerosol formation from the OH-radical-initiated oxidation of alkanes and alkenes. *International Reviews in Physical Chemistry* **2011**, *30*, 161–195.
- [28] Yee, L. D.; Craven, J. S.; Loza, C. L.; Schilling, K. A.; Ng, N. L.; Canagaratna, M. R.; Ziemann, P. J.; Flagan, R. C.; Seinfeld, J. H. Effect of chemical structure on secondary organic aerosol formation from C12 alkanes. *Atmospheric Chemistry and Physics* **2013**, *13*, 11121–11140.
- [29] Atkinson, R.; Arey, J. Atmospheric degradation of volatile organic compounds. *Chemical Reviews* **2003**, *103*, 4605–4638.
- [30] Grieshop, A. P.; Logue, J. M.; Donahue, N. M.; Robinson, A. L. Laboratory investigation of photochemical oxidation of organic aerosol from wood fires 1: measurement and simulation of organic aerosol evolution. *Atmospheric Chemistry and Physics* **2009**, *9*, 1263–1277.
- [31] Pfaffenberger, L.; Barmet, P.; Slowik, J. G.; Praplan, A. P.; Dommen, J.; Prévôt, A. S. H.; Baltensperger, U. The link between organic aerosol mass loading and degree of oxygenation: an  $\alpha$ -pinene photooxidation study. *Atmospheric Chemistry and Physics* **2013**, *13*, 6493–6506.

- [32] Wong, J. P. S.; Zhou, S.; Abbatt, J. P. D. Changes in Secondary Organic Aerosol Composition and Mass due to Photolysis: Relative Humidity Dependence. *The journal of physical chemistry. A* **2014**,
- [33] Lignell, H.; Hinks, M. L.; Nizkorodov, S. A. Exploring matrix effects on photochemistry of organic aerosols. *Proceedings of the National Academy of Sciences of the United States of America* **2014**, *111*, 13780–5.
- [34] Matsunaga, A.; Ziemann, P. J. Gas-Wall Partitioning of Organic Compounds in a Teflon Film Chamber and Potential Effects on Reaction Product and Aerosol Yield Measurements. *Aerosol Science and Technology* **2010**, *44*, 881–892.
- [35] Zhang, X.; Cappa, C. D.; Jathar, S. H.; McVay, R. C.; Ensberg, J. J.; Kleeman, M. J.; Seinfeld, J. H. Influence of vapor wall loss in laboratory chambers on yields of secondary organic aerosol. *Proceedings of the National Academy of Sciences of the United States of America* **2014**, 1–6.
- [36] Virtanen, A.; Joutsensaari, J.; Koop, T.; Kannosto, J.; Yli-Pirilä, P.; Leskinen, J.; Mäkelä, J. M.; Holopainen, J. K.; Pöschl, U.; Kulmala, M.; Worsnop, D. R.; Laaksonen, A. An amorphous solid state of biogenic secondary organic aerosol particles. *Nature* **2010**, *467*, 824–7.
- [37] Vaden, T. D.; Imre, D.; Beránek, J.; Shrivastava, M.; Zelenyuk, A. Evaporation kinetics and phase of laboratory and ambient secondary organic aerosol. *Proceedings of the National Academy of Sciences of the United States of America* **2011**, *108*, 2190–5.
- [38] Perraud, V.; Bruns, E. A.; Ezell, M. J.; Johnson, S. N.; Yu, Y.; Alexander, M. L.; Zelenyuk, A.; Imre, D.; Chang, W. L.; Dabdub, D.; Pankow, J. F.; Finlayson-Pitts, B. J. Nonequilibrium atmospheric secondary organic aerosol formation and growth. *Proceedings of the National Academy of Sciences of the United States of America* **2012**, *109*, 2836–41.
- [39] Kuwata, M.; Zorn, S. R.; Martin, S. T. Using elemental ratios to predict the density of organic material composed of carbon, hydrogen, and oxygen. *Environmental science & technology* **2012**, *46*, 787–94.
- [40] Bones, D. L.; Reid, J. P.; Lienhard, D. M.; Krieger, U. K. Comparing the mechanism of water condensation and evaporation in glassy aerosol. *Proceedings of the National Academy of Sciences of the United States of America* **2012**, *109*, 11613–8.
- [41] Donahue, N. M. et al. Aging of biogenic secondary organic aerosol via gas-phase OH radical reactions. *Proceedings of the National Academy of Sciences of the United States of America* **2012**, *109*, 13503–8.
- [42] Renbaum-Wolff, L.; Grayson, J. W.; Bateman, A. P.; Kuwata, M.; Sellier, M.; Murray, B. J.; Shilling, J. E.; Martin, S. T.; Bertram, A. K. Viscosity of  $\alpha$ -pinene

secondary organic material and implications for particle growth and reactivity. *Proceedings of the National Academy of Sciences of the United States of America* **2013**, *110*, 8014–9.

- [43] Gentner, D. R.; Isaacman, G.; Worton, D. R.; Chan, A. W. H.; Dallmann, T. R.; Davis, L.; Liu, S.; Day, D. A.; Russell, L. M.; Wilson, K. R.; Weber, R.; Guha, A.; Harley, R. A.; Goldstein, A. H. Elucidating secondary organic aerosol from diesel and gasoline vehicles through detailed characterization of organic carbon emissions. *Proceedings of the National Academy of Sciences* **2012**, *109*, 18318–18323.
- [44] Worton, D. R.; Isaacman, G.; Gentner, D. R.; Dallmann, T. R.; Chan, A. W. H.; Ruehl, C.; Kirchstetter, T. W.; Wilson, K. R.; Harley, R. a.; Goldstein, A. H. Lubricating oil dominates primary organic aerosol emissions from motor vehicles. *Environmental science & technology* **2014**, *48*, 3698–706.
- [45] Barmet, P.; Dommen, J.; Decarlo, P. F.; Tritscher, T.; Praplan, A. P.; Platt, S. M.; Prévôt, A. S. H.; Donahue, N. M.; Baltensperger, U. OH clock determination by proton transfer reaction mass spectrometry at an environmental chamber. *Atmospheric Measurement Techniques* **2012**, *5*, 647–656.
- [46] DeCarlo, P. F.; Kimmel, J. R.; Trimborn, A.; Northway, M. J.; Jayne, J. T.; Aiken, A. C.; Gonin, M.; Fuhrer, K.; Horvath, T.; Docherty, K. S.; Worsnop, D. R.; Jimenez, J. L. Field-deployable, high-resolution, time-of-flight aerosol mass spectrometer. *Analytical chemistry* **2006**, *78*, 8281–9.
- [47] Aiken, A. C. et al. O/C and OM/OC Ratios of Primary, Secondary, and Ambient Organic Aerosols with High-Resolution Time-of-Flight Aerosol Mass Spectrometry. *Environmental Science & Technology* **2008**, *42*, 4478–4485.
- [48] Hildebrandt, L.; Donahue, N. M.; Pandis, S. N. High formation of secondary organic aerosol from the photo-oxidation of toluene. *Atmospheric Chemistry and Physics* **2009**, *9*, 2973–2986.
- [49] Donahue, N. M.; Chuang, W.; Epstein, S. a.; Kroll, J. H.; Worsnop, D. R.; Robinson, a. L.; Adams, P. J.; Pandis, S. N. Why do organic aerosols exist? Understanding aerosol lifetimes using the two-dimensional volatility basis set. *Environmental Chemistry* **2013**, *10*, 151.
- [50] Kwok, E. S. C.; Atkinson, R. Estimation Of Hydroxyl Radical Reaction-Rate Constants For Gas-Phase Organic-Compounds Using A Structure-Reactivity Relationship - An Update. *Atmospheric Environment* **1995**, *29*, 1685–1695.
- [51] Henry, K. M.; Donahue, N. M. Photochemical Aging of  $\alpha$ -Pinene Secondary Organic Aerosol: Effects of OH Radical Sources and Photolysis. *The Journal of Physical Chemistry A* **2012**, *116*, 5932–5940.
- [52] Presto, A. A.; Miracolo, M. A.; Donahue, N. M.; Robinson, A. L. Secondary Organic Aerosol Formation from High-NO<sub>x</sub> Photo-Oxidation of Low Volatility

- Precursors: *n*-Alkanes. *Environmental Science & Technology* **2010**, *44*, 2029–2034.
- [53] Daumit, K. E.; Kessler, S. H.; Kroll, J. H. Average chemical properties and potential formation pathways of highly oxidized organic aerosol. *Faraday Discussions* **2013**, *165*, 181.
- [54] Faust, B. C.; Allen, J. M. Aqueous-phase photochemical sources of peroxy radicals and singlet molecular oxygen in clouds and fog. *Journal of Geophysical Research* **1992**, *97*, 12913–12926.
- [55] Hunter, J. F.; Carrasquillo, A. J.; Daumit, K. E.; Kroll, J. H. Secondary organic aerosol formation from acyclic, monocyclic, and polycyclic alkanes. *Environmental science & technology* **2014**, *48*, 10227–34.
- [56] Griffin, R. J.; Cocker, D. R.; Flagan, R. C.; Seinfeld, J. H. Organic aerosol formation from the oxidation of biogenic hydrocarbons. *Journal of Geophysical Research* **1999**, *104*, 3555–3567.
- [57] Ng, N. L.; Kroll, J. H.; Chan, A. W. H.; Chhabra, P. S.; Flagan, R. C.; Seinfeld, J. H. Secondary organic aerosol formation from *m*-xylene, toluene, and benzene. *Atmospheric Chemistry and Physics* **2007**, *7*, 3909–3922.
- [58] Lim, Y. B.; Ziemann, P. J. Chemistry of Secondary Organic Aerosol Formation from OH Radical-Initiated Reactions of Linear, Branched, and Cyclic Alkanes in the Presence of NO<sub>x</sub>. *Aerosol Science and Technology* **2009**, *43*, 604–619.
- [59] Ziemann, P. J.; Atkinson, R. Kinetics, products, and mechanisms of secondary organic aerosol formation. *Chemical Society reviews* **2012**, *41*, 6582–605.
- [60] US EPA, Estimation Programs Interface Suite™ for Microsoft® Windows 8. 2014.
- [61] Atkinson, R.; Aschmann, S. M.; Carter, W. P. L. Rate constants for the gas-phase reactions of OH radicals with a series of bi- and tricycloalkanes at 299 ± 2 K: Effects of ring strain. *International Journal Of Chemical Kinetics* **1983**, *15*, 37–50.
- [62] Benson, S. W. *Thermochemical Kinetics*, second ed. ed.; Wiley Interscience, 1976.
- [63] Bahreini, R.; Keywood, M. D.; Ng, N. L.; Varutbangkul, V.; Gao, S.; Flagan, R. C.; Seinfeld, J. H.; Worsnop, D. R.; Jimenez, J. L. Measurements of Secondary Organic Aerosol from Oxidation of Cycloalkenes, Terpenes, and *m*-Xylene Using an Aerodyne Aerosol Mass Spectrometer. *Environmental Science & Technology* **2005**, *39*, 5674–5688.
- [64] Stanier, C. O.; Donahue, N. M.; Pandis, S. N. Parameterization of secondary organic aerosol mass fractions from smog chamber data. *Atmospheric Environment* **2008**, *42*, 2276–2299.

- [65] Lambe, A. T.; Onasch, T. B.; Croasdale, D. R.; Wright, J. P.; Martin, A. T.; Franklin, J. P.; Massoli, P.; Kroll, J. H.; Canagaratna, M. R.; Brune, W. H.; Worsnop, D. R.; Davidovits, P. Transitions from functionalization to fragmentation reactions of laboratory secondary organic aerosol (SOA) generated from the OH oxidation of alkane precursors. *Environmental science & technology* **2012**, *46*, 5430–7.
- [66] Atkinson, R. Rate constants for the atmospheric reactions of alkoxy radicals: An updated estimation method. *Atmospheric Environment* **2007**, *41*, 8468–8485.
- [67] Kanakidou, M. et al. Organic aerosol and global climate modelling: a review. *Atmospheric Chemistry and Physics* **2005**, *5*, 1053–1123.
- [68] Gagosian, R. B.; Peltzer, E. T. The importance of atmospheric input of terrestrial organic material to deep sea sediments. *Organic Geochemistry* **1986**, *10*, 661–669.
- [69] Roberts, J. M.; Bertman, S. B.; Jobson, T.; Niki, H.; Tanner, R. Measurement of total nonmethane organic carbon ( $C_y$ ): Development and application at Chebogue Point, Nova Scotia, during the 1993 North Atlantic Regional Experiment campaign. *Journal of Geophysical Research* **1998**, *103*, 13581.
- [70] Chung, M. Y.; Maris, C.; Krischke, U.; Meller, R.; Paulson, S. E. An investigation of the relationship between total non-methane organic carbon and the sum of speciated hydrocarbons and carbonyls measured by standard GC/FID: Measurements in the Los Angeles air basin. *Atmospheric Environment* **2003**, *37*, S159–S170.
- [71] Lee, A.; Goldstein, A. H.; Kroll, J. H.; Ng, N. L.; Varutbangkul, V.; Flagan, R. C.; Seinfeld, J. H. Gas-phase products and secondary aerosol yields from the photooxidation of 16 different terpenes. *Journal of Geophysical Research* **2006**, *111*, D17305.
- [72] Pankow, J. F.; Barsanti, K. C. The carbon number-polarity grid: A means to manage the complexity of the mix of organic compounds when modeling atmospheric organic particulate matter. *Atmospheric Environment* **2009**, *43*, 2829–2835.
- [73] Heald, C. L.; Kroll, J. H.; Jimenez, J. L.; Docherty, K. S.; Decarlo, P. F.; Aiken, A. C.; Chen, Q.; Martin, S. T.; Farmer, D. K.; Artaxo, P. A simplified description of the evolution of organic aerosol composition in the atmosphere. *Geophysical Research Letters* **2010**, *37*, n/a–n/a.
- [74] Donahue, N. M.; Epstein, S. A.; Pandis, S. N.; Robinson, A. L. A two-dimensional volatility basis set: 1. organic-aerosol mixing thermodynamics. *Atmospheric Chemistry and Physics* **2011**, *11*, 3303–3318.

- [75] Kroll, J. H.; Donahue, N. M.; Jimenez, J. L.; Kessler, S. H.; Canagaratna, M. R.; Wilson, K. R.; Altieri, K. E.; Mazzoleni, L. R.; Wozniak, A. S.; Bluhm, H.; Mysak, E. R.; Smith, J. D.; Kolb, C. E.; Worsnop, D. R. Carbon oxidation state as a metric for describing the chemistry of atmospheric organic aerosol. *Nature chemistry* **2011**, *3*, 133–9.
- [76] Cappa, C. D.; Wilson, K. R. Multi-generation gas-phase oxidation, equilibrium partitioning, and the formation and evolution of secondary organic aerosol. *Atmospheric Chemistry and Physics* **2012**, *12*, 9505–9528.
- [77] Ortega, J. et al. Overview of the Manitou Experimental Forest Observatory: site description and selected science results from 2008 to 2013. *Atmospheric Chemistry and Physics* **2014**, *14*, 6345–6367.
- [78] Faulhaber, A. E.; Thomas, B. M.; Jimenez, J. L.; Jayne, J. T.; Worsnop, D. R.; Ziemann, P. J. Characterization of a thermodenuder-particle beam mass spectrometer system for the study of organic aerosol volatility and composition. *Atmospheric Measurement Techniques* **2009**, *2*, 15–31.
- [79] Hansel, A.; Jordan, A.; Holzinger, R.; Prazeller, P.; Vogel, W.; Lindinger, W. Proton transfer reaction mass spectrometry: on-line trace gas analysis at the ppb level. *International Journal of Mass Spectrometry and Ion Processes* **1995**, *149-150*, 609–619.
- [80] Jordan, A.; Haidacher, S.; Hanel, G.; Hartungen, E.; Märk, L.; Seehauser, H.; Schotchkowsky, R.; Sulzer, P.; Märk, T. A high resolution and high sensitivity proton-transfer-reaction time-of-flight mass spectrometer (PTR-TOF-MS). *International Journal of Mass Spectrometry* **2009**, *286*, 122–128.
- [81] Kaser, L.; Karl, T.; Schnitzhofer, R.; Graus, M.; Herdinger-Blatt, I. S.; DiGangi, J. P.; Sive, B.; Turnipseed, A.; Hornbrook, R. S.; Zheng, W.; Flocke, F. M.; Guenther, A.; Keutsch, F. N.; Apel, E.; Hansel, A. Comparison of different real time VOC measurement techniques in a ponderosa pine forest. *Atmospheric Chemistry and Physics* **2013**, *13*, 2893–2906.
- [82] Yatavelli, R. L. N.; Lopez-Hilfiker, F.; Wargo, J. D.; Kimmel, J. R.; Cubison, M. J.; Bertram, T. H.; Jimenez, J. L.; Gonin, M.; Worsnop, D. R.; Thornton, J. A. A Chemical Ionization High-Resolution Time-of-Flight Mass Spectrometer Coupled to a Micro Orifice Volatilization Impactor (MOVI-HRToF-CIMS) for Analysis of Gas and Particle-Phase Organic Species. *Aerosol Science and Technology* **2012**, *46*, 1313–1327.
- [83] Yatavelli, R. L. N.; Stark, H.; Thompson, S. L.; Kimmel, J. R.; Cubison, M. J.; Day, D. A.; Campuzano-Jost, P.; Palm, B. B.; Hodzic, A.; Thornton, J. A.; Jayne, J. T.; Worsnop, D. R.; Jimenez, J. L. Semicontinuous measurements of gas-particle partitioning of organic acids in a ponderosa pine forest using a MOVI-HRToF-CIMS. *Atmospheric Chemistry and Physics* **2014**, *14*, 1527–1546.



- [84] Zhao, Y.; Kreisberg, N. M.; Worton, D. R.; Teng, A. P.; Hering, S. V.; Goldstein, A. H. Development of an In Situ Thermal Desorption Gas Chromatography Instrument for Quantifying Atmospheric Semi-Volatile Organic Compounds. *Aerosol Science and Technology* **2013**, *47*, 258–266.
- [85] Williams, B. J. et al. The First Combined Thermal Desorption Aerosol Gas Chromatograph-Aerosol Mass Spectrometer (TAG-AMS). *Aerosol Science and Technology* **2014**, *48*, 358–370.
- [86] Cross, E. S.; Hunter, J. F.; Carrasquillo, A. J.; Franklin, J. P.; Herndon, S. C.; Jayne, J. T.; Worsnop, D. R.; Miake-Lye, R. C.; Kroll, J. H. Online measurements of the emissions of intermediate-volatility and semi-volatile organic compounds from aircraft. *Atmospheric Chemistry and Physics* **2013**, *13*, 7845–7858.
- [87] Kaser, L.; Karl, T.; Guenther, A.; Graus, M.; Schnitzhofer, R.; Turnipseed, A.; Fischer, L.; Harley, P.; Madronich, M.; Gochis, D.; Keutsch, F. N.; Hansel, A. Undisturbed and disturbed above canopy ponderosa pine emissions: PTR-TOF-MS measurements and MEGAN 2.1 model results. *Atmospheric Chemistry and Physics* **2013**, *13*, 11935–11947.
- [88] Zhang, L.; Gong, S.; Padro, J.; Barrie, L. A size-segregated particle dry deposition scheme for an atmospheric aerosol module. *Atmospheric Environment* **2001**, *35*, 549–560.
- [89] Farmer, D. K.; Chen, Q.; Kimmel, J. R.; Docherty, K. S.; Nemitz, E.; Artaxo, P. A.; Cappa, C. D.; Martin, S. T.; Jimenez, J. L. Chemically Resolved Particle Fluxes Over Tropical and Temperate Forests. *Aerosol Science and Technology* **2013**, *47*, 818–830.
- [90] Heald, C. L. et al. Total observed organic carbon (TOOC) in the atmosphere: a synthesis of North American observations. *Atmospheric Chemistry and Physics* **2008**, *8*, 2007–2025.
- [91] de Gouw, J. A. et al. Emission and chemistry of organic carbon in the gas and aerosol phase at a sub-urban site near Mexico City in March 2006 during the MILAGRO study. *Atmospheric Chemistry and Physics* **2009**, *9*, 3425–3442.
- [92] Aiken, A. C.; DeCarlo, P. F.; Jimenez, J. Elemental Analysis of Organic Species with Electron Ionization High-Resolution Mass Spectrometry. *Analytical Chemistry* **2007**, *79*, 8350–8358.
- [93] Canagaratna, M. R.; Jimenez, J. L.; Kroll, J. H.; Chen, Q.; Kessler, S. H.; Massoli, P.; Hildebrandt Ruiz, L.; Fortner, E.; Williams, L. R.; Wilson, K. R.; Surratt, J. D.; Donahue, N. M.; Jayne, J. T.; Worsnop, D. R. Elemental ratio measurements of organic compounds using aerosol mass spectrometry: characterization, improved calibration, and implications. *Atmospheric Chemistry and Physics Discussions* **2014**, *14*, 19791–19835.

- [94] Pankow, J. F.; Asher, W. E. SIMPOL.1: a simple group contribution method for predicting vapor pressures and enthalpies of vaporization of multifunctional organic compounds. *Atmospheric Chemistry and Physics* **2008**, *8*, 2773–2796.
- [95] Eddingsaas, N. C.; VanderVelde, D. G.; Wennberg, P. O. Kinetics and products of the acid-catalyzed ring-opening of atmospherically relevant butyl epoxy alcohols. *The journal of physical chemistry. A* **2010**, *114*, 8106–13.
- [96] Worton, D. R. et al. Observational insights into aerosol formation from isoprene. *Environmental science & technology* **2013**, *47*, 11403–13.
- [97] Bouvier-Brown, N. C.; Goldstein, A. H.; Gilman, J. B.; Kuster, W. C.; de Gouw, J. A. In-situ ambient quantification of monoterpenes, sesquiterpenes, and related oxygenated compounds during BEARPEX 2007—implications for gas- and particle-phase chemistry. *Atmospheric Chemistry and Physics Discussions* **2009**, *9*, 10235–10269.
- [98] Jayne, J. T.; Leard, D. C.; Zhang, X.; Davidovits, P.; Smith, K. A.; Kolb, C. E.; Worsnop, D. R. Development of an Aerosol Mass Spectrometer for Size and Composition Analysis of Submicron Particles. *Aerosol Science and Technology* **2000**, *33*, 49–70.